

P82

THE DYNAMICS AND CONTROL OF LARGE FLEXIBLE  
SPACE STRUCTURES - XIII

FINAL REPORT

NASA GRANT: NSG-1414, Supplement 12

by

Peter M. Bainum  
Professor of Aerospace Engineering  
Principal Investigator

and

Feiyue Li  
Jianke Xu  
Graduate Research Assistants

September 1990

DEPARTMENT OF MECHANICAL ENGINEERING  
SCHOOL OF ENGINEERING  
HOWARD UNIVERSITY  
WASHINGTON, D.C. 20059

(NASA-CR-186930) THE DYNAMICS AND CONTROL  
OF LARGE FLEXIBLE SPACE STRUCTURES - 13  
Final Report (Howard Univ.) 82 p CSCL 222

N90-29591

Unclas  
G3/19 0302640

## ABSTRACT

The optimal control of three-dimensional large-angle rapid maneuvers and vibrations of a Shuttle-mast-reflector system is considered. The nonlinear equations of motion are formulated by using Lagrange's formula, with the mast modeled as a continuous beam subject to three dimensional deformations. The nonlinear terms in the equations come from the coupling between the angular velocities, the modal coordinates, and the modal rates. Pontryagin's Maximum Principle is applied to the slewing problem, to derive the necessary conditions for the optimal controls, which are bounded by given saturation levels. The resulting two-point boundary-value problem is then solved by using the quasilinearization algorithm and the method of particular solutions. The numerical results for both the linearized system and the nonlinear system are presented to compare the differences in their time responses.

The study of the large-angle maneuvering of the Shuttle-beam-reflector spacecraft in the plane of a circular earth orbit is extended to consider the effects of the structural offset connection, the axial shortening, and the gravitational torque on the slewing motion. The offset effect is analyzed by changing the attachment point of the reflector to the beam. As the attachment point is moved away from the mass center of the reflector, the responses of the nonlinear system deviate from those of the linearized system. The axial geometric shortening effect induced by the deformation of the beam contributes to the system equations through second order terms in the modal

amplitudes and rates. The gravitational torque effect is relatively small.

Finally the effect of additional design parameters (such as related to additional payload requirement) on the LQR based design of an orbiting control/structural system is examined. Based on the introduction of some desired control properties to the optimal system design, the multi-objectives for the integral control structural design are defined as the quadratic cost function and its partial variation about the redesigned parameters. The constraints not only include the limited mass and control forces for the system but also include the control properties (such as the transient response time of the system). Optimal multicriteria are derived for minimizing the cost function and setting the variation of the cost function with respect to the design variables to zero. The simple models of uniform solid and tubular beams are demonstrated here with two typical additional payload masses: (1) symmetrically distributed with respect to the center of the beam; (2) asymmetrically distributed with respect to the center of the beam. For the solid and tubular beams, the length and material properties are assumed equal. By considering the transient response of pitch angle and free-free beam deformations in the orbital plane, the optimal outer diameter of the beam and all feedback control can be determined by numerical analysis with this multicriteria approach.

TABLE OF CONTENTS

ABSTRACT

CHAPTER I INTRODUCTION

CHAPTER II OPTIMAL LARGE ANGLE MANEUVERS OF A FLEXIBLE SPACECRAFT

CHAPTER III EFFECT OF STRUCTURAL OFFSET, AXIAL SHORTENING, AND GRAVITATIONAL TORQUE ON THE SLEWING OF A FLEXIBLE SPACECRAFT

CHAPTER IV THE EFFECT OF ADDITIONAL DESIGN PARAMETERS ON THE LQR BASED DESIGN OF A CONTROL/STRUCTURAL SYSTEM

CHAPTER V CONCLUSIONS AND RECOMMENDATIONS

## I. INTRODUCTION

The present grant, NSG-1414, Suppl. 12 extends the research initiated in May 1977 and reported in Refs. 1-16<sup>1</sup> for the grant years May 1977 - May 1989. This effort has focused on the problem of shape and orientation control of large, inherently flexible proposed space systems. Possible applications proposed for these large space systems (LSS) include: Earth observation and resource sensing systems; orbitally based electronic mail transmission; large scale multi-beam antenna communication systems; as platforms for orbital-based telescope systems; and as in-orbit test models designed to compare the performance of LSS systems with that predicted based on scale model Earth-based laboratory experiments and/or computer simulations. In the last several years the grant research has focused on the orbital model of the Spacecraft Control Laboratory Experiment (SCOLE).<sup>17</sup>

The present report is divided into five chapters. Chapter II is based on a paper presented at the 1990 International Conference on the Dynamics of Flexible Structures in Space and describes rapid three dimensional maneuvers and vibration suppression of the asymmetrical flexible SCOLE configuration. Pontryagin's maximum principle is applied to both the linearized and nonlinear system equations to develop the necessary conditions for the optimal multi-control problem. The resulting two point boundary value problem is then solved based on the

---

<sup>1</sup>References cited in this report are listed separately at the end of each chapter.

quasilinearization algorithm and the method of particular solutions. The numerical results for both the linear and nonlinear systems are presented to compare the differences in their time responses.

Chapter III is motivated by a paper presented at the 17th International Symposium on Space Technology and Science in which the effects of the structural offset for asymmetrical configurations (such as SCOLE), axial shortening, and gravitational torque during a rapid slew are evaluated. For this study a two dimensional model of the SCOLE Shuttle - (flexible) beam-reflector system is considered. Both linear and nonlinear system models are treated.

In Chapter IV the effect of additional system design parameters (such as those related to the placement of additional payloads) on the LQR based design of an orbiting control/structural system is analyzed. This multicriteria numerical optimization approach is considered for minimizing an LQR type cost function where the system design parameter is the outside diameter of a solid and/or tubular beam, subject to constraints on the total system mass, control saturation levels, and transient settling time. Different combinations of additional payload masses are considered.

Finally, Chapter V describes the main general conclusions together with general recommendations. The thrust of this effort has been redirected to provide more direct support to the new NASA Controls/Structures Interaction Program (CSI), particularly as evidenced by Chapter IV, and our follow-on proposal, Ref. 18.

References - Chapter I

1. Bainum, P.M. and Sellappan, R., "The Dynamics and Control of Large Flexible Space Structures," Final Report NASA Grant: NSG-1414, Part A: Discrete Model and Modal Control, Howard University, May 1978.
2. Bainum, Peter M., Kumar, V.K., and James, Paul K., "The Dynamics and Control of Large Flexible Space Structures," Final Report, NASA Grant: NSG-1414, Part B: Development of Continuum Model and Computer Simulation, Howard University, May 1978.
3. Bainum, P.M. and Reddy, A.S.S.R., "The Dynamics and Control of Large Flexible Space Structures II," Final Report, NASA Grant NSG-1414, Suppl. I, Part A: Shape and Orientation Control Using Point Actuators, Howard University, June 1979.
4. Bainum, P.M., James, P.K., Krishna, R., and Kumar, V.K., "The Dynamics and Control of Large Flexible Space Structures II," Final Report, NASA Grant NSG-1414, Suppl. 1, Part B: Model Development and Computer Simulation, Howard University, June 1979.
5. Bainum, P.M., Krishna, R., and James, P.K., "The Dynamics and Control of Large Flexible Space Structures III," Final Report, NASA Grant NSG-1414, Suppl. 2, Part A: Shape and Orientation Control of a Platform in Orbit Using Point Actuators, Howard University, June 1980.
6. Bainum, P.M. and Kumar, V.K., "The Dynamics and Control of Large Flexible Space Structures III," Final Report, NASA Grant NSG-1414, Suppl. 2, Part B: The Modelling, Dynamics and Stability of Large Earth Pointing Orbiting Structures, Howard University, September 1980.
7. Bainum, P.M., Kumar, V.K., Krishna, R. and Reddy, A.S.S.R., "The Dynamics and Control of Large Flexible Space Structures IV," Final Report, NASA Grant NSG-1414, Suppl. 3, NASA CR-165815, Howard University, August 1981.
8. Bainum, P.M., Reddy, A.S.S.R., Krishna, R., Diarra, C.M., and Kumar, V.K., "The Dynamics and Control of Large Flexible Space Structures V", Final Report, NASA Grant NSG-1414, Suppl. 4, NASA CR-169360, Howard University, August 1982.
9. Bainum, P.M., Reddy, A.S.S.R., Krishna, R., and Diarra, C.M., "The Dynamics and Control of Large Flexible Space Structures VI," Final Report NASA Grant NSG-1414, Suppl. 5, Howard University, Sept. 1983.

10. Bainum, P.M., Reddy, A.S.S.R., Krishna, R., Diarra, C.M. and Ananthakrishnan, S., "The Dynamics and Control of Large Flexible Space Structures-VII," Final Report NASA Grant NSG-1414, Suppl. 6, Howard University, June 1984.
11. Bainum, P.M., Reddy, A.S.S.R., Diarra, C.M. and Ananthakrishnan, S., "The Dynamics and Control of Large Flexible Space Structures-VIII," Final Report NASA Grant NSG-1414 Suppl. 7, Howard University, June 1985.
12. Bainum, P.M., Reddy, A.S.S.R. and Diarra, C.M., "The Dynamics and Control of Large Flexible Space Structures -IX," Final Report NASA Grant NSG-1414, Suppl. 8, Howard University, July 1986.
13. Bainum, P.M., Reddy, A.S.S.R., Li, Feiyue, and Diarra, C.M., "The Dynamics and Control of Large Flexible Space Structures X-Part I", Final Report NASA Grant NSG-1414, Suppl. 9, Howard University, August 1987.
14. Bainum, P.M., Reddy, A.S.S.R., Diarra, C.M., and Li, Feiyue, "The Dynamics and Control of Large Flexible Space Structures X-Part II", Final Report NASA Grant NSG-1414, Suppl. 9, Howard University, January 1988.
15. Bainum, P.M., Reddy, A.S.S.R., Diarra, C.M., and Li, Feiyue, "The Dynamics and Control of Large Flexible Space Structures-XI," Final Report NASA Grant NSG-1414, Suppl. 10, Howard University, August 1988.
16. Bainum, P.M., Reddy, A.S.S.R., Li, Feiyue and Xu, Jianke, "The Dynamics and Control of Large Flexible Space Structures XII," Final Report NASA Grant NSG-1414, Suppl. 11, Howard University, Sept. 1989.
17. Taylor, L.W. and Balakrishnan, A.V., "A Mathematical Problem and a Spacecraft Control Laboratory Experiment (SCOLE) Used to Evaluate Control Laws for Flexible Spacecraft...NASA/IEEE Design Challenge," (Rev.), January 1984. (Originally presented at AIAA/VP&SU Symposium on Dynamics and Control of Large Structures, June 6-8, 1983.)
18. Bainum, P.M., "Proposal for Research Grant on: "Control Structural Interaction of Large Articulated Space Systems with Telerobots" (submitted to NASA), April 1, 1990.

## II. OPTIMAL LARGE ANGLE MANEUVERS OF A FLEXIBLE SPACECRAFT

### 1. INTRODUCTION

Many authors have considered the problem of large-angle rapid maneuvers of flexible spacecraft [1-5]. The direct solution of the open-loop two-point boundary-value problem (TPBVP) for three-dimensional (3-D) slews of flexible spacecraft resulted in numerical problems with rank-deficient matrices as stated by Chun [3]. However, a different numerical method may be used to overcome this difficulty. In this paper, the problem has been solved successfully by using the quasilinearization algorithm and the method of particular solutions for 3-D slews of an asymmetrical flexible spacecraft, namely, the Spacecraft Control Laboratory Experiment (SCOLE) configuration.

The open-loop slewing approach has several obvious distinct properties. First, the control law is easy to implement in practice for both ground tests and space flight tests. Second, the open-loop solution may serve as a good reference for the feedback control law design, as proposed by Chun [3], and Meirovitch [4], in which the open-loop solution for a rigid (instead of a flexible) spacecraft is used as the nominal reference trajectory. As an extension to Refs. [3] and [4], it may be helpful if the open-loop solution for the 3-D slew of a flexible spacecraft system could also be used as a nominal reference solution. In addition, through the present study, we can also see how different are the responses of the nonlinear system from those of the linearized system, and the differences between the flexible and rigidized systems.

### 2. FORMULATION OF THE STATE EQUATIONS

#### 2.1 System Configuration

As shown in Fig. 1, the orbiting SCOLE configuration [6] is composed of a Shuttle, a flexible mast, and a reflector antenna. Both the Shuttle and the reflector are considered to be rigid bodies. One end of the mast is fixed to

the Shuttle at its mass center,  $o_s$ , while the other end is firmly connected to the reflector at an offset point,  $a_r$ .

Three coordinate systems,  $(\hat{i}_o \hat{j}_o \hat{k}_o)$ ,  $(\hat{i}_s \hat{j}_s \hat{k}_s)$ , and  $(\hat{i}_r \hat{j}_r \hat{k}_r)$ , representing the orbit's local vertical/horizontal reference system, the Shuttle body axis coordinates, and the reflector axes, respectively, are adopted in Figure 1. The mass center of the reflector,  $o_r$ , is located at  $(x_r, y_r)$  in the reflector axis system. Three Euler angles  $(\theta_1, \theta_2, \theta_3)$  or four quaternions  $(q_0, q_1, q_2, q_3)$  are used to describe the attitude of the Shuttle with respect to the orbiting reference system.

The undeformed mast is assumed to be oriented along the z axis of the Shuttle coordinate system. The 3-D deformation of the mast consists of two bending deflections  $U(z,t)$  and  $V(z,t)$  in the x-z and y-z planes, respectively, and torsion  $\phi(z,t)$  about the z axis. It is assumed that these deformations are small as compared with the length of the mast and can be expressed by the following modal superposition formula [7]:

$$U = \sum_1 \xi_i(z) \alpha_i(t), \quad V = \sum_1 \eta_i(z) \alpha_i(t), \quad \phi = \sum_1 \zeta_i(z) \alpha_i(t), \quad (1)$$

where  $\xi_i$ ,  $\eta_i$ , and  $\zeta_i$  are modal shape function vector components normalized by a common factor, and  $\alpha_i$  is a scaled modal amplitude associated with the ith mode. The free vibration of this structure can be considered as a space free-free beam vibration problem with boundary conditions including the masses and moments of inertia of the Shuttle and the reflector. The partial differential equation formulation for this problem [6,7] can be solved by using the separation of variables method. The first five natural frequencies and mode shapes have been obtained by Robertson [7], and will be used in this paper.

## 2.2 Kinetic Energy

The kinetic energy of the system about the mass center of the system,  $c$ , can be expressed as

$$\begin{aligned}
T &= \frac{1}{2} \int_s |\dot{\bar{r}}|^2 dm + \frac{1}{2} \left[ \int_b |\dot{\bar{r}}|^2 dm - \frac{1}{m_t} \left( \int_b |\dot{\bar{r}}| dm \right)^2 \right] \\
&+ \frac{1}{2} \left[ \int_r |\dot{\bar{r}}|^2 dm - \frac{1}{m_t} \left( \int_r |\dot{\bar{r}}| dm \right)^2 \right] - \frac{1}{m_t} \left( \int_b \dot{\bar{r}} dm \right) \cdot \left( \int_r \dot{\bar{r}} dm \right) \\
&= T_s + T_b + T_r - T_c
\end{aligned} \tag{2}$$

where  $\bar{r}$  is the position vector from  $o_s$  to an arbitrary mass element in the system and  $m_t$  is the total mass of the system. The integration subscripts, "s", "b", and "r", mean that the corresponding integration is throughout the Shuttle, the beam, and the reflector, respectively.

Kinetic Energy of the Shuttle The first term in Equation (2) is the rotational kinetic energy of the Shuttle about  $o_s$ ,

$$T_s = \frac{1}{2} \omega^T J_s \omega \tag{3}$$

where  $\omega$  is the matrix describing the angular velocity vector of the Shuttle,  $\bar{\omega}$ , and  $J_s$  is the inertia matrix of the Shuttle.

Kinetic Energy of the Mast As Shown in Figure 2, the position vector of an element  $dm$  and its velocity are, respectively,

$$\bar{r} = \bar{b} + \bar{p}, \quad \bar{b} = U \hat{i}_s + V \hat{j}_s + z \hat{k}_s \tag{4}$$

$$\dot{\bar{r}} = \bar{v}_b + \bar{\omega}_b(z) \times \bar{p} \tag{5}$$

where  $\bar{p}$  is a vector within the cross section of the beam and

$$\bar{v}_b = U \hat{i}_s + V \hat{j}_s + \bar{\omega} \times \bar{b} \tag{6}$$

$\bar{\omega}_b(z)$  is the angular velocity of the element,

$$\bar{\omega}_b(z) = \bar{\omega} + \dot{\phi}_x \hat{i}_s + \dot{\phi}_y \hat{j}_s + \dot{\phi}_z \hat{k}_s \tag{7}$$

where  $\phi_x = -(\partial V / \partial z)$ ,  $\phi_y = \partial U / \partial z$ , and  $\phi_z = \phi$ .

During the integration process of equation (2), one needs to do the following calculations,

$$\int_b |\bar{\omega}_b \times \bar{p}|^2 dm = \int_0^L \left\{ \rho \omega_b^T \left[ \int_A (p^T p E - p p^T) dA \right] \omega_b \right\} dz \quad (8)$$

where  $\omega_b$  is the matrix representation of  $\bar{\omega}_b$  and E is an identity matrix. For the circular cross section of the beam assumed here, the inner integration in Equation (8) turns out, in the local beam coordinates, to be,

$$\left[ \int_A (p^T p E - p p^T) dA \right] = I_p \begin{bmatrix} \frac{1}{2} & 0 & 0 \\ 0 & \frac{1}{2} & 0 \\ 0 & 0 & 1 \end{bmatrix} = J^{(r)} \quad (9)$$

where  $I_p$  is the polar moment of inertia of the beam. Due to the small deformation of the beam, the local beam axes is assumed to be related to the Shuttle axes by a transformation matrix,

$$R^{sr} = \begin{bmatrix} 1 & -\phi_z & \phi_y \\ \phi_z & 1 & -\phi_x \\ -\phi_y & \phi_x & 1 \end{bmatrix} \quad (10)$$

Therefore,  $J^{(r)}$  in Equation (9) can be transformed to the Shuttle axes by the following similarity transformation:

$$J^{(s)} = R^{sr} J^{(r)} (R^{sr})^T \quad (11)$$

After substituting all related terms into the second term of Equation (2), and neglecting all the third and higher order terms in the modal amplitude vector,  $\alpha$ , the modal rate vector,  $\dot{\alpha}$ , and their coupling, one can arrive at

$$T_b = \frac{1}{2} \omega^T J_b \omega + \frac{1}{2} \dot{\alpha}^T I_b \dot{\alpha} + \omega^T h_b \quad (12)$$

where  $I_b$  is a constant matrix. The elements of matrix  $J_b$  and the vector  $h_b$  have the following forms,

$$(J_b)_{ij} = c_{ij} + \alpha^T m_{ij} + \alpha^T M_{ij} \alpha, \quad (h_b)_i = \dot{\alpha}^T g_i + \dot{\alpha}^T G_i \alpha \quad (13)$$

where  $c_{ij}$ ,  $m_{ij}$ ,  $g_i$ ,  $M_{ij}$ , and  $G_i$  are constants, constant vectors, and constant matrices, respectively.

Kinetic Energy of the Reflector After using a development process similar to that for the mast, one can obtain,

$$T_r = \frac{1}{2} \omega^T J_r \omega + \frac{1}{2} \dot{\alpha}^T I_r \dot{\alpha} + \omega^T h_r \quad (14)$$

Here the inertia matrix of the reflector needs to be considered in the development process.

The Coupling Term in Equation (2) can also be written in the form of Equation (12) for consistence,

$$T_c = \frac{1}{2} \omega^T J_c \omega + \frac{1}{2} \dot{\alpha}^T I_c \dot{\alpha} + \omega^T h_c \quad (15)$$

After substituting Equations (12,14,15) into Equation (2), one obtains,

$$T = \frac{1}{2} \omega^T \{ J_0 + J_1 + J_2 \} \omega + \frac{1}{2} \dot{\alpha}^T I \dot{\alpha} + \omega^T \{ h_1 + h_2 \} \quad (16)$$

where  $J_0$ ,  $J_1$ ,  $J_2$  are  $3 \times 3$  matrices,  $h_1$ ,  $h_2$  are  $3 \times 1$  vectors,  $I$  is an  $n \times n$  constant matrix, and

$$\begin{aligned} (J_0)_{ij} &= \text{constant}, & (J_1)_{ij} &= \alpha^T m_{ij}, & (J_2)_{ij} &= \alpha^T M_{ij} \alpha \\ (h_1)_i &= \alpha^T g_i, & (h_2)_i &= \alpha^T G_i \alpha \end{aligned} \quad (17)$$

where  $m_{ij}$ ,  $g_i$ ,  $M_{ij}$ , and  $G_i$  are constant vectors and matrices.

### Potential Energy

The elastic potential energy of the flexible part is

$$V = \frac{1}{2} \left\{ \int_0^L EI \left( \frac{\partial^2 U}{\partial z^2} \right)^2 dz + \int_0^L EI \left( \frac{\partial^2 v}{\partial z^2} \right)^2 dz + \int_0^L GI_p \left( \frac{\partial \phi}{\partial z} \right)^2 dz \right\} = \frac{1}{2} \alpha^T K \alpha \quad (18)$$

where  $EI$  is the bending stiffness and  $G$  is the modulus of rigidity of the beam.

### Generalized Forces

The virtual work done by the controls is

$$\delta W = \bar{N}_1 \cdot \delta \bar{\theta} + \sum_{j=2}^4 \bar{N}_j \cdot \delta \bar{r}_j \quad (19)$$

where  $\delta \bar{\theta}$  is a variation vector which has the direction of an axis of rotation of the Shuttle and the magnitude of the rotation angle about this axis,  $\delta \bar{r}_j$  are the virtual displacements of the position vector  $\bar{r}$  at the location of the controls,  $\bar{N}_1$  is the control torque vector on the Shuttle, and  $\bar{N}_j$  are the control force vectors on the beam and the reflector. The shift of the center of mass of the system is also considered in this development. After expanding these terms by using the associated relations and the transformation matrix (10), dropping all third and higher order terms in  $\alpha$ , one can get,

$$\delta W = \delta \theta^T [f_1 + \sum_{j=2}^4 \Gamma_j f_j] + \delta \alpha^T \sum_{j=2}^4 \Psi_j f_j \quad (20)$$

where  $f_1 = [f_{1x} \ f_{1y} \ f_{1z}]^T$ ,  $f_j = [f_{jx} \ f_{jy}]^T$ , are control variables; the elements of matrices  $\Gamma_j$  and  $\Psi_j$  have the similar form as those in Equation (17), and up to the first order terms in  $\alpha$  have been retained for later use. Then, the generalized forces are,

$$Q_\theta = f_1 + \sum_{j=2}^4 \Gamma_j f_j, \quad Q_\alpha = \sum_{j=2}^4 \Psi_j f_j \quad (21)$$

### Dynamical Equations

After constructing the Lagrangian,  $L=T-V$ , and using

$$\frac{d}{dt} \left( \frac{\partial L}{\partial \dot{\omega}} \right) + \tilde{\omega} \left( \frac{\partial L}{\partial \dot{\omega}} \right) = Q_\theta, \quad \frac{d}{dt} \left( \frac{\partial L}{\partial \dot{\alpha}} \right) - \left( \frac{\partial L}{\partial \alpha} \right) = Q_\alpha \quad (22)$$

one can get the following equations by discarding second order terms in  $\alpha$ ,  $\dot{\alpha}$ , and their coupling, and retaining a constant mass matrix represented by the coefficients for  $\dot{\omega}$  and  $\ddot{\alpha}$ ,

$$J_0 \dot{\omega} + [g_1 \ g_2 \ g_3]^T \ddot{\alpha} = [\bar{m} + \bar{M}(\alpha)] \ddot{\omega} + \bar{H}(\dot{\alpha}) \omega + Q_\theta \quad (23)$$

$$[g_1 \ g_2 \ g_3] \dot{\omega} + I \ddot{\alpha} = [\bar{n} + \bar{N}(\alpha)] \ddot{\omega} + \bar{G}(\dot{\alpha}) \omega + Q_\alpha - K \alpha \quad (24)$$

where

$$\bar{\omega} = \left[ \omega_1^2 \quad \omega_2^2 \quad \omega_3^2 \quad \omega_2 \omega_3 \quad \omega_3 \omega_1 \quad \omega_1 \omega_2 \right]^T \quad (25)$$

After finding the inverse of the mass matrix, a state form of Equations (23) and (24) can be obtained as,

$$\dot{y} = \begin{bmatrix} \dot{\omega} \\ \dot{\beta} \end{bmatrix} = (A + \bar{B}_\alpha) \bar{\omega} + (\bar{C}_\beta) \omega + D\alpha + (E + \bar{F}_\alpha) u \quad (26)$$

where  $\beta = \alpha$ ,  $\bar{B}_\alpha = [B_1 \alpha \mid B_2 \alpha \mid \dots \mid B_6 \alpha]$ ,  $\bar{C}_\beta = [C_1 \beta \mid C_2 \beta \mid C_3 \beta]$ , and  $\bar{F}_\alpha = [F_1 \alpha \mid F_2 \alpha \mid \dots \mid F_9 \alpha]$ , with  $A, B_i, C_i, D, E, F_i$  being constant matrices; and  $u = [f_{1x} \quad f_{1y} \quad f_{1z} \mid f_{2x} \quad f_{2y} \mid f_{3x} \quad f_{3y} \mid f_{4x} \quad f_{4y}]^T$ . For the purpose of comparison, the dynamical equations for the rigidized (rigid) spacecraft can be obtained by deleting all terms related to  $\alpha$  and  $\beta$ , this is,

$$\dot{\omega} = \bar{A} \bar{\omega} + \bar{E} u \quad (27)$$

where  $\bar{A}$  and  $\bar{E}$  are  $3 \times 6$  and  $3 \times 9$  constant matrices, respectively. A linearized form of Equation (27) can also be obtained by deleting all nonlinear terms,

$$\dot{y} = D\alpha + Eu \quad (28)$$

The kinematic equations for the quaternions are

$$\dot{q} = \frac{1}{2} \bar{\omega} \tilde{q}, \quad \text{where} \quad \tilde{\omega} = \begin{bmatrix} 0 & -\omega_1 & -\omega_2 & -\omega_3 \\ \omega_1 & 0 & \epsilon_3 & -\omega_2 \\ \omega_2 & -\omega_3 & 0 & \epsilon_1 \\ \omega_3 & \epsilon_2 & -\omega_1 & 0 \end{bmatrix} \quad (29)$$

where  $q$  is the  $4 \times 1$  quaternion vector.

### 3. DERIVATION OF THE OPTIMAL CONTROL PROBLEM

#### Necessary Conditions

A quadratic cost function is used,

$$J = \frac{1}{2} \int_0^{t_f} (\alpha^T Q_1 \alpha + \omega^T Q_2 \omega + \beta^T Q_3 \beta + u^T R u) dt \quad (30)$$

where  $Q_1$ , and  $R$  are weighting matrices,  $t_f$  is the given slewing time. The magnitudes of the controls,  $u$ , are bounded,

$$|u_i| \leq u_{ib}, \quad i=1, \dots, 9. \quad (31)$$

The following technique is used to solve this problem [8]. First, the necessary conditions based on Equations (26, 29, 30) are derived. Then, the constraints (31) are imposed on these necessary conditions to modify the controls.

The Hamiltonian of the system is,

$$\begin{aligned} H = & \frac{1}{2} (\alpha^T Q_1 \alpha + \omega^T Q_2 \omega + \beta^T Q_3 \beta + u^T R u + p^T \dot{\omega} q) + \gamma^T \beta \\ & + \lambda^T [(A + \bar{B}_\alpha) \bar{\omega} + (\bar{C}_\beta) \omega + D \alpha + (E + \bar{F}_\alpha) u] \end{aligned} \quad (32)$$

where  $p$ ,  $\gamma$ , and  $\lambda = [\lambda_1 \ \lambda_2]^T$  are the costate vectors associated with  $q$ ,  $\alpha$ ,  $\omega$ , and  $\beta$ , respectively. By using the Maximum Principle, the necessary conditions for the unrestricted optimal control problem are the dynamical equations (26, 29) plus the following differential equations for the costates,

$$\dot{p} = -\frac{\partial H}{\partial q} = \frac{1}{2} \dot{\omega} p \quad (33)$$

$$\dot{\gamma} = -\frac{\partial H}{\partial \alpha} = -Q_1 \alpha - D^T \lambda - (\bar{B}_\alpha^T \lambda) \bar{\omega} - (\bar{F}_\alpha^T \lambda) u \quad (34)$$

$$\dot{\lambda}_1 = -\frac{\partial H}{\partial \omega} = -Q_2 \omega - \frac{1}{2} [q] p - [\lambda^T (A + \bar{B}_\alpha)] \omega - (\bar{C}_\beta)^T \lambda \quad (35)$$

$$\dot{\lambda}_2 = -\frac{\partial H}{\partial \beta} = -Q_3 \beta - \gamma - (\bar{C}_\beta^T \lambda) \omega \quad (36)$$

and the optimal control,

$$\frac{\partial H}{\partial u} = 0, \implies u = -R^{-1}(E + \bar{P}_\alpha)^T \lambda \quad (37)$$

The control resulting from Equation (37) is then modified by the following saturation considerations,

$$u_i = \begin{cases} -u_{ib}, & \text{if } u_{ic} \leq -u_{ib} \\ u_{ib}, & \text{if } u_{ic} \geq u_{ib} \end{cases}, \quad \text{otherwise,} \quad u_i = u_{ic} = -[R^{-1}(E + \bar{P}_\alpha)^T \lambda]_i \quad (38)$$

$i = 1, \dots, 9.$

By substituting the control expressions into Equations (26) and (34), one can obtain a set of  $4(n+3)+2$  differential equations for the states and the costates. To obtain the control,  $u$ , one needs to solve these equations with the given conditions:  $q(0)$ ,  $\alpha(0)$ ,  $\omega(0)$ ,  $\dot{\alpha}(0)$ , and  $q(t_f)$ ,  $\alpha(t_f)$ ,  $\omega(t_f)$ ,  $\dot{\alpha}(t_f)$ .

#### 4. Two-Point Boundary-Value Problem (TPBVP)

One way of obtaining the optimal control law is to transform the above necessary conditions into the following TPBVP. Let  $x$  represent the state vector, and  $\lambda$  represent the costate vector. After substituting the control expressions (38) into equations (26) and (34), one can obtain two sets of ordinary differential equations for the states and the costates,

$$\dot{x} = f_1(x, \lambda)_{(7+2n) \times 1} \quad (39a)$$

$$\dot{\lambda} = f_2(x, \lambda)_{(7+2n) \times 1} \quad (39b)$$

with the following boundary conditions,

$$x(0) \text{ and } x(t_f) \text{ prescribed, } \lambda(0) \text{ and } \lambda(t_f) \text{ unknown.} \quad (40)$$

Due to the known boundary conditions being specified at the two ends of the slewing time, this problem is usually called the two-point boundary-value problem. This kind of split boundary conditions usually result from the large-angle maneuver requirements, in which the initial ( $t=0$ ) and final ( $t=t_f$ )

states of the system are specified. By solving this problem, we can obtain the optimal control (based on the necessary conditions). The often used solution strategy is to change the boundary value problem to the initial value problem, i.e., find  $\lambda(0)$ , the missing initial costates. Once  $\lambda(0)$  is obtained, one can solve the equations (39) as an initial value problem by using any numerical integration method. However, owing to the nonlinearity of the equations, there is generally no analytical solution to this problem or simple numerical method to obtain the solution except for some very simple cases such as the linear time-invariant case. The numerical iteration method is the general approach to the this problem.

To start an iteration process, one usually needs an initial guess of  $\lambda^{(0)}(0)$ . Then, equations (39) or their equivalent form (the linearized version of (39)) are solved and a  $x^{(0)}(t_f)$  is obtained. Based on the difference  $\Delta x(t_f) = x^{(0)}(t_f) - x(t_f)$ , the correction to  $\lambda(0)$ ,  $\Delta\lambda(0)$ , is obtained. This gives us a new initial value of  $\lambda(0)$ ,  $\lambda^{(1)}(0)$ . Hence, the next iteration begins. The iteration process can be terminated when  $|\lambda^{(k+1)}(0) - \lambda^{(k)}(0)|$  is less than a given error limit. One can see immediately that if the beginning guess  $\lambda^{(0)}(0)$  is close to the true value (converged value) of  $\lambda(0)$ , the solution will converge and less iterations are needed. However, a "good" guess of  $\lambda(0)$  is often difficult to obtain for the general nonlinear problems.

Therefore, the effort for solving the TPBVP is two fold. The first is try to establish a good iteration (correction) method with a wide convergence interval so that it can guarantee convergence even for a "poor" initial guess. The other is try to find a "good" initial guess based on the characteristics of the practical problem and using some simplified mathematical models. In this report, we use the quasilinearization method. We also use the solution of  $\lambda(0)$  from the simplified linear, time-invariant model of the system as the initial guess for starting the iteration process.

#### 4.1 Linear and Time-Invariant TPBVP

For linear, time-invariant versions of equations (39) (refs. 1-2),

$$\dot{z} = Az, \quad \text{where } z^T = [x^T, \lambda^T] \quad (41)$$

its transition matrix (constant exponential matrix),

$$e^{At_f} = \begin{bmatrix} A_{11} & A_{12} \\ A_{21} & A_{22} \end{bmatrix}$$

can be used to obtain the initial costates (closed form solution):

$$\lambda(0) = A_{12}^{-1} [x(t_f) - A_{11} x(0)] \quad (42)$$

#### 4.2 Nonlinear TPBVP

The continuation (relaxation) process (to increase the participation of the nonlinearity in the solution) and the differential correction (for determination of the initial costate variables) have been used in references 1-2 for the 2-D slewing problem. However, as stated in ref. 3, the extension of these techniques to the 3-D slewing problem has encountered a numerical problem: rank deficiency.

In refs. 5, 10, and 11, the quasilinearization method has been successfully used. In this method, one needs to linearize the differential equations (39),

$$\dot{z} = g(z), \quad \text{where } z^T = [x^T, \lambda^T], \quad g^T = [f_1^T, f_2^T] \quad (43)$$

about an approximate solution of this equation in the following form (a series of linearized, time-variant, nonhomogeneous equations):

$$\dot{z}^{(k+1)} = (\partial g / \partial z) z^{(k+1)} + h(z^{(k)}) \quad (44)$$

where  $z^{(k)}$  is the  $k$ th solution of the same linearized equation. It is also the  $k$ th approximate solution of the original nonlinear equations (43). Here, the boundary conditions, (40), are naturally adopted as the boundary conditions of the linearized equations, (44). The control expressions, (37), also need to be linearized (ref. 8):

$$u^{(k+1)} = u^{(k)} - R^{-1} [\bar{P}(\Delta\alpha)]^T \lambda^{(k)} - R^{-1} [E + \bar{P}(\alpha^{(k)})]^T \Delta\lambda \quad (45)$$

where  $\Delta\alpha = \alpha^{(k+1)} - \alpha^{(k)}$ , and  $\Delta\lambda = \lambda^{(k+1)} - \lambda^{(k)}$ . By assuming that

$$u^{(k)} = -R^{-1}[E + \bar{P}(\alpha^{(k)})]^T \lambda^{(k)} \quad (46)$$

for the unbounded control case, equation (45) can be rewritten as,

$$u^{(k+1)} = -R^{-1}[\bar{P}(\Delta\alpha)]^T \lambda^{(k)} - R^{-1}[E + \bar{P}(\alpha^{(k)})]^T \lambda^{(k+1)} \quad (47)$$

However, in the bounded control case, equations (38) are considered, that is,

$$u_i^{(k)} = \begin{cases} -u_{ib} \text{ or } u_{ib} \\ -\{R^{-1}[E + \bar{P}(\alpha^{(k)})]^T \lambda^{(k)}\}_i \end{cases} \quad (48)$$

Accordingly, at the (k+1)st step,  $u^{(k+1)}$  can be determined by

$$u_i^{(k+1)} = \begin{cases} -u_{ib} \text{ or } u_{ib}, & \text{if } |\{R^{-1}[E + \bar{P}(\alpha^{(k)})]^T \lambda^{(k)}\}_i| \geq u_{ib} \\ -\{R^{-1}[\bar{P}(\Delta\alpha)]^T \lambda^{(k)} - R^{-1}[E + \bar{P}(\alpha^{(k)})]^T \lambda^{(k+1)}\}_i \end{cases} \quad (49)$$

So far, an iteration process is formed. In each iteration, only a linear TPBVP is solved. It is this property that gives this approach the name quasilinearization method.

The linear TPBVP can be solved by many ready-made methods. One of the frequently used algorithms is the method of particular solutions (ref. 9). Let  $m$  represent the number of the states (also the costates). Equations (44) can also be rewritten in the following form,

$$\dot{x}(t) = G(t)x(t) + H(t)\lambda(t), \quad \dot{\lambda}(t) = I(t)x(t) + J(t)\lambda(t) \quad (50a, b)$$

From the theorem of the linear system, any solution equation (50a) can be expressed as the linear combination of its  $m+1$  particular solutions, i.e.,

$$x(t) = \sum_{i=1}^{m+1} c_i x^i(t), \quad \text{as long as } \sum_{i=1}^{m+1} c_i = 1 \quad (51)$$

where  $c_i$  are constants and  $x^i(t)$  are the  $i$ th particular solution vectors. The

method begins by integrating equations (50a, b) forward  $m+1$  times, with the initial conditions,

$$z^1(0) = \begin{bmatrix} x(0) \\ 1 \\ 0 \\ 0 \\ \vdots \\ 0 \end{bmatrix}, \quad z^2(0) = \begin{bmatrix} x(0) \\ 0 \\ 1 \\ 0 \\ \vdots \\ 0 \end{bmatrix}, \quad \dots, \quad z^m(0) = \begin{bmatrix} x(0) \\ 0 \\ 0 \\ \vdots \\ 0 \\ 1 \end{bmatrix}, \quad \text{and} \quad z^{m+1}(0) = \begin{bmatrix} x(0) \\ 0 \\ 0 \\ 0 \\ \vdots \\ 0 \end{bmatrix}.$$

This gives us  $m+1$  particular solutions,  $x^1(t)$ ,  $x^2(t)$ ,  $\dots$ ,  $x^{m+1}(t)$ . Substituting these solutions into equations (51), and setting  $t=t_f$ , we have

$$\sum_{i=1}^{m+1} c_i x^i(t_f) = x(t_f), \quad \sum_{i=1}^{m+1} c_i = 1 \quad (52)$$

This is a set of  $m+1$  algebra equations for  $m+1$  unknown constants,  $c_i$ . By assuming the existence of inverse of the coefficient matrix, we can obtain the solution,  $c = [c_1 \ c_2 \ \dots \ c_m]^T$  and  $c_{m+1}$ . By doing the following manipulation,

$$z(0) = \sum_{i=1}^{m+1} c_i z^i(0) = \begin{bmatrix} \sum_{i=1}^{m+1} c_i x^i(0) \\ c_1 \\ c_2 \\ \vdots \\ c_m \end{bmatrix} = \begin{bmatrix} x(0) \\ c_1 \\ c_2 \\ \vdots \\ c_m \end{bmatrix}$$

one immediately realizes that  $c = \lambda(0)$ , the missing initial costates.

#### 4.3 Transformation of Attitude States and Costates

The following procedure is designed to obtain the solution of the nonlinear TPBVP. First, the linear TPBVP based on equation (28) is solved and a nominal trajectory is produced, in which the control is unbounded and the initial costates are calculated by using the transition matrix method. Then, a converged solution for the linear TPBVP with bounded controls is obtained by iterations starting from the previously obtained trajectory. Note that the Euler angles are used in all the above computations.

Next, to obtain the starting solution for the nonlinear TPBVP, the 3 Euler angles and the 3 associated costates are transformed to the 4 quaternions and their 4 costates (from  $t=0$  to  $t=t_f$ ). Refs. 10-11 provides us the following relationship between the quaternions,  $q(t)$  and their costates,  $p(t)$ :

$$\begin{bmatrix} p_0 \\ p_1 \\ p_2 \\ p_3 \end{bmatrix} = \begin{bmatrix} d_0 & -d_1 & -d_2 & -d_3 \\ d_1 & d_0 & -d_3 & d_2 \\ d_2 & d_3 & d_0 & -d_1 \\ d_3 & -d_2 & d_1 & d_0 \end{bmatrix} \begin{bmatrix} q_0 \\ q_1 \\ q_2 \\ q_3 \end{bmatrix} \quad (53)$$

where  $d_i$  are constants. For the case  $q(0)=[1 \ 0 \ 0 \ 0]^T$ , we can choose  $p_0(0)=0$ ,  $d_0=0$ . Then,

$$[p_1(0) \ p_2(0) \ p_3(0)] = [d_1 \ d_2 \ d_3] = d^T \quad (54)$$

The vector  $d$  can be determined by

$$d = 2 [\text{initial Euler angle costate vector}] \quad (55)$$

This result can be proved if one compares the related state and costate equations for both linear and nonlinear TPBVPs (for the case  $\omega(0)=0$ ). After finding the  $q(t)$  by using a nonsingular transformation between  $q(t)$  and the Euler angles,  $\theta_1(t)$ ,  $\theta_2(t)$ , and  $\theta_3(t)$ , one can use equations (53-55) to obtain  $p(t)$ .

Finally, the nonlinear TPBVP is solved through the quasilinearization process and the method of particular solutions [9].

## 5. NUMERICAL RESULTS

The following parameters of the orbiting SCOLE are used in this paper [6]. The inertia matrices of the Shuttle and the reflector, about the mass center,  $o_s$  and  $o_r$ , respectively, are (slug-ft<sup>2</sup>):

$$\begin{bmatrix} 905443 & 0 & 145393 \\ 0 & 6789100 & 0 \\ 145393 & 0 & 7086601 \end{bmatrix}, \quad \begin{bmatrix} 4881.375 & 0 & 0 \\ 0 & 4969.594 & 0 \\ 0 & 0 & 9921.969 \end{bmatrix}$$

The material properties of the mast are:  $EI=GI_p=4E+7$  lb-ft<sup>2</sup>,  $\rho A=0.09554$  slug/ft,  $\rho I_p=.9089$  slug-ft, and  $L=130$  ft. The masses of the Shuttle, the mast, and the reflector are (slug): 6366.46, 12.42, and 12.42, respectively. The location of the mass center of the reflector is  $x_r=18.75$  ft, and  $y_r=32.5$  ft. The control saturation levels are:  $|f_{1x}|=|f_{1y}|=|f_{1z}| \leq 1E+4$  ft-lb,  $|f_{2x}|=|f_{2y}|=|f_{3x}|=|f_{3y}| \leq 10$  lb,  $|f_{4x}|=|f_{4y}| \leq 800$  lb. The first five natural frequencies are (hz): .2740493, .3229025, .7487723, 1.244013, 2.051804.

The numerical tests based on the previously described method have been performed for the roll-axis slews, pitch-axis slews, as well as arbitrary-axis slews. All these tests are rest-to-rest slews and the iteration process is terminated after the initial costates are reached within five digit accuracy.

The following procedure is designed to obtain the solution of the nonlinear TPBVP. First, the linear TPBVP based on Equation (28) is solved and a nominal trajectory is produced, in which the control is unbounded and the initial costates are calculated by using the transition matrix method. Then, a converged solution for the linear TPBVP with bounded controls is obtained by iterations starting from the previously obtained trajectory. Note that the Euler angles are used in all above computations. Next, the Euler angles and the associated costates are transformed to the quaternions and their costates [10, 11], to obtain the starting solution for the nonlinear TPBVP. Finally, the nonlinear TPBVP is solved through the quasilinearization process and the method of particular solutions.

Case 1 is a 90 deg slew about the roll(x) axis with only three torques on the Shuttle as the control, i.e.,  $u=[f_{1x} \ f_{1y} \ f_{1z}]^T$ . The weightings for the state,  $Q_1$ ,  $Q_2$ , and  $Q_3$  are chosen to be zero matrices, with the consideration that a non-zero choice will improve the responses [5]. The control weighting is selected as  $R=\text{Diag}[1E-6, 1E-6, 1E-6]^T$ , since the small values here imply the small costates (which is advantageous for the numerical convergence) for the same control (see Equation (37)). The slewing time,  $t_f=28$  sec, makes the slew near the minimum-time-slew as used in [5] for the planar SCOPE configuration.

The results for this slew are shown in Figs. 3, in which the solid lines represent the responses of the linearized system (27), while the dotted lines stand for those of the nonlinear system. The three attitude angles are plotted in Figs. 3a-c. The roll angle,  $\theta_1$ , for both systems is almost the same, but the pitch (y) and yaw (z) angles are different although the magnitudes are quite small. Associated with these differences are the differences in the controls  $f_{1y}$  and  $f_{1z}$ , shown in Figs. 3j-k. The roll-axis torque,  $f_{1x}$ , (Fig. 3i) is near the bang-bang type. There are little differences in the first three modal amplitudes (Figs. 3d-f) between the two systems, but the 4th and the 5th modal amplitudes (Figs. 3g-h) present larger relative differences. Since the second mode describes mainly the deformation of the mast in the y-z plane, which is perpendicular to the slew (x) axis, the second modal amplitude has the largest peak value among all the five modes.

Case 2 is a 90 deg slew about the x axis, but using all 9 controls.  $Q_1 = 0$ ,  $i=1,2,3$ , and  $R = \text{Diag}[1E-6, 1E-6, 1E-6, 8E-2, 2E-2, 9E-2, 4E-2, 8E-4, 3E-4]^T$ . Due to the increase in the control effort, the slewing time can be shortened.  $t_f = 12$  sec is selected numerically by the judgment that the maximum displacement of the mast at the reflector end is less than 10% of its total length, to be consistent with the small deformation assumption. To make a comparison, the slewing results for the rigid spacecraft model (Equation (27)) are also obtained by using the same  $Q_1$ 's and R. Figs. 4 give the results for the present slew, where the dashed lines represent the time histories of the rigid nonlinear system.

The three systems have less differences in  $\theta_1$  (Fig. 4a).  $\theta_2$  and  $\theta_3$  (Figs. 4b-c) are still very small, but the peak values are several times larger than those in Figs. 3b-c. The differences between the flexible and rigid nonlinear systems are small, but the differences between the flexible nonlinear and the flexible linear systems are relatively large. The reason is that the quadratic terms of the angular velocity of the Shuttle,  $\bar{\omega}$ , (Equation (25)), have been used both in the rigid and flexible nonlinear systems, but do not appear in the flexible linearized system. Therefore, these quadratic terms play an important role the 3-D large-angle rapid slewing problems. The similar differences in the three systems are also reflected in the control histories (Figs. 4i-p). The small differences between the flexible and rigid nonlinear systems are caused by the deformation of the flexible mast. For the rapid

slews with large control torques and forces, the deformation will further increase, and so will the differences between these two systems.

The five modal responses are quite different from those in Case 1. Some of the peak values increase about 30 times, and the response phases change. For example, before  $t=t_f/2$ ,  $\alpha_2$  is mostly positive in Case 1, but negative in Case 2, and this change reverses after  $t=t_f/2$ . This change is caused by the controls at the reflector [5].

In the present slew,  $\theta_1$  is the main attitude angle and mode 2 has the largest deformation in the  $y$ - $z$  plane among all the five modes (Figs. 4d-h). Within Figs. 4, after comparing the responses of the linearized system with those of the nonlinear systems, we see that there are less relative differences in  $\theta_1$  and  $\alpha_2$  than in  $\theta_2$  ( $\theta_3$ ) and other modes. These results imply, for the slew considered here, the major modes (rigid  $\theta_1$  and flexible  $\alpha_2$ ) have the largest overall displacements but the smallest relative differences between the linear and nonlinear systems. On the other hand, the secondary modes ( $\theta_2$ ,  $\theta_3$ ,  $\alpha_1$ ,  $\alpha_3$ ,  $\alpha_4$ ,  $\alpha_5$ ) have smaller overall displacements but larger relative differences. As a consequence, the major controls ( $f_{4y}$ ) (Figs. 4q) and all the remaining secondary controls (Figs. 4i-p), as well as the major deformation  $V(z,t)$  and secondary deformations  $U(z,t)$  and  $\phi(z,t)$  (Figs. 4r-t) also yield the same results. These results may lead to the following conclusion: the linearized equations can represent very well the nonlinear equations for the major slewing motion even for large displacements, but not so well for the secondary motions, even for small displacements. The explanation for this fact might be that the magnitudes of the nonlinear terms have a certain level which is less than that of the linear terms representative of the major motions, but is great enough to compete with that of the linear terms for the secondary motions.

It should be mentioned that these facts can not be observed in the planar slewing problems studied by many authors (for example, Refs. 1, 2, and 5). In those researches, the differences between the linearized system and the nonlinear system are very small because all the modes are planar modes and, hence, the first several modes are all major modes.

Case 3 Figs. 5 show the results for a simultaneous three-axis slew ( $\theta_1=60$ ,  $\theta_2=30$ ,  $\theta_3=45$  deg). The weightings for the states are  $Q_1=Q_2=Q_3=0$ . In this case, The Shuttle torques ( $f_{1x}$ ,  $f_{1y}$ , and  $f_{1z}$ ) and the reflector forces ( $f_{4x}$ , and  $f_{4y}$ ) are used. The associated weighting for the control is  $R=DIAG(1E-4, 1E-4, 1E-4, 0.6, 1.4-3)$ . The slewing time,  $t_f$ , is 40 sec. The solid lines in the figures 5a-h responses of the rigidized nonlinear system, equation (27), while the dotted lines represent the slew results for the flexible nonlinear system.

## 6. CONCLUSIONS

The application of Pontryagin's Maximum Principle to the large angle slewing maneuver problem has been extended to the slewing of a 3-D flexible spacecraft (SCOLE). A numerical simulation procedure based on the quasilinearization algorithm for solving the resulting nonlinear TPBVP has been established and tested successfully for several examples. The general nonlinear dynamical equations developed here contain all the quadratic terms of the angular velocity of the main body and their coupling with the first order modal amplitudes and modal rates. It is suggested that higher order terms be included if a further analysis is conducted. The numerical results show an important fact that the linearized system can represent the nonlinear system adequately for predicting the major motions but not as well for the secondary motions. The quadratic terms (nonlinear) of the angular velocity of the main body (Shuttle) cannot be neglected for large-angle rapid maneuvers. The differences between the responses of the rigid and flexible nonlinear systems are small because the deformation of the flexible part (mast) is small. For further research, it is recommended that the applicability of this method to more complicated systems be established.

## REFERENCES

1. J.D. Turner and J.L. Junkins, Optimal Large-Angle Single-Axis Rotational Maneuvers of Flexible Spacecraft. *Journal of Guidance and Control*, Vol. 3, No. 6, pp. 578-585, (1980).

2. J.D. Turner and H.M. Chun, Optimal Distributed Control of a Flexible Spacecraft During a Large-Angle Maneuver. *Journal of Guidance, Control, and Dynamics*, Vol. 7, No. 3, pp. 257-264, (1984).
3. H.M. Chun, J.D. Turner, and J.-N. Juang, Frequency-Shaped Large-Angle Maneuvers. *Journal of the Astronautical Sciences*, Vol. 36, No. 3, pp. 219-234, (1988).
4. L. Meirovitch and R.D. Quinn, Maneuvering and Vibration Control of Flexible Spacecraft. *Journal of the Astronautical Sciences*, Vol. 35, No. 3, pp. 301-328, (1987).
5. P.M. Bainum and F. Li, Rapid In-Plane Maneuvering of the Flexible Orbiting SCOLE. *AAS/AIAA Astrodynamics Specialist Conference*, Stowe, Vermont, Aug. 7-10, (1989), AAS Paper 89-422. To appear in *J. of the Astronautical Sciences*, (1990).
6. L.W. Taylor and A.V. Balakrishnan, A Mathematical Problem and a Spacecraft Control Laboratory Experiment (SCOLE) Used to Evaluate Control Laws for Flexible Spacecraft ... NASA/IEEE Design Challenge. *Proc. of the Fourth VPI&SU Symposium on Dynamics and Control of Large Structures*, Blacksburg, VA, June 1983. Revised Jan. (1984).
7. D.K. Robertson, Three-Dimensional Vibration Analysis of a Uniform Beam with Offset Inertial Masses at the Ends. *NASA Technical Memorandum 86393*, Sept. (1985).
8. B.P. Yeo, K.J. Waldron, and B.S. Goh, Optimal Initial Choice of Multipliers in the Quasilinearization Method for Optimal Control Problems with Bounded Controls. *Int. Journal of Control*, Vol. 20, No. 1, pp. 17-33, (1974).
9. A. Miele and R.R. Iyer, General Technique for Solving Nonlinear Two-Point Boundary-Value Problems via the Method of Particular Solutions. *Journal of Optimization Theory and Applications*, Vol. 5, No. 5, pp. 382-399, (1970).
10. F. Li and P.M. Bainum, Minimum Time Attitude Maneuvers of a Rigid Spacecraft. *AIAA 26th Aerospace Sciences Meeting*, Reno, Nevada, Jan. 11-14, (1988). Paper No. 88-0675.
11. F. Li and P.M. Bainum, Numerical Approach for Solving Rigid Spacecraft Minimum Time Attitude Maneuvers. *Journal of Guidance, Control, and Dynamics*, Vol. 13, No. 1, pp. 38-45, (1990).

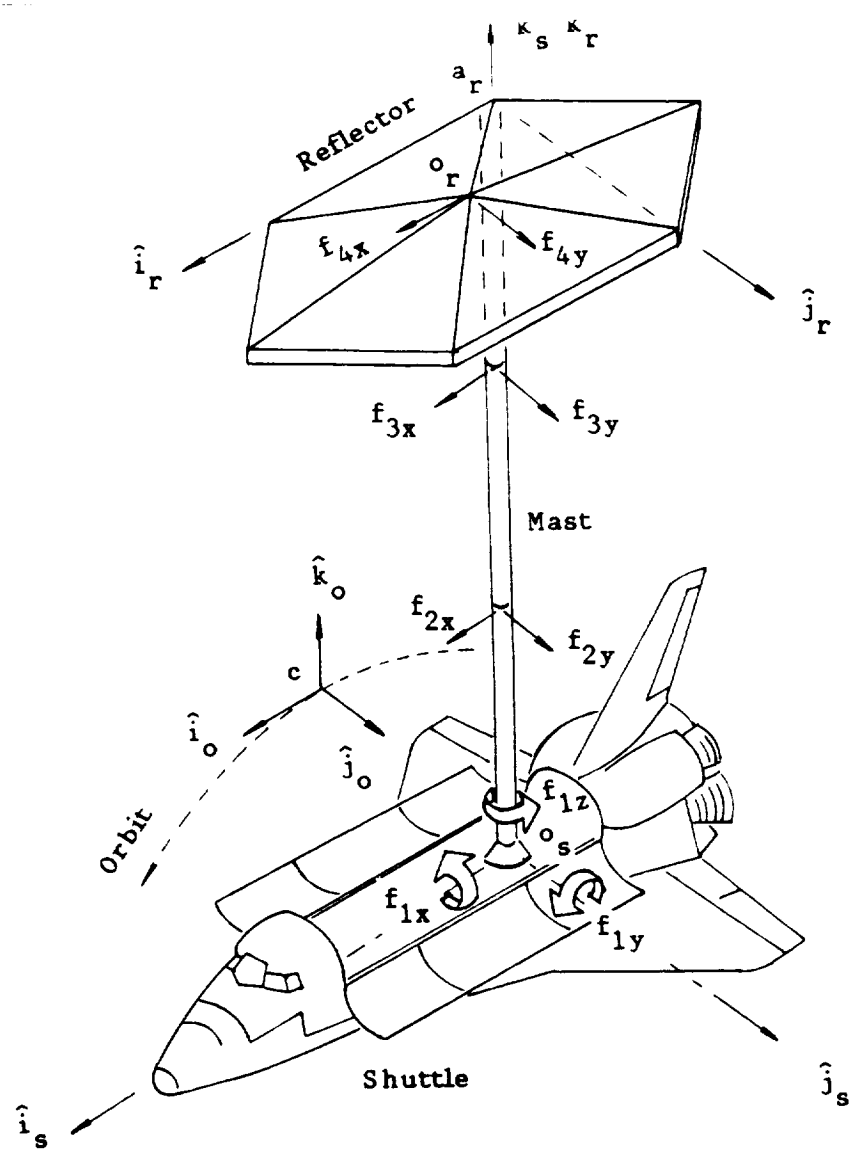


Figure 1. Drawing of the orbiting SCOLE configuration.

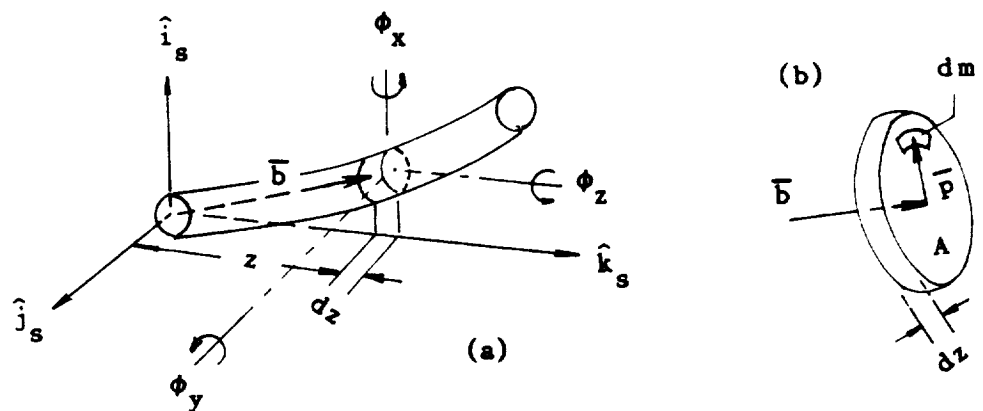


Figure 2. (a) Deformation of the mast, (b) An element in the mast.

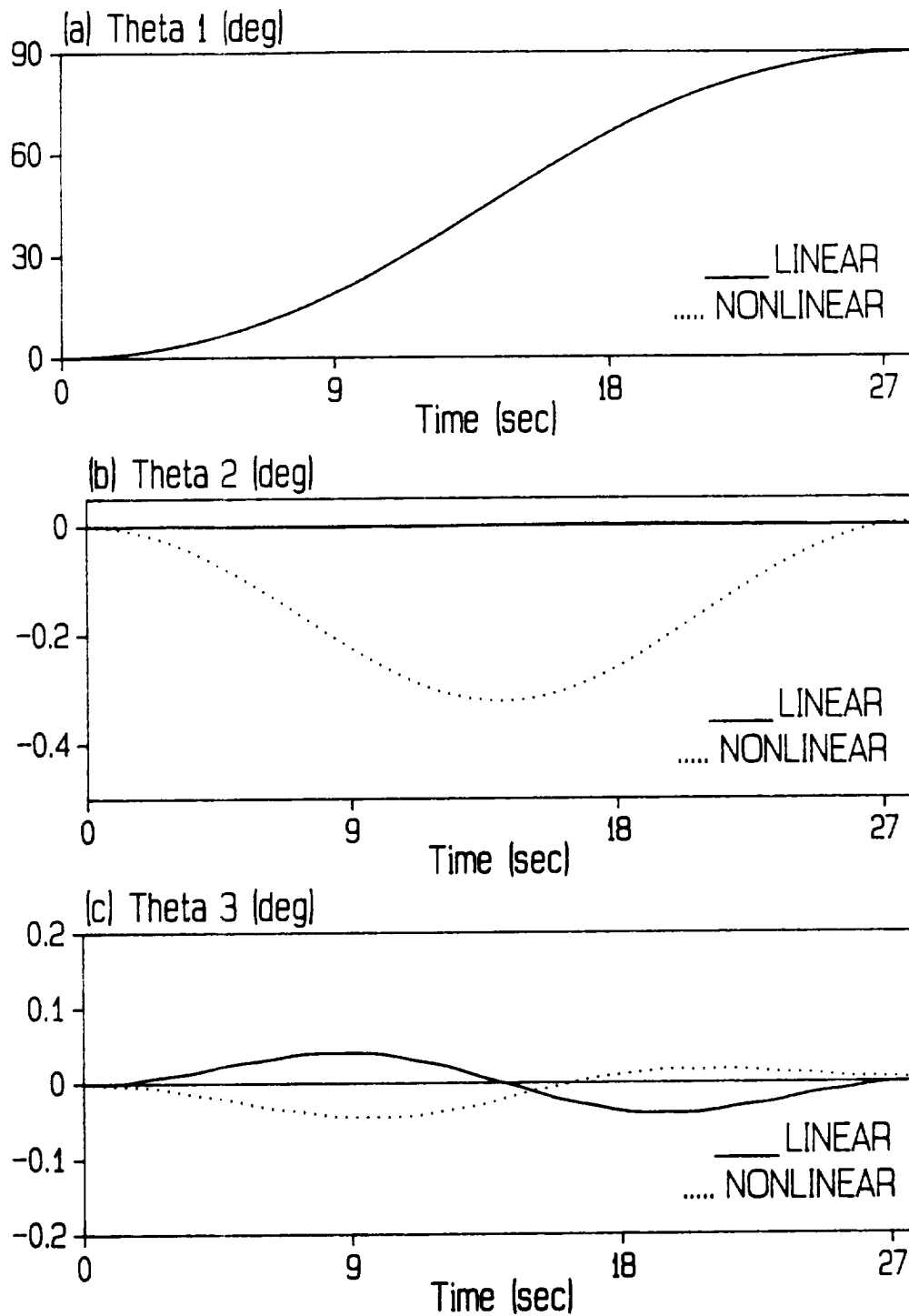


Fig. 3. Case 1, 90 degree roll axis slew, Shuttle torques only.

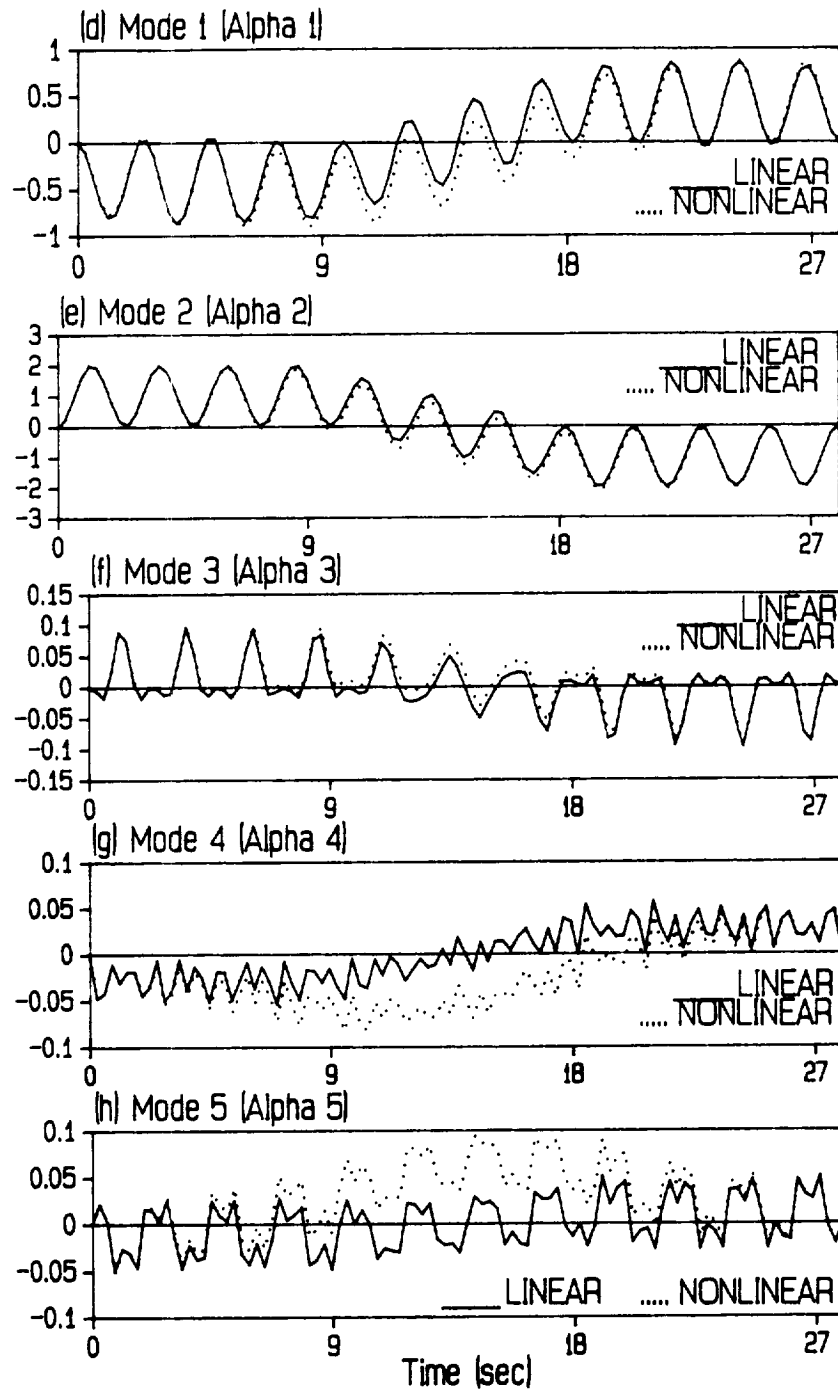


Fig. 3. (continued) Case 1, 90 degree roll axis slew, Shuttle torques only.

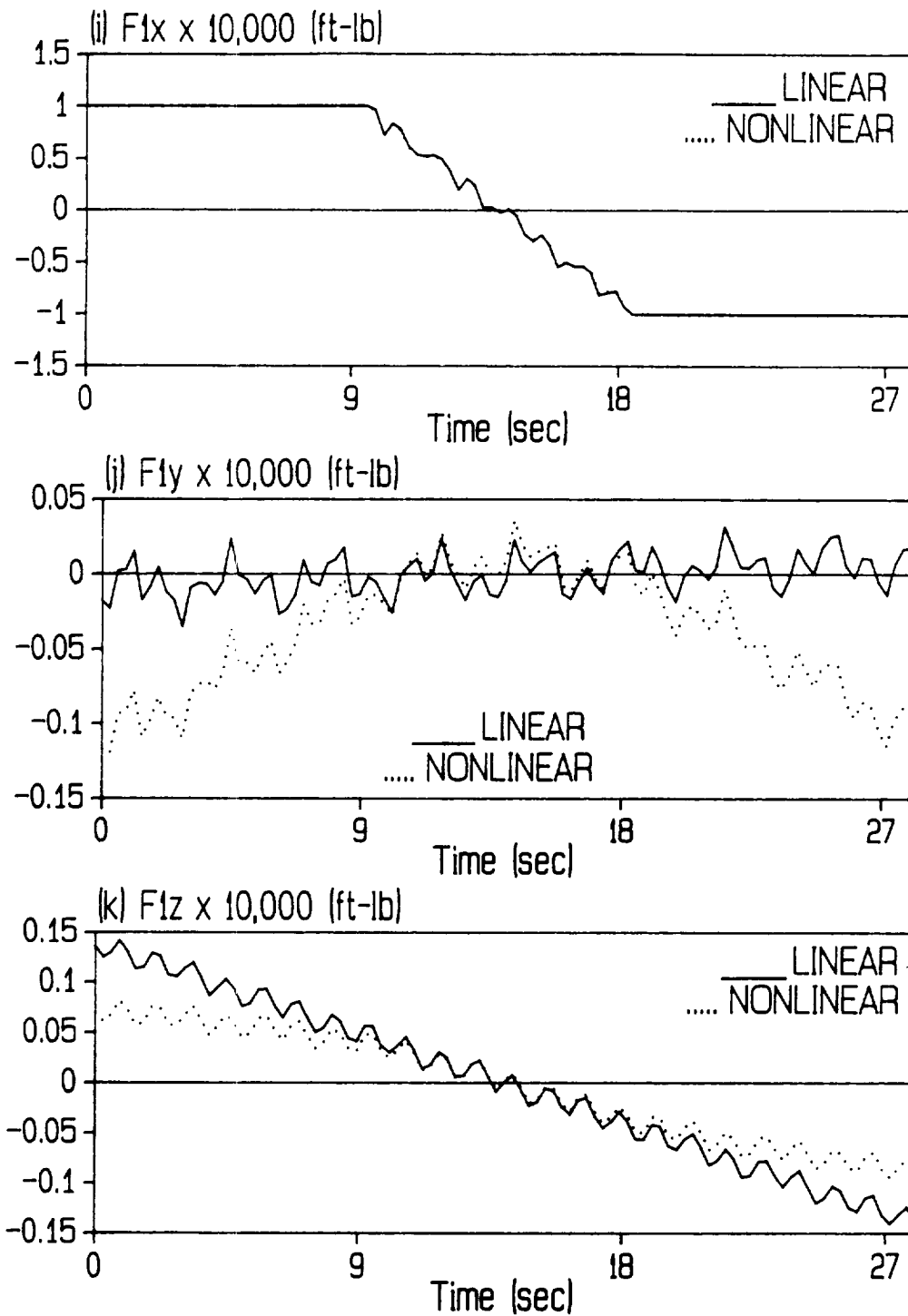


Fig. 3. (continued) Case 1, 90 degree roll axis slew, Shuttle torques only.

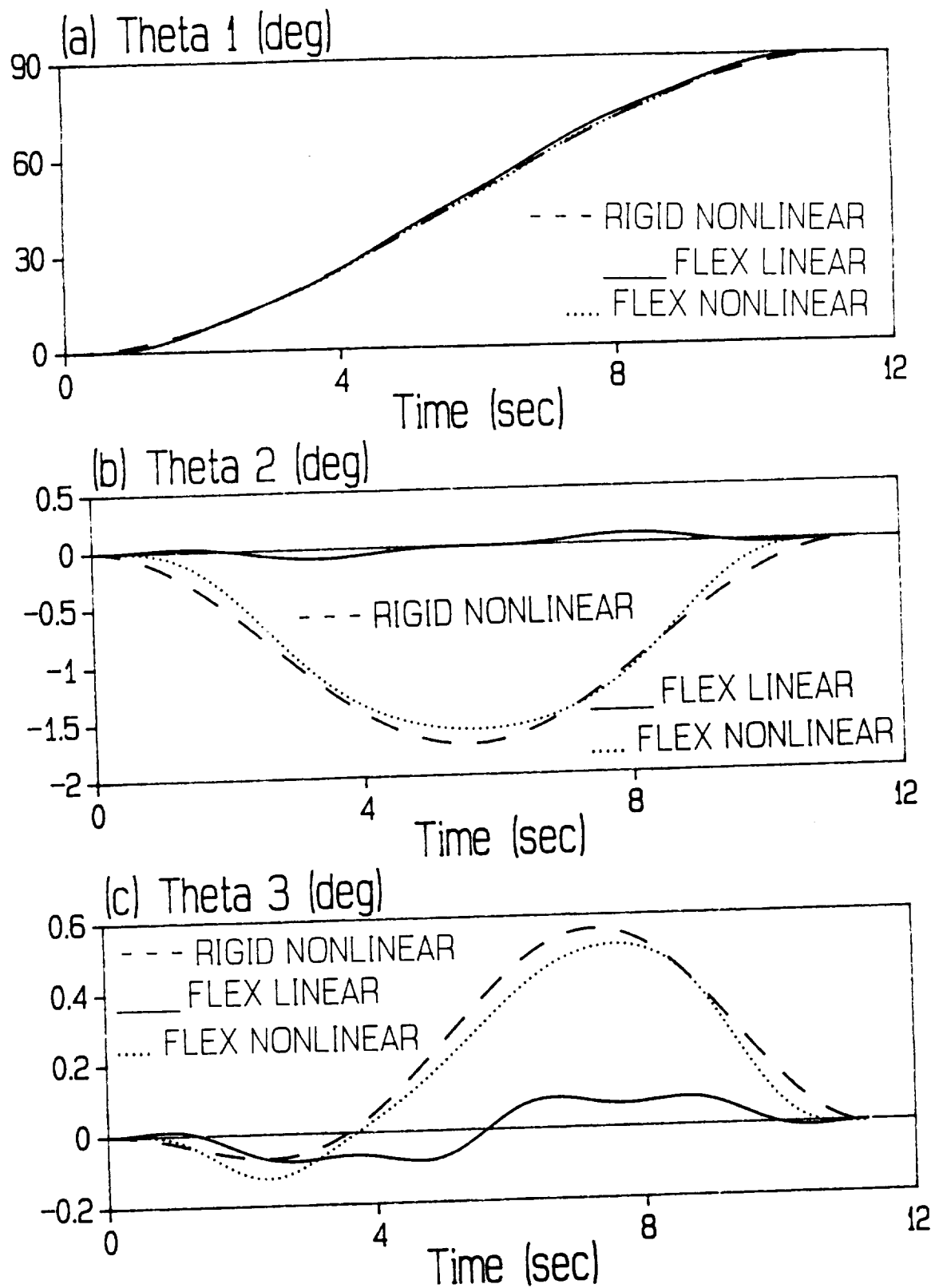


Fig. 4. Case 2, 90 degree roll axis slew, all controls.

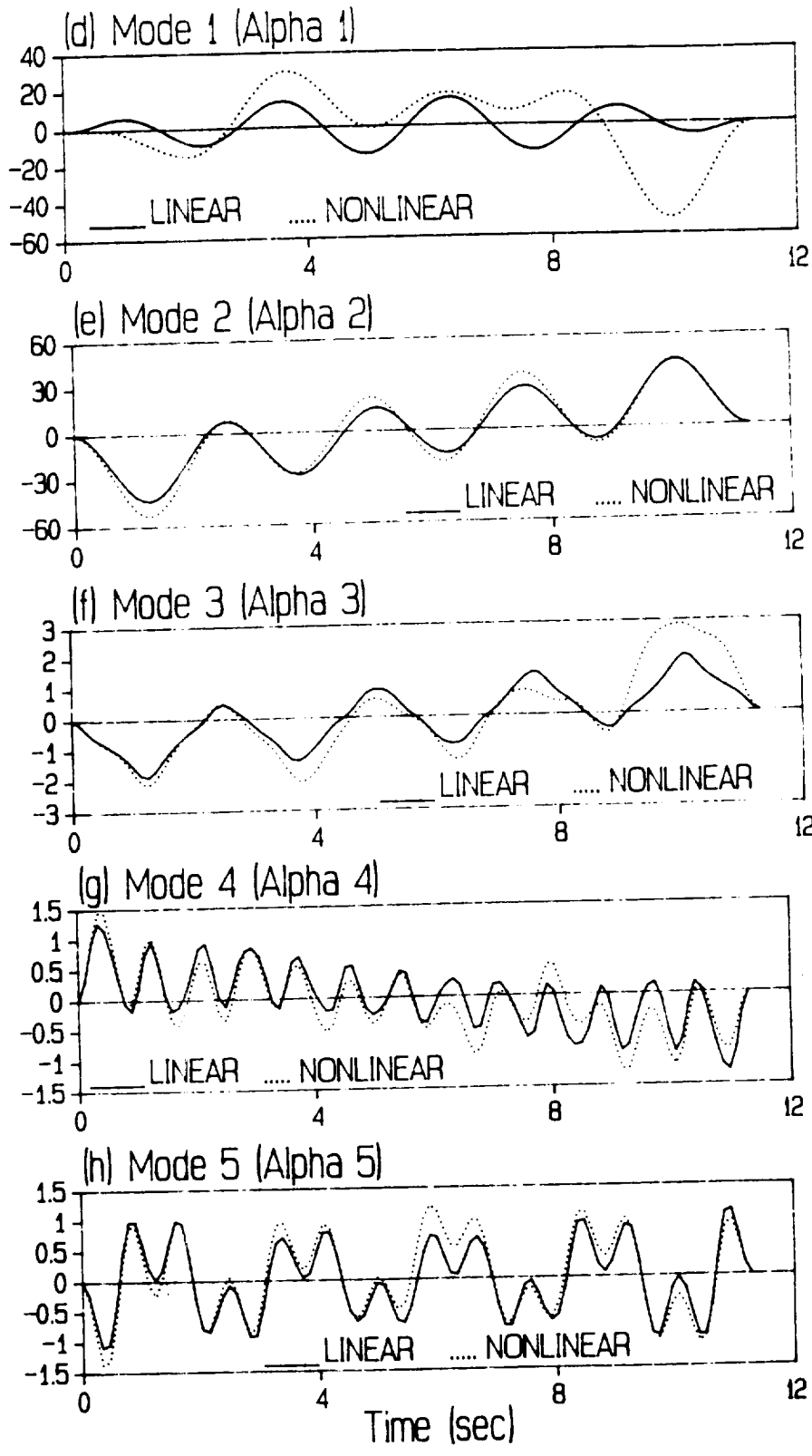


Fig. 4. (continued) Case 2, 90 degree roll axis slew, all controls.

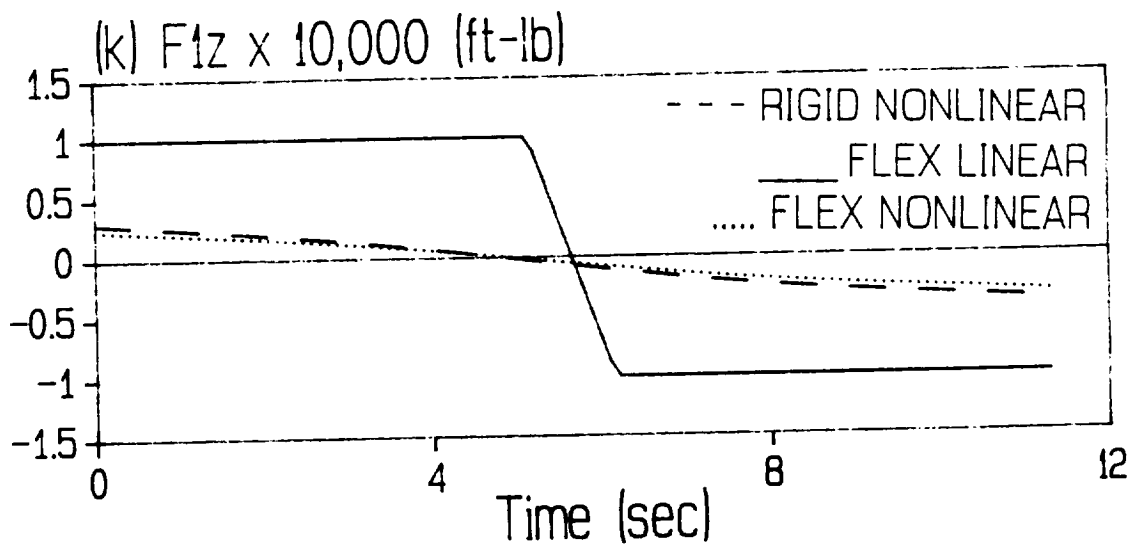
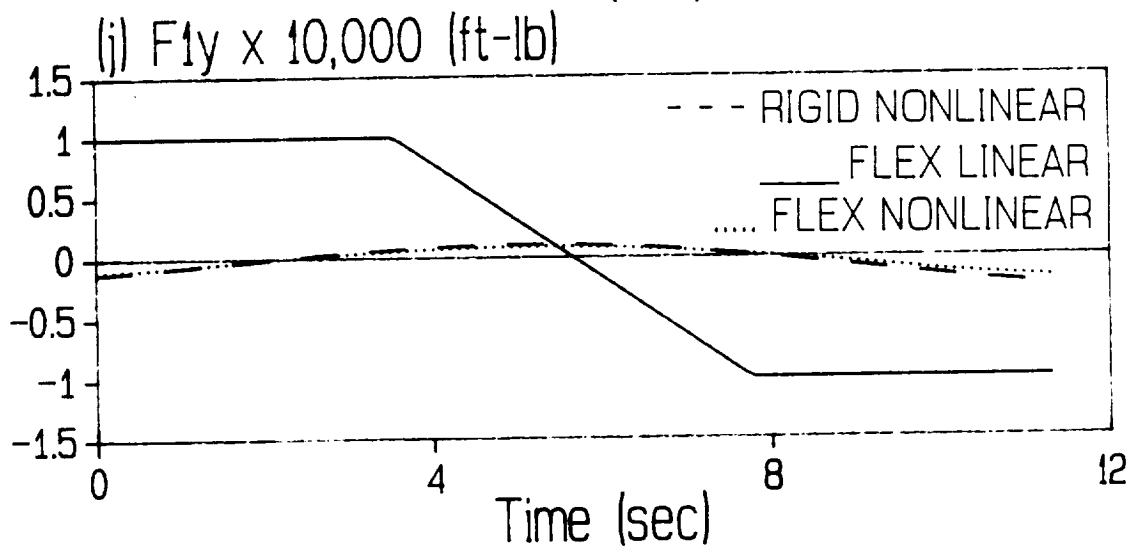
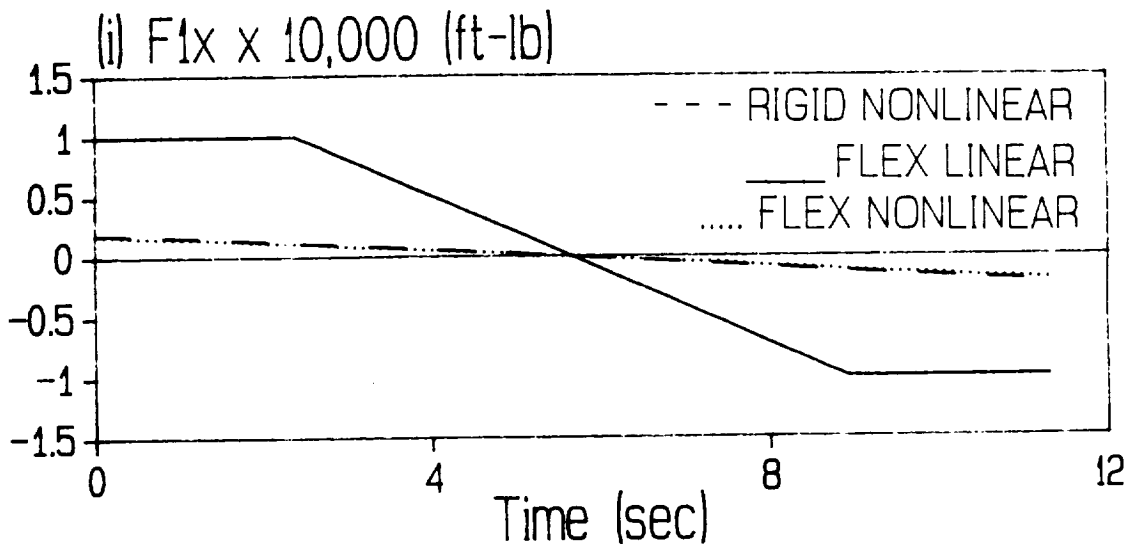


Fig. 4. (continued) Case 2, 90 degree roll axis slew, all controls.

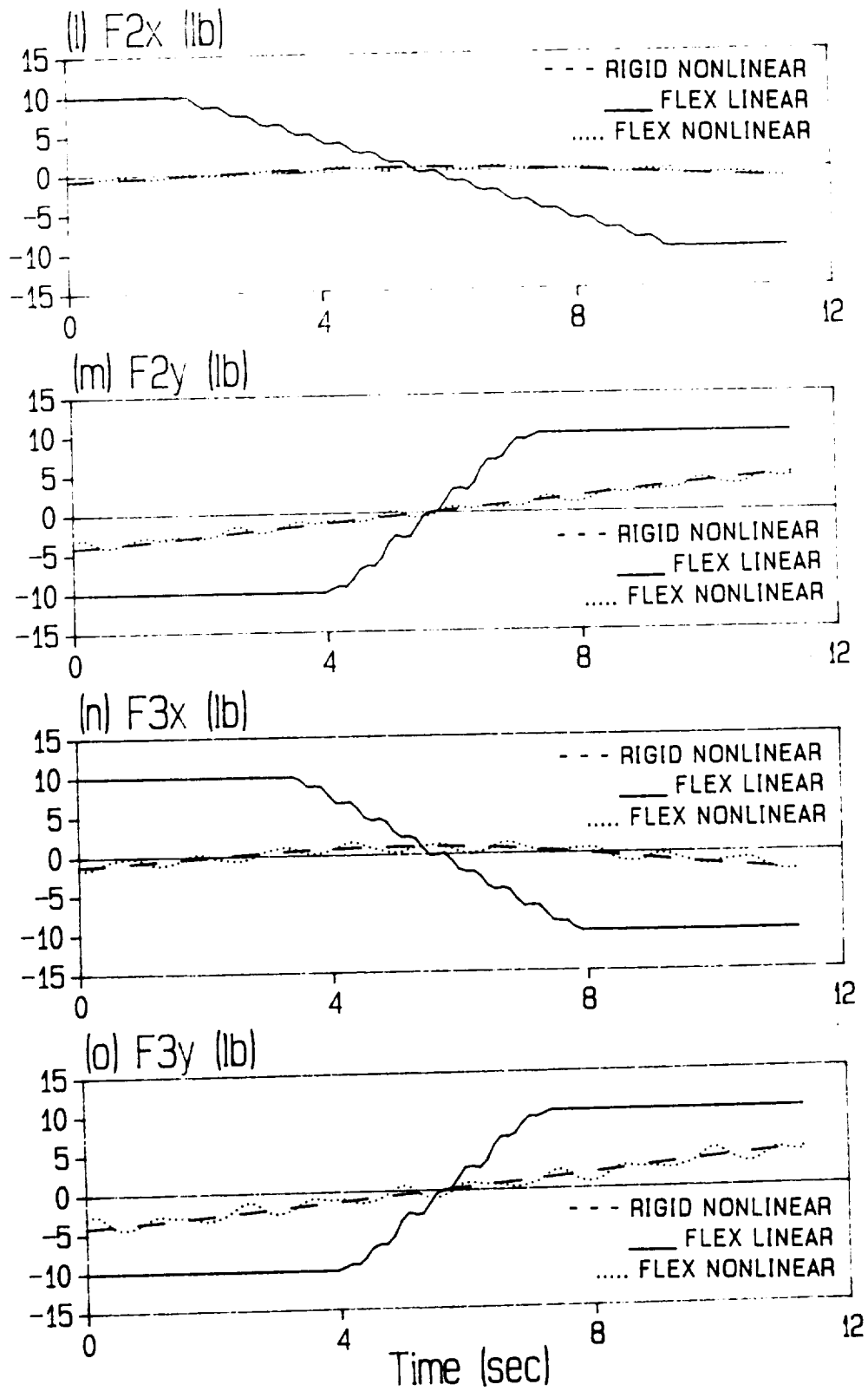


Fig. 4. (continued) Case 2, 90 degree roll axis slew, all controls.

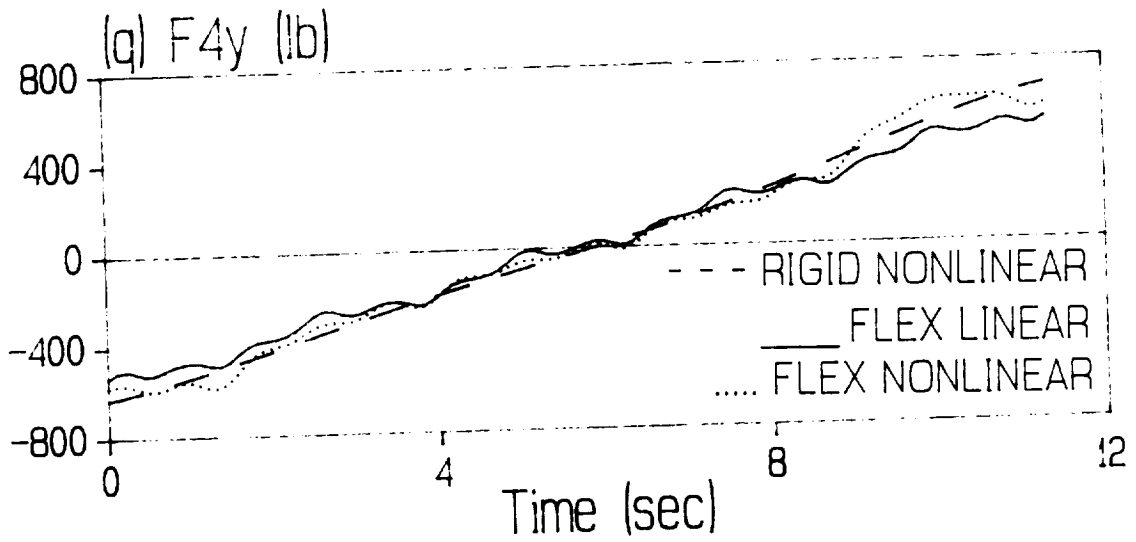
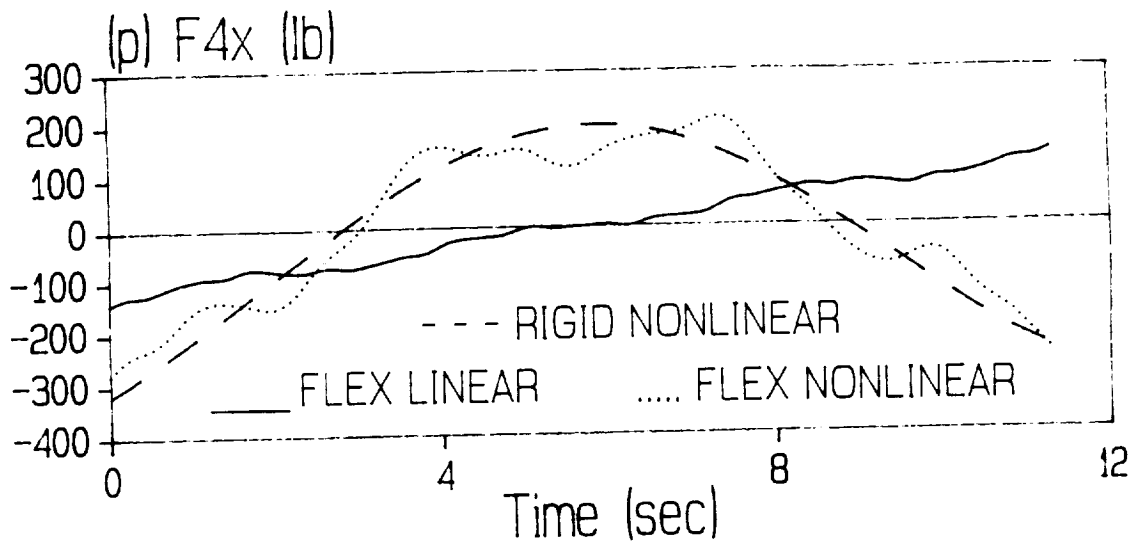


Fig. 4. (continued) Case 2, 90 degree roll axis slew, all controls.

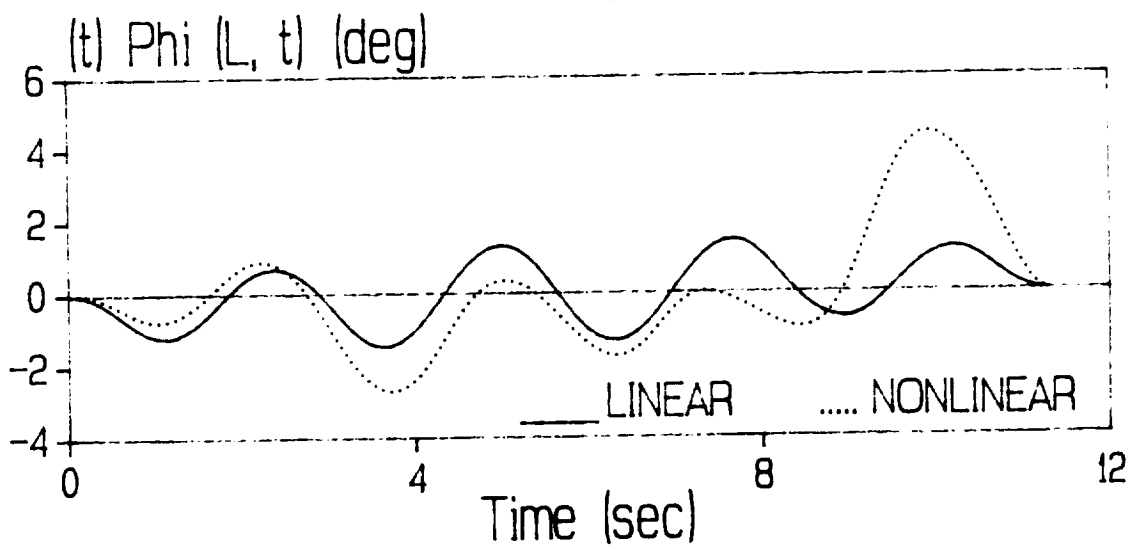
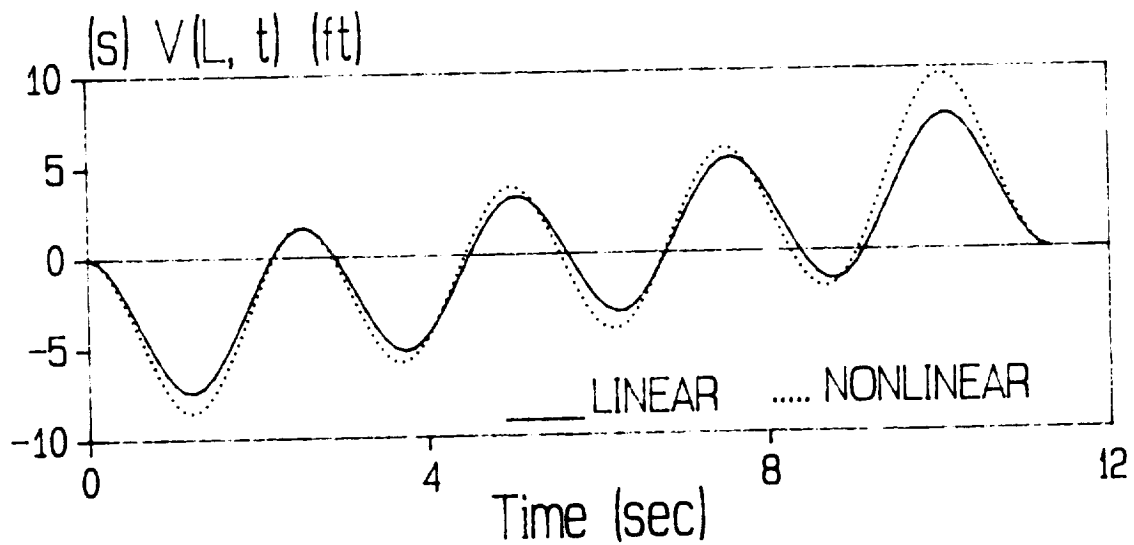
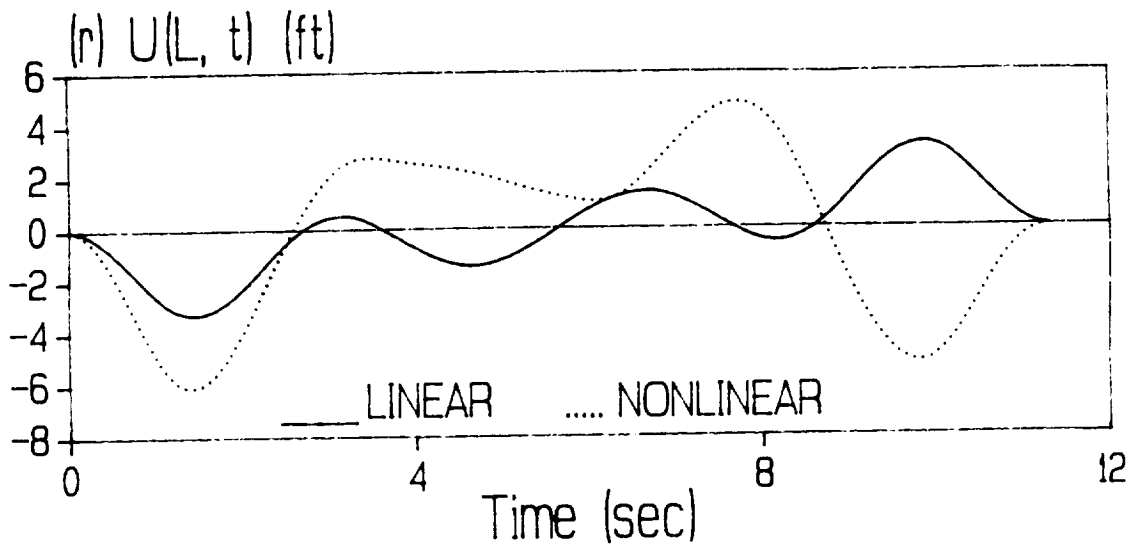


Fig. 4. (continued) Case 2, 90 degree roll axis slew, all controls.

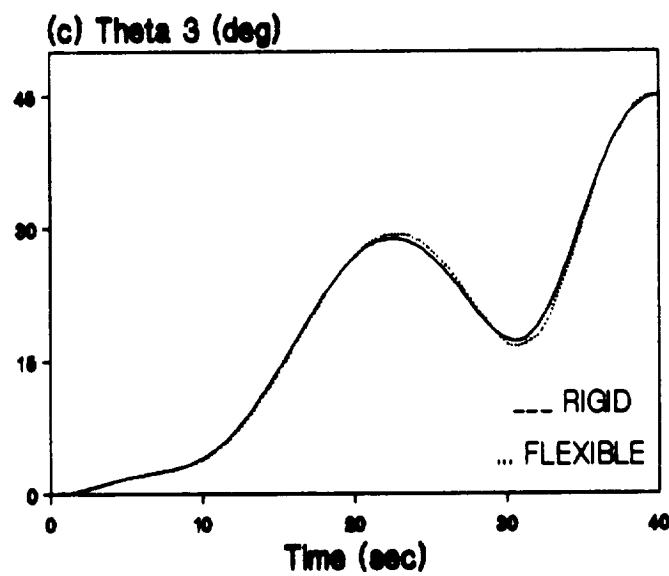
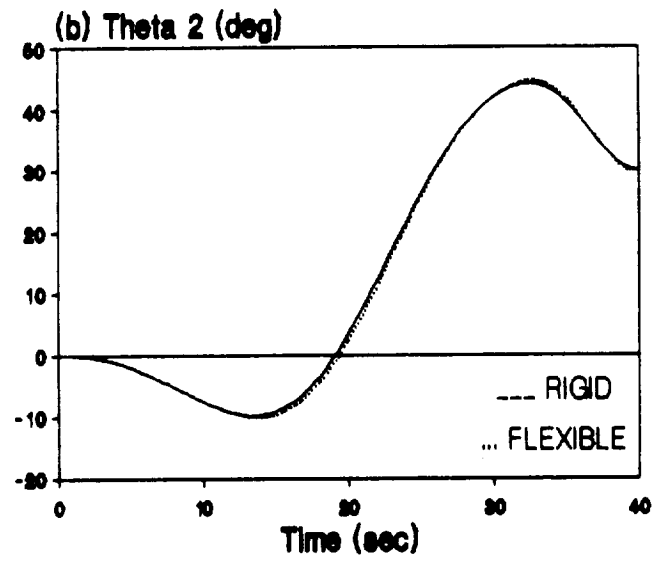
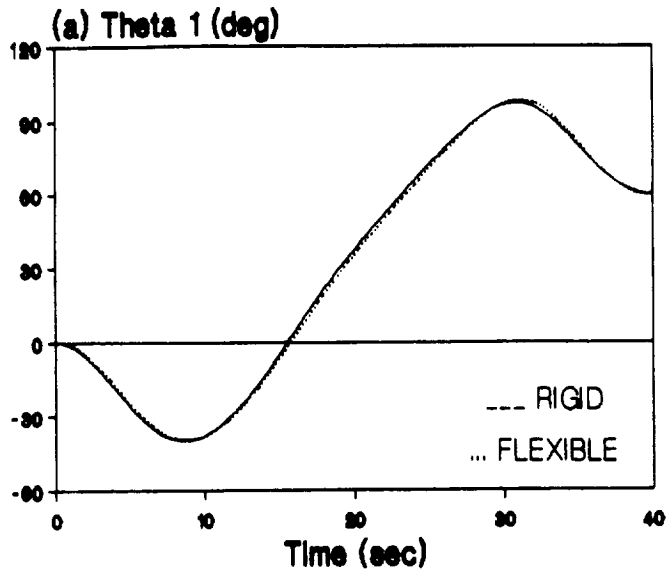


Fig. 5. Results for the 3-D slew, Case 3: 60-30-45 deg-Slew, Shuttle Torques + Reflector Forces,  $R = \text{Diag}(1E-4, 1E-4, 1E-4, 0.6, 1.4E-3)$ .

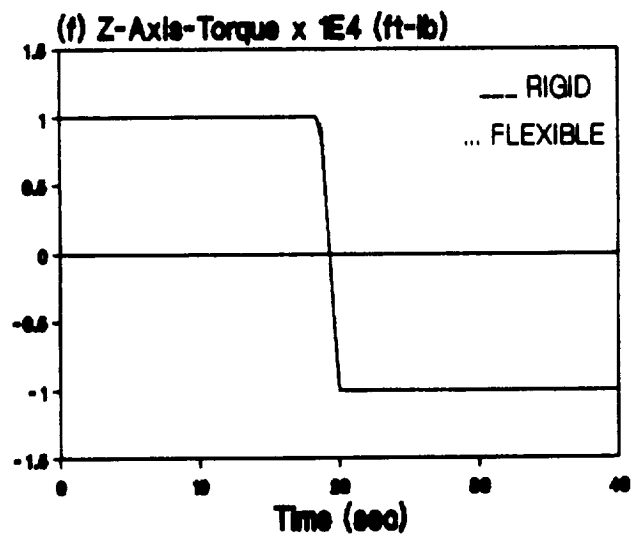
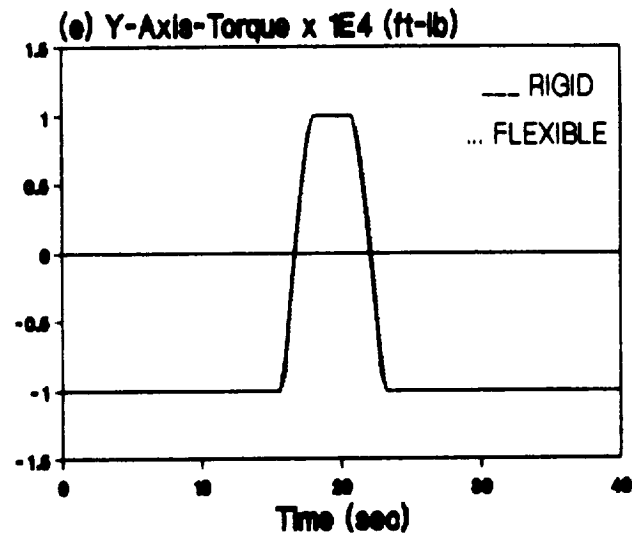
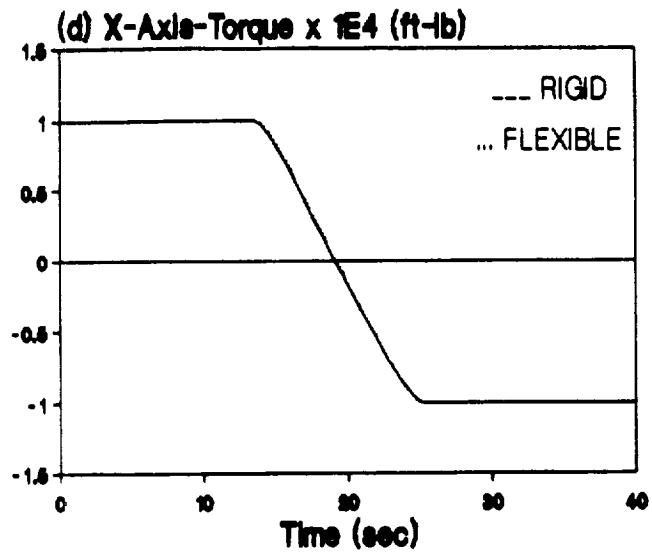
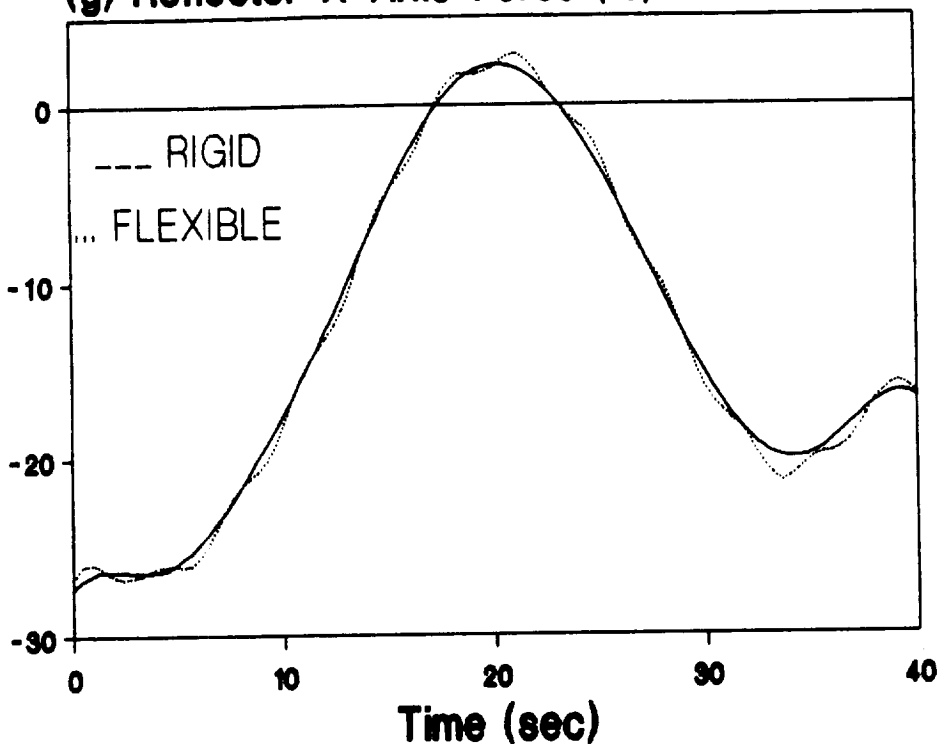
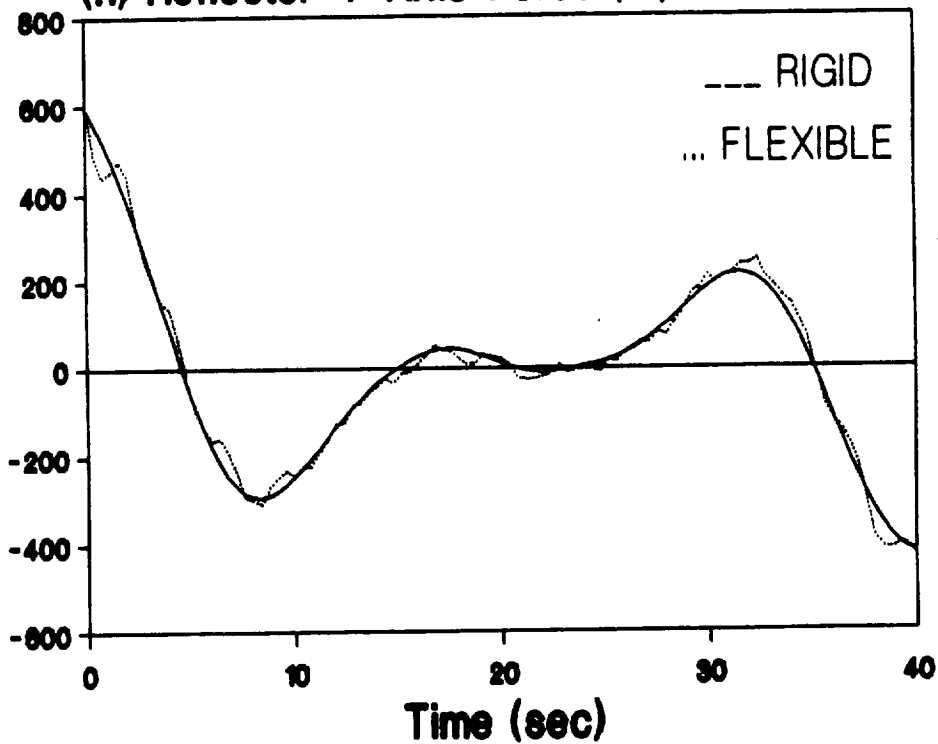


Fig. 5. Results for the 3-D slew, Case 3: 60-30-45 deg-Slew, Shuttle Torques + Reflector Forces,  $R = \text{Diag}(1E-4, 1E-4, 1E-4, 0.6, 1.4E-3)$ .

**(g) Reflector-X-Axis-Force (lb)**



**(h) Reflector-Y-Axis-Force (lb)**



**Fig. 5. Results for the 3-D slew, Case 3: 60-30-45 deg-Slew, Shuttle Torques + Reflector Forces,  $R = \text{Diag}(1E-4, 1E-4, 1E-4, 0.6, 1.4E-3)$ .**

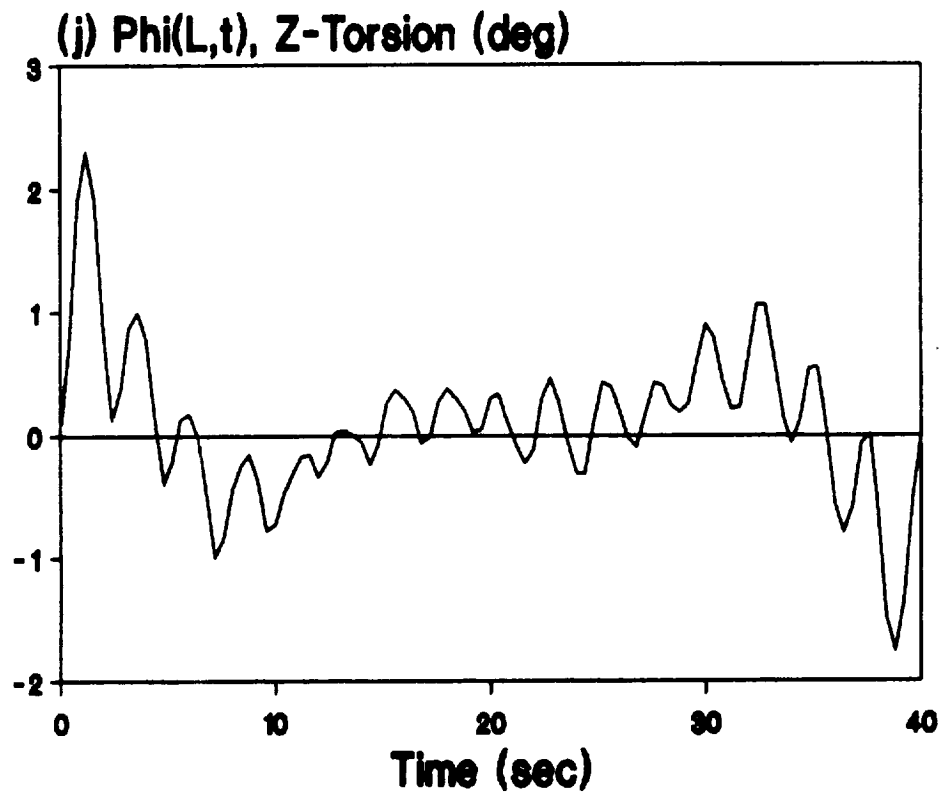
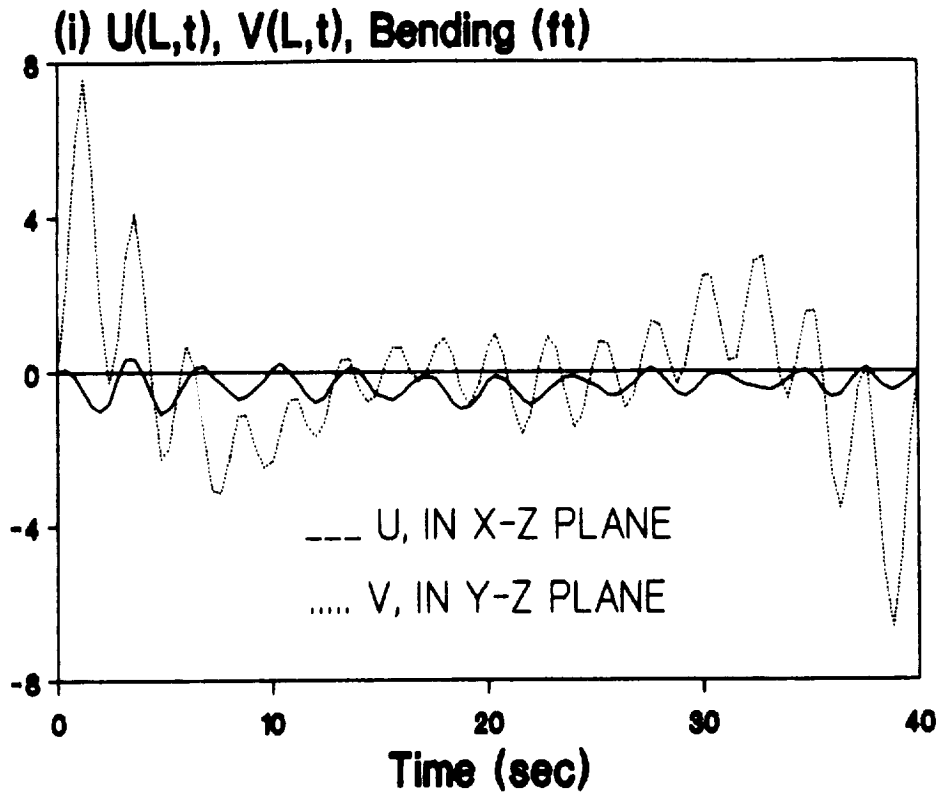


Fig. 5. Results for the 3-D slew, Case 3: 60-30-45 deg-Slew, Shuttle Torques + Reflector Forces,  $R = \text{Diag}(1E-4, 1E-4, 1E-4, 0.6, 1.4E-3)$ .

### III. EFFECT OF STRUCTURAL OFFSET AXIAL SHORTENING, AND GRAVITATIONAL TORQUE ON THE SLEWING OF A FLEXIBLE SPACECRAFT

#### 1. Introduction

The direct application of Pontryagin's Maximum Principle to the attitude maneuvers of spacecraft has been conducted by many authors (Refs. 1-2). Recently, some effort has been made to utilize this principle to more complicated structures (Refs. 3-4). In Ref. 3, the rapid slewing of a 2-dimensional flexible orbiting spacecraft, a Shuttle-beam-reflector system, has been considered. It is observed (Ref. 3) that the time response history of the nonlinear system has a shift from that of the linearized system, but the reason for this was not clear. In continuation of this study, the present paper will first answer this question by examining the equations of motion and by presenting more numerical examples.

The so called axial shortening effect of a beam induced by its transverse displacement has been brought to attention by some authors (Refs. 1-2, 5). Although the shortening terms have been included in the equations (Refs. 1-2), their effect on the slew lacked quantitative analysis; specifically, the numerical examples with and without these terms were not provided. On the other hand, a numerical example in Ref. 5 shows that large differences do result between models with and without the shortening effect. But the numerical example is only for an uncontrolled dynamical response case and the main body's motion is prescribed. In the present paper, therefore, the shortening terms are considered in the formulation of the equations of motion and numerical examples both with and without these terms are presented to compare the difference between them.

Finally, the gravitational torque terms are modeled and included in the equations to show their effect on the slewing motion.

## 2. Dynamical Equations

### System Configuration

The spacecraft model used here (see Fig. 1) is composed of two rigid bodies, representing the Shuttle and a reflector (Refs. 3-4, 6), connected by a flexible beam through fixed joints, in the plane of the Earth orbit. One end of the beam is assumed to be connected to the mass center of the Shuttle, while the other end is, in general, not connected to the mass center of the reflector. This offset is represented by  $x_r$  in the  $\hat{i}_r$  direction of the reflector's coordinate system,  $(\hat{i}_r, \hat{k}_r)$ . It is this offset parameter that will be examined in this paper.  $\theta$  is the rotation angle of the Shuttle fixed coordinate system,  $(\hat{i}_s, \hat{k}_s)$ , with respect to the orbital coordinate system,  $(\hat{i}_o, \hat{k}_o)$ .  $u(z,t)$  and  $\phi(z,t) = \partial u / \partial z$  describe the transverse displacement of the beam and the rotation angle of its cross section from its undeformed position, respectively. Both  $u$  and  $\phi$  are assumed small and can be expressed by the modal superposition formula  $u = \sum_1 \xi_i(z) \alpha_i(t)$ ,  $\phi = \sum_1 \xi'_i(z) \alpha_i(t)$ ; where  $\xi_i$  is the  $i$ th modal function,  $\alpha_i$  is the  $i$ th scaled modal amplitude, and  $\xi'_i = d\xi_i/dz$ .

The effect of the offset on the slewing is analyzed by changing the value of  $x_r$ . Towards this purpose, the partial differential equation for the free vibration of this structure has been solved by using the separation of variable method. The natural frequencies and modal shape functions have been obtained (the assumed mode method was used in Refs. 1-2, 5), for different value of  $x_r$ . It is observed that the natural frequencies decrease as the offset distance increases.

### Kinetic Energy

The kinetic energy of the system about the mass center of the system,  $c$ , can be expressed as  $T = T_s + (T_b + T_r) - T_c$ , or

$$\begin{aligned}
 T = & \frac{1}{2} \int_s |\dot{r}|^2 dm + \frac{1}{2} \left[ \int_{b+r} |\dot{r}|^2 dm - \frac{1}{m_t} \left( \int_b |\dot{r}| dm \right)^2 - \frac{1}{m_t} \left( \int_r |\dot{r}| dm \right)^2 \right] \\
 & - \frac{1}{m_t} \left( \int_b \dot{r} dm \right) \cdot \left( \int_r \dot{r} dm \right) \quad (1)
 \end{aligned}$$

where  $\bar{r}$  is the position vector from  $o_s$  (Shuttle mass center) to an arbitrary mass element in the system and  $m_t$  is the total mass of the system. The integration subscripts, "s", "b", and "r", mean that the corresponding integration is throughout the Shuttle, the beam, and the reflector, respectively.  $T_s$  in Eq. (1) represents the kinetic energy of the Shuttle about  $o_s$ ,  $T_s = \frac{1}{2} I_s \dot{\theta}_t^2$ , where  $\dot{\theta}_t = \dot{\theta} + \omega_0$ ,  $\omega_0$  is the orbital rate and  $I_s$  is the moment of inertia of the Shuttle.

Two assumptions for the deformation of the beam have been made: (1) The length of the beam does not change; (2) The rotary inertia and the shearing force are neglected. Consider now an element  $dm$  on the beam (see Fig. 1), which has a coordinate,  $z$ , before deformation and,  $z - \Delta z$ , after deformation along the  $\hat{k}_s$  axis, where  $\Delta z$  is the "shortening" amount due to the deformation and can be determined by solving the following functional,

$$z = \int_0^{z - \Delta z} \sqrt{1 + \left(\frac{\partial u}{\partial z}\right)^2} dz \quad \text{or approximately,} \quad z \approx \int_0^{z - \Delta z} \left[1 + \frac{1}{2} \left(\frac{\partial u}{\partial z}\right)^2\right] dz$$

where small  $(\partial u / \partial z)$  is assumed. Then,

$$\begin{aligned} \Delta z &\approx \frac{1}{2} \int_0^{z - \Delta z} \left(\frac{\partial u}{\partial z}\right)^2 dz = \frac{1}{2} \int_0^z \left(\frac{\partial u}{\partial z}\right)^2 dz + \frac{1}{2} \int_z^{z - \Delta z} \left(\frac{\partial u}{\partial z}\right)^2 dz \\ &\approx \frac{1}{2} \int_0^z \left(\frac{\partial u}{\partial z}\right)^2 dz + \frac{1}{2} (-\Delta z) \left(\frac{\partial u}{\partial z}\right)^2 \Big|_{z = \bar{z} \in [z - \Delta z, z]} \end{aligned}$$

By dropping the second term, which is a higher order term, we have

$$\Delta z = \frac{1}{2} \int_0^z \left(\frac{\partial u}{\partial z}\right)^2 dz$$

This indicates that  $\Delta z$  is a function of  $z$  and  $u(z, t)$  (a function). Also,  $\Delta z$  is a second order term in the modal amplitude,  $\alpha$ . Equivalent developments for the shortening effect are also presented in Refs. 1 and 5. The position and velocity vectors of a mass element  $dm$  on the beam and the reflector are, respectively,

$$\begin{aligned} \bar{r} &= u\hat{i} + (z - \Delta z)\hat{k}; & \dot{\bar{r}} &= [\dot{\theta}_t(z - \Delta z) + \dot{u}]\hat{i} - (\dot{\theta}_t u + \Delta \dot{z})\hat{k}; & (\hat{k}, \hat{i}) &= (\hat{k}_0, \hat{i}_0); \\ \bar{r} &= (u_r + x)\hat{i} + (L - \Delta L - x\phi_r)\hat{k}; & \text{and} & & \dot{\bar{r}} &= [\dot{\theta}_t(L - \Delta L - x\phi_r) + \dot{u}_r]\hat{i} - [\dot{\theta}_t(u_r + x) + \Delta \dot{L} + x\dot{\phi}_r]\hat{k} \end{aligned}$$

where  $L$  is the length of the beam.  $T_b$ ,  $T_r$ , and  $T_c$  in Eq. (1) can be obtained by using the following equations:

$$\begin{aligned} \int_b z \Delta z dm &= \frac{1}{2} \int_0^L \rho A z \left[ \int_0^z \left( \frac{\partial u}{\partial y} \right)^2 dy \right] dz \\ &= \frac{1}{2} \rho A \left\{ \left[ \frac{z^2}{2} \int_0^z \left( \frac{\partial u}{\partial y} \right)^2 dy \right]_0^L - \int_0^L \frac{z^2}{2} \left( \frac{\partial u}{\partial z} \right)^2 dz \right\} = \frac{1}{2} \rho A \left[ \int_0^L \frac{1}{2} (L^2 - z^2) \left( \frac{\partial u}{\partial z} \right)^2 dz \right] \\ \int_b \Delta z dm &= \frac{1}{2} \int_0^L \rho A \left[ \int_0^z \left( \frac{\partial u}{\partial y} \right)^2 dy \right] dz \\ &= \frac{1}{2} \rho A \left\{ \left[ z \int_0^z \left( \frac{\partial u}{\partial y} \right)^2 dy \right]_0^L - \int_0^L z \left( \frac{\partial u}{\partial z} \right)^2 dz \right\} = \frac{1}{2} \rho A \int_0^L (L - z) \left( \frac{\partial u}{\partial z} \right)^2 dz \end{aligned}$$

After dropping third and higher order terms in modal amplitudes,  $\alpha$ , we obtain

$$T = \frac{1}{2} (\dot{\theta} + \omega_0)^2 (I + 2\alpha^T m_a + \alpha^T M_2 \alpha) + (\dot{\theta} + \omega_0) \dot{\alpha}^T (m_2 + M_4 \alpha) + \frac{1}{2} \dot{\alpha}^T M_3 \dot{\alpha}$$

where  $I$ ,  $m_a$ ,  $m_2$ ,  $M_2$ ,  $M_4$ , and  $M_3$  are constants, vectors, and matrices, respectively.

### Potential Energy

The gravitational energy and the elastic energy of the beam are

$$\begin{aligned} V_g + V_s &= \frac{1}{2} \int_0^L EI \left( \frac{\partial^2 u}{\partial z^2} \right)^2 dz + \frac{3}{2} \omega_0^2 \hat{k}_0 \cdot \mathbf{J} \cdot \hat{k}_0 \\ &= \frac{1}{2} \alpha^T K \alpha + \frac{3}{2} \omega_0^2 (J_{11} \sin^2 \theta + J_{33} \cos^2 \theta - J_{13} \sin 2\theta) \end{aligned}$$

where  $\hat{k}_0 = -\hat{i} \sin \theta + \hat{k} \cos \theta$ ,  $EI$  is the constant flexural rigidity of the cross section of the beam, and  $\mathbf{J}$  is the inertia tensor of the system, with  $J_{ij}$  being the functions of the modal amplitudes,  $\alpha$ .

## Generalized Forces

The shortening effect is also considered in developing the virtual work of the controls and the associated generalized forces,  $Q_\theta$  and  $Q_\alpha$ . For example, the force arm for a control force is affected by the shortening effect.

## Dynamical Equations

By using the Lagrangian equations, we can obtain the dynamical equations of the system in the following matrix form

$$\begin{bmatrix} I+2\alpha^T m_a + \alpha^T M_2 \alpha & (m_2 + M_4 \alpha)^T \\ \hline m_2 + M_4 \alpha & M_3 \end{bmatrix} \begin{bmatrix} \ddot{\theta} \\ \ddot{\alpha} \end{bmatrix} = \begin{bmatrix} -2\dot{\theta}\dot{\alpha}^T (m_a + M_2 \alpha) - \dot{\alpha}^T M_5 \dot{\alpha} - \partial V_g / \partial \theta + Q_\theta \\ \hline -2\dot{\theta} M_a \dot{\alpha} + \dot{\theta}^2 (m_a + M_2 \alpha) - K\alpha - \partial V_g / \partial \alpha + Q_\alpha \end{bmatrix} \quad (2)$$

where  $M_4 = M_a + M_5$ .  $m_a$ ,  $M_a$  and  $M_5$  are linear functions of  $x_r$ .  $M_2$ ,  $M_3$  and  $M_5$  contain the components of the shortening terms. From these equations, we see that the terms containing  $m_a$  and  $M_a$  are nonlinear terms of first order in  $\alpha$  or  $\dot{\alpha}$ , while the terms containing  $M_2$ ,  $M_4$  and  $M_5$  are of second order. Therefore, for moderate nonzero values of  $x_r$ , the influence of the structural offset can be greater than the shortening effect. The linearized equations can be obtained by neglecting all nonlinear terms,

$$\begin{bmatrix} I & m_2^T \\ \hline m_2 & M_3 \end{bmatrix} \begin{bmatrix} \ddot{\theta} \\ \ddot{\alpha} \end{bmatrix} = \begin{bmatrix} 0 \\ -K\alpha \end{bmatrix} + \begin{bmatrix} -\partial V_g / \partial \theta + Q_\theta \\ \hline -\partial V_g / \partial \alpha + Q_\alpha \end{bmatrix}_{\text{LIN}} \quad (3)$$

where "LIN" means constant and linear terms. Note that on the right side of Eq. (3), the structural offset and the shortening terms disappear.

### 3. Optimal Control

The optimal control for the slew problem is derived by using the techniques similar to those used in Ref. 3 and will not be repeated here. The controllers are provided by one control torquer on the Shuttle ( $u_1$ ), one control force on the reflector ( $u_4$ ), and two force actuators on the beam ( $u_2$  at  $L/3$  and  $u_3$  at  $2L/3$ ). Each of the controls has its own upper and lower saturation levels. The cost functional,  $J = \frac{1}{2} \int_0^T \bar{u}^T R \bar{u} dt$ , is used in the present paper, where  $\bar{u}$  is the control vector,  $R$  is the control weighting matrix, and  $T$  is the slewing time. The resulting two-point boundary-value problem is solved by using the quasilinearization algorithm.

### 4. Numerical Results

The parameters of the orbiting SCOLE (Ref. 6) (Spacecraft Control Laboratory Experiment) are:  $EI=4E7$  lb-ft<sup>2</sup>,  $\rho A=0.09554$  slug/ft,  $L=130$  ft,  $m_g=6366.46$  slug,  $m_r=12.42$  slug,  $I_g=12.42$  slug-ft<sup>2</sup>,  $I_r=4881.375$  slug-ft<sup>2</sup>,  $\omega_0=0.001$  (rad/s) (orbital altitude  $h=981$  km). The natural frequencies (hz) for  $x_r=0$  and  $x_r=32.5$  (ft) are: 0.3365257, 2.062547, 5.316669; and 0.3199540, 1.287843, 4.800169, respectively. All numerical simulations are 90 degree rest-to-rest slews and can be represented by:

Case 1  $x_r=0$ ,  $\bar{u}=u_1$ ,  $R=1E-6$ ,  $T=27.6$  (s)

Case 2  $x_r=0$ ,  $\bar{u}=[u_1 \ u_2 \ u_3 \ u_4]^T$ ,  $R=DIAG(1E-6, .15, .21, 1E-4)$ ,  $T=8.196$  (s)

Case 3  $x_r=32.5$  (ft),  $\bar{u}=u_1$ ,  $R=1E-6$ ,  $T=27.6$  (s)

Case 4  $x_r=32.5$  (ft),  $\bar{u}=[u_1 \ u_2 \ u_3 \ u_4]^T$ ,  $R=DIAG(1E-6, .15, .21, 1E-4)$ ,  $T=8.196$  (s)

Figs. 2a-g display the time histories of  $\theta(t)$ ,  $u(L,t)$ ,  $\phi(L,t)$ ,  $\bar{u}(t)$  for Case 4. Clearly, the response of  $\theta(t)$  for both linear and nonlinear systems are very close. However, there exist some differences between the two systems in  $u(L,t)$ ,  $\phi(L,t)$  and the controls,  $\bar{u}$ . The difference is primarily due to the offset  $x_r$  (here,  $x_r=32.5$  ft). When  $x_r=0$ , this difference can be reduced markedly, regardless of whether the shortening effect and gravitation are considered. It is also interesting to know that the controls have large differences only around the mid-slew-time.

Table 1 Tip Displacement and Tip Angle

		Max-Disp (ft)	Min-Disp (ft)	Max-Ang (deg)	Min-Ang (deg)	e-Disp
Case 1 $x_r = 0, \bar{u} = u_1$ T=27.6 s	Linearized	0.37727	-0.37727	0.27402	-0.27404	—
	$\Delta L = 0, \omega_0 = 0$	0.37727	-0.37727	0.27403	-0.27404	0.0%
	$\Delta L \neq 0, \omega_0 = 0$	0.37727	-0.37727	0.27402	-0.27404	0.0%
	$\Delta L \neq 0, \omega_0 \neq 0$	0.37728	-0.37728	0.27403	-0.27405	0.0%
Case 2 $x_r = 0, \bar{u} = \bar{u}$ T=8.196 s	Linearized	13.072	-13.072	9.6216	-9.6216	—
	$\Delta L = 0, \omega_0 = 0$	13.186	-13.186	9.7050	-9.7050	0.87%
	$\Delta L \neq 0, \omega_0 = 0$	13.154	-13.154	9.6847	-9.6847	0.63%
	$\Delta L \neq 0, \omega_0 \neq 0$	13.153	-13.154	9.6842	-9.6845	0.62%
Case 3 $x_r \neq 0, \bar{u} = u_1$ T=27.6 s	Linearized	0.38812	-0.38812	0.30342	-0.30340	—
	$\Delta L = 0, \omega_0 = 0$	0.38590	-0.40802	0.29110	-0.33940	5.13%
	$\Delta L \neq 0, \omega_0 = 0$	0.38600	-0.40732	0.29118	-0.33884	4.95%
	$\Delta L \neq 0, \omega_0 \neq 0$	0.38586	-0.40803	0.29094	-0.33981	5.13%
Case 4 $x_r \neq 0, \bar{u} = \bar{u}$ T=8.196 s	Linearized	12.191	-12.191	9.1082	-9.1082	—
	$\Delta L = 0, \omega_0 = 0$	12.734	-12.061	9.4541	-9.1299	4.45%
	$\Delta L \neq 0, \omega_0 = 0$	12.796	-12.052	9.5067	-9.2030	4.96%
	$\Delta L \neq 0, \omega_0 \neq 0$	12.795	-12.054	9.5052	-9.2061	4.95%

Table 1 lists the maximum (minimum) values for the displacement,  $u(L,t)$ , and angle,  $\phi(L,t)$ , of the beam during the associated slews for all cases. The first line in each case lists the results for the linearized system, while all remaining lines represent those for the nonlinear system with different considerations. For example,  $\Delta L=0$  means the shortening effect is not considered. The last column gives the largest relative displacement error, with respect to the linear results, based on

$$(e_{Disp})_* = \text{Max} \left( \left| \frac{\text{MAX}_* - \text{MAX}_{LIM}}{\text{MAX}_{LIM}} \right|, \left| \frac{\text{MIN}_* - \text{MIN}_{LIM}}{\text{MIN}_{LIM}} \right| \right)$$

Nonlinear System vs. Linearized System First, let us examine line 1 and line 2 in each case. In Case 1, since no offset, the differences between the two lines are very small. In Case 2, where more controllers are used and the slewing time is shortened, the differences increase symmetrically ( $|\text{MAX}| = |\text{MIN}|$ ), in spite of  $x_r = 0$ . Case 3 uses the same slewing conditions as used in Case 1, except  $x_r = 32.5$  ft. This offset shifts the envelop of the response downwards and results in a larger relative displacement error than that in Case 2. Case 4 is the combination of Cases 2 and 3. The shift now is upwards which is due to the inclusion of more controllers. When more controllers are used (Ref. 3), the phase of the response reverses, so do the maximum (minimum) amplitudes.

Shortening Effect By comparing line 2 and line 3 in each case, we can see that the shortening terms (1) reduce the amplitude (Cases 2 and 3); (2) increase the amplitude (Case 4); and shift the response upwards (Cases 3 and 4). These observations coincide with the fact that  $\Delta z$  is only a second order effect compared with the offset effect.

Gravitational Effect By observing lines 3 and 4, we can conclude that the addition of the gravitational torques into the equations of motion has a very small effect on the slew, although they shift the response downwards. This is because the orbital rate is much smaller than the slewing rate and the magnitude of the gravitational torque term is much smaller than that of the active control torque term.

## 5. Conclusion

Generally, the linearized system can predict the system dynamics very well in the slow slewing case. However, in the rapid large-angle slewing problem, the responses of the system deviate noticeably from those described by the linearized equations if the effects of structural offset and axial shortening are included in the simulations. The structural offset (if any) results in a first order nonlinear effect. The shortening effect causes only a second order nonlinear effect and may not be considered, in the controlled simulations, unless the deformation is out of the linear range. The gravitational effect can be safely neglected in the slew motions considered here.

## References

1. J.L. Junkins and J.D. Turner, Optimal Spacecraft Rotational Maneuvers, Elsevier, Amsterdam, 1986.
2. J.D. Turner and H.M. Chun, "Optimal Distributed Control of a Flexible Spacecraft During a Large-Angle Maneuver," *Journal of Guidance, Control, and Dynamics*, Vol. 7, No. 3, 1984, pp. 257-264.
3. P.M. Bainum and F. Li, "Rapid In-Plane Maneuvering of the Flexible Orbiting SCOLE," AAS/AIAA Astrodynamics Specialist Conference, Stowe, Vermont, Aug. 7-10, 1989, AAS Paper 89-422.
4. P.M. Bainum and F. Li, "Optimal Large Angle Maneuvers of a Flexible Spacecraft," presented at the International Conference: Dynamics of Flexible Structures in Space, Cranfield, Bedford, UK, May 15-18, 1990.
5. T.R. Kane, R.R. Ryan, and A.K. Banerjee, "Dynamics of a Cantilever Beam Attached to a Moving Base," *Journal of Guidance, Control, and Dynamics*, Vol. 10, No. 2, 1987, pp. 139-151.
6. L.W. Taylor and A.V. Balakrishnan, "A Mathematical Problem and a Spacecraft Control Laboratory Experiment (SCOLE) Used to Evaluate Control Laws for Flexible Spacecraft ... NASA/IEEE Design Challenge," *Proc. of the 4th VPI&SU Symposium on Dynamics and Control of Large Structures*, Blacksburg, VA, June 1983; Revised Jan. 1984.

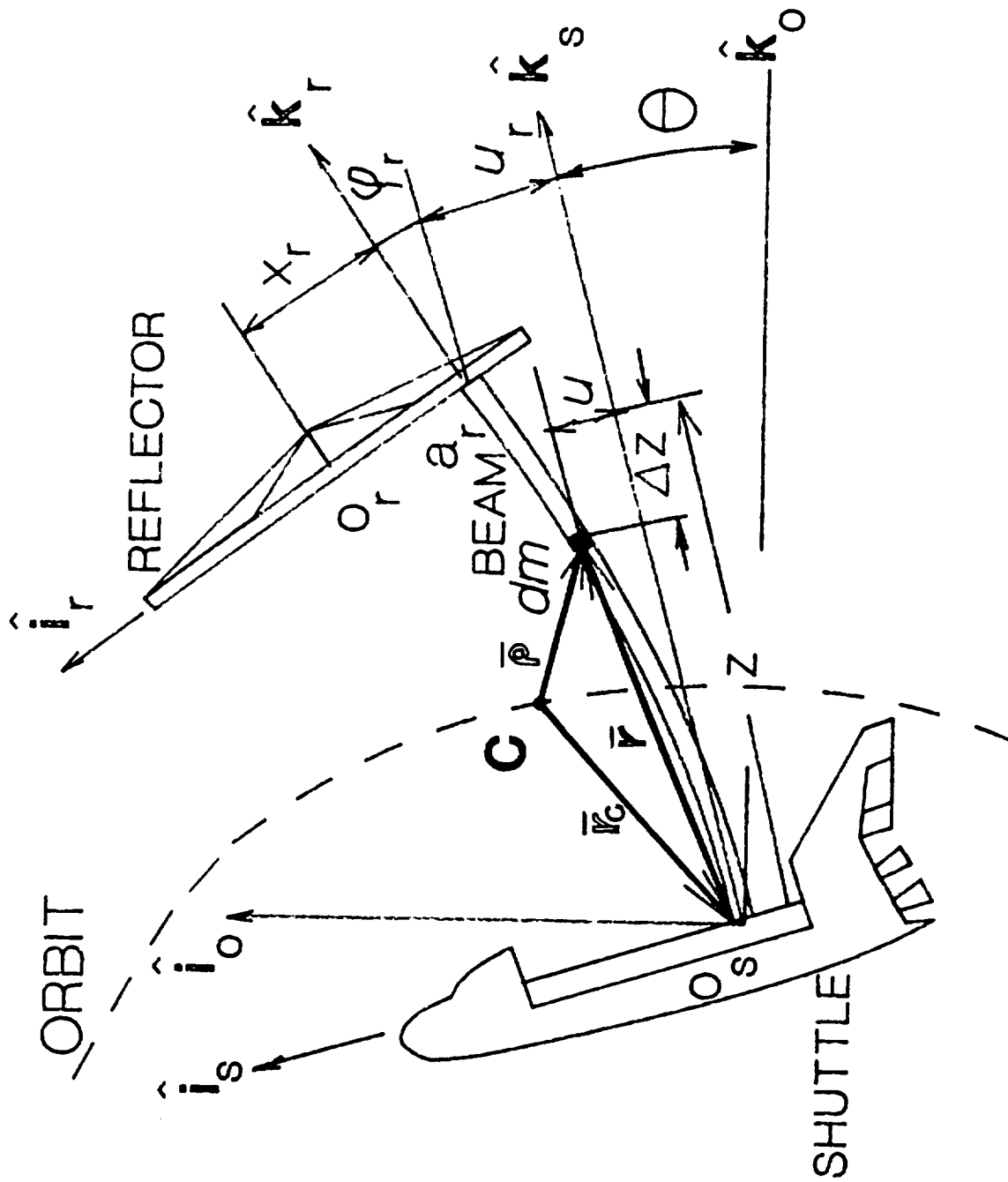


Fig. 1. 2-D Orbiting SCOLE Configuration and Beam Element

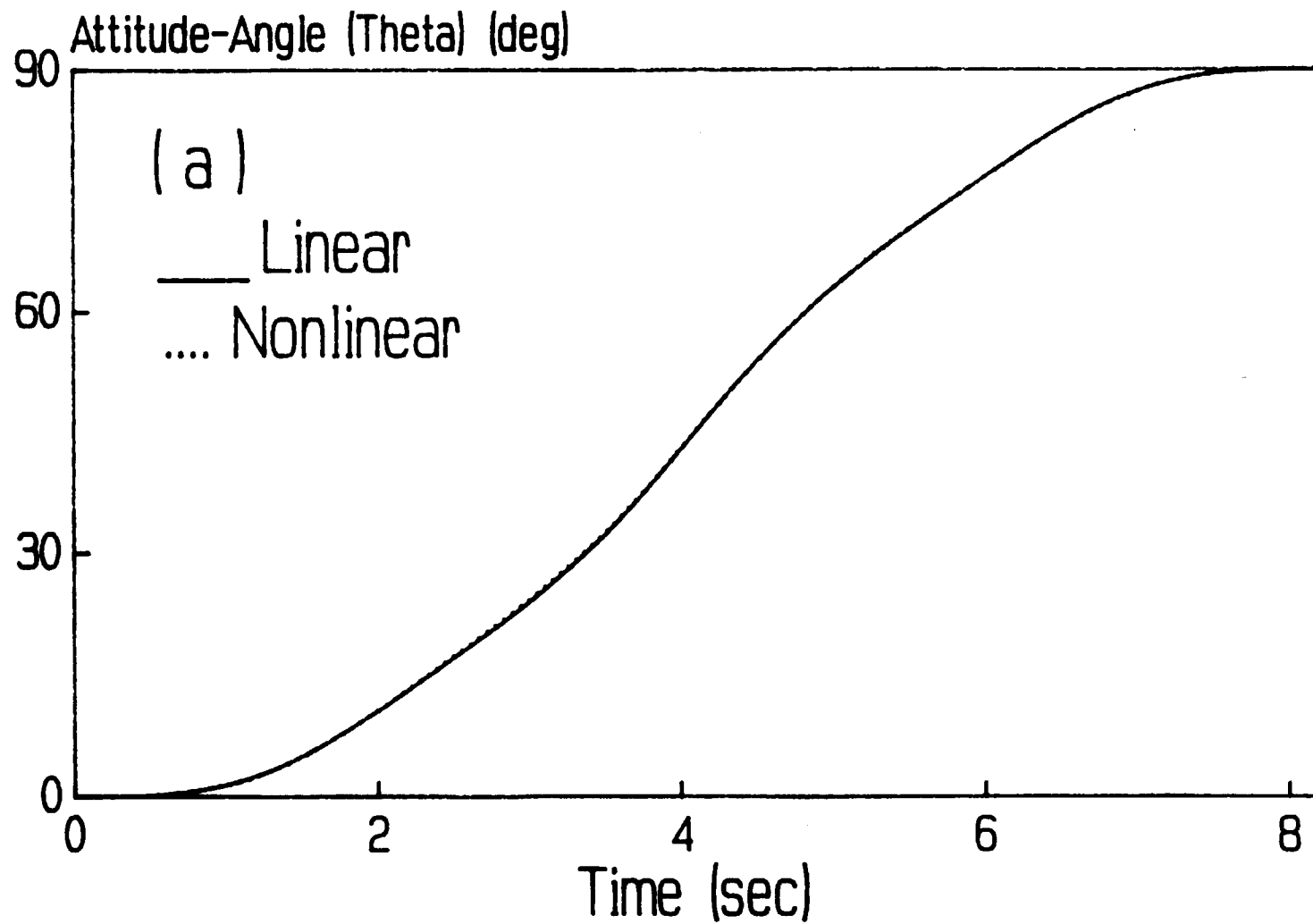


Fig. 2. Results for the 2-D Slew, Case 4:  $x_r = 32.5$  ft,  
 $u = [u_1 \ u_2 \ u_3 \ u_4]^T$ ,  $t_r = 8.196$  sec.

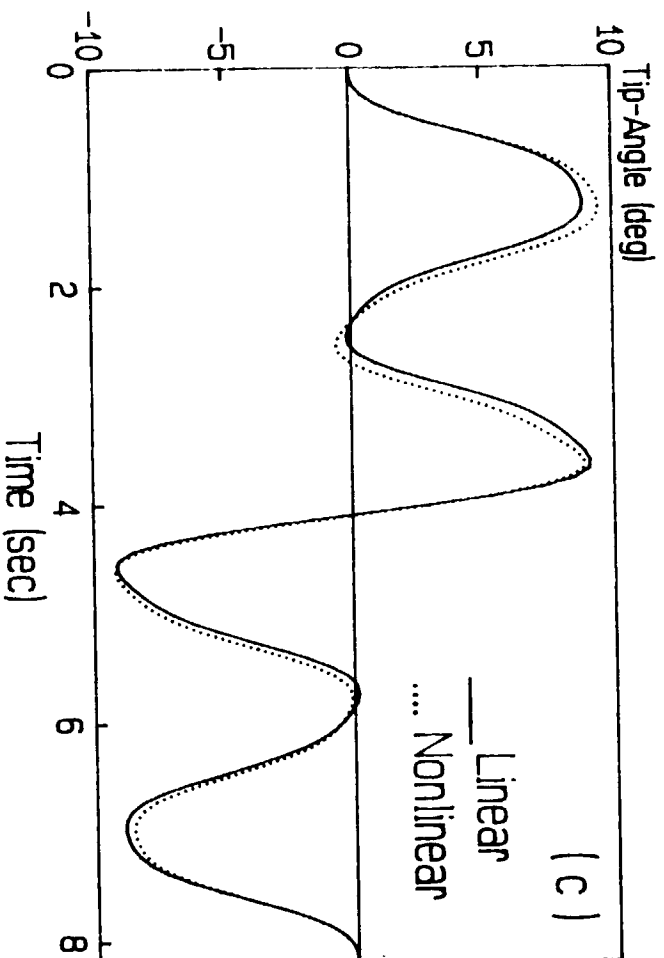
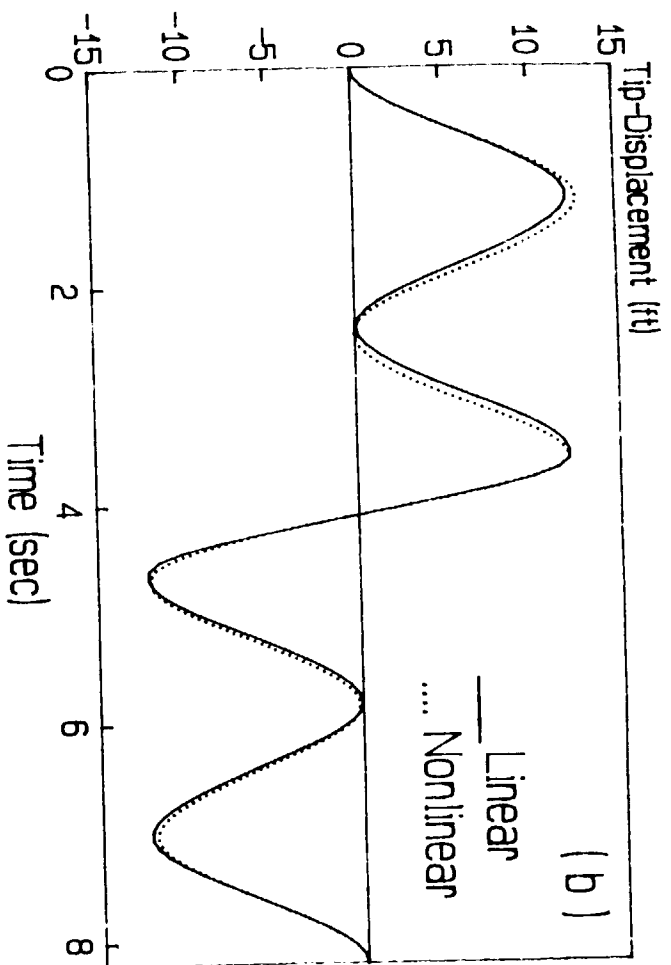


Fig. 2. Results for the 2-D Slew, Case 4:  $x_r = 32.5$  ft,  
 $u = [u_1 \ u_2 \ u_3 \ u_4]^T$ ,  $t_r = 8.196$  sec.

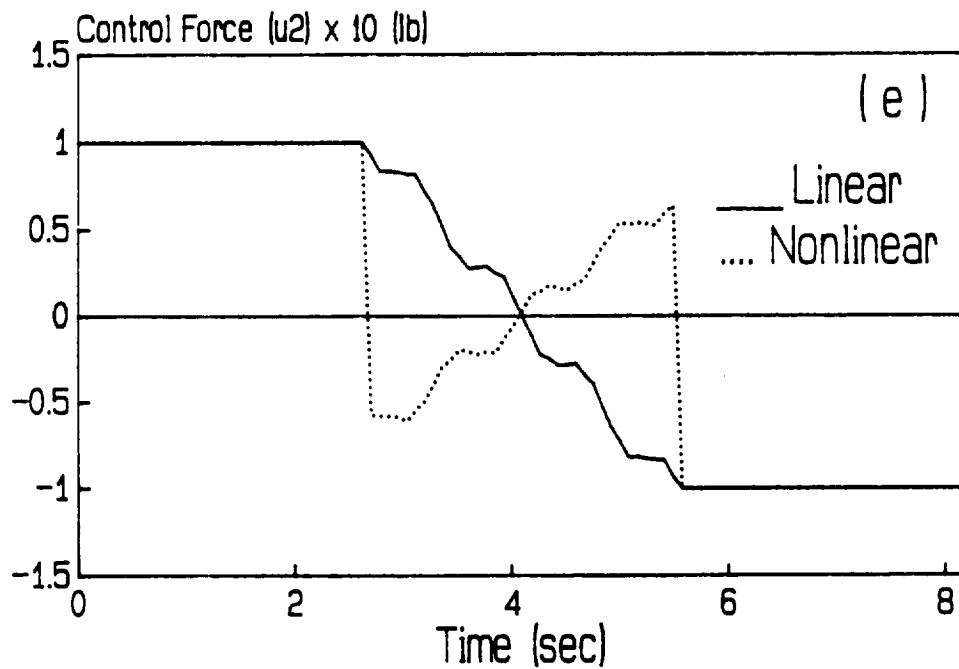
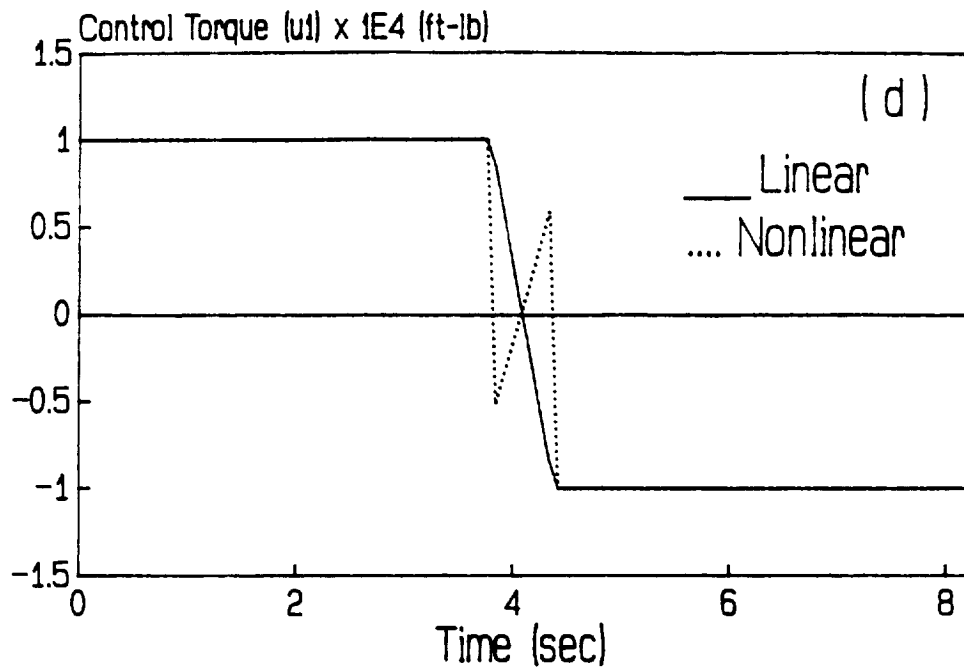


Fig. 2. Results for the 2-D Slew, Case 4:  $x_r = 32.5$  ft,  $u = [u_1 \ u_2 \ u_3 \ u_4]^T$ ,  $t_r = 8.196$  sec.

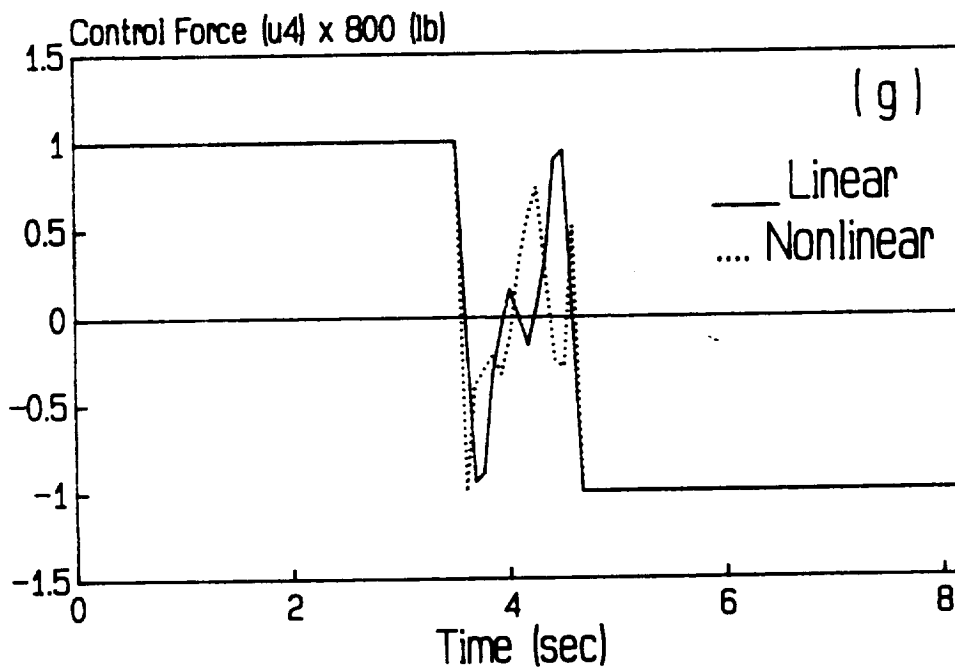
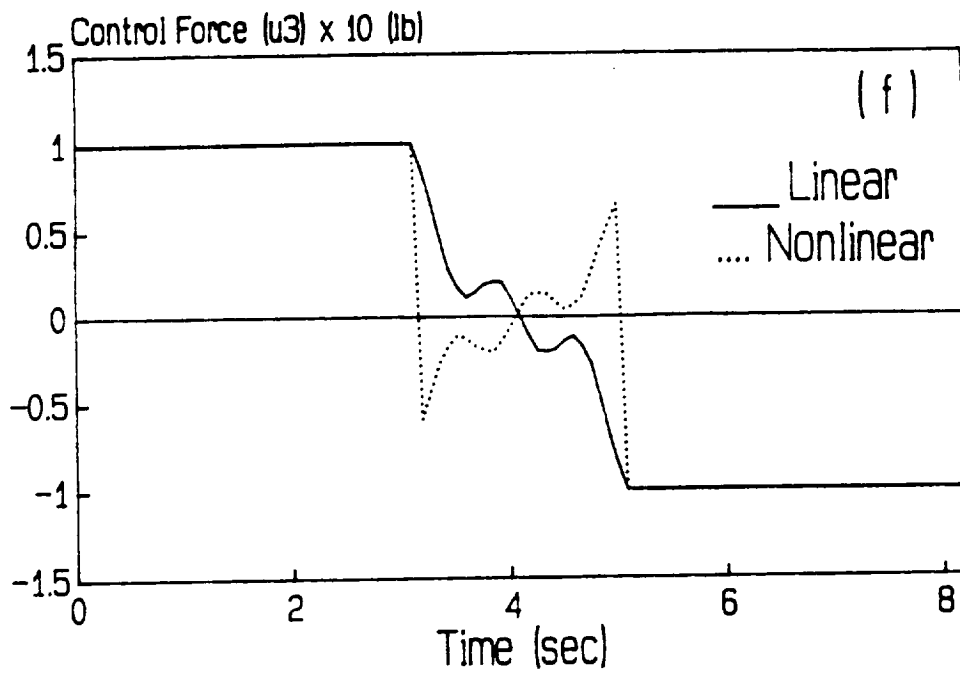


Fig. 2. Results for the 2-D Slew, Case 4:  $x_r = 32.5$  ft,  
 $u = [u_1 \ u_2 \ u_3 \ u_4]^T$ ,  $t_r = 8.196$  sec.

#### IV. THE EFFECT OF ADDITIONAL DESIGN PARAMETERS ON THE LQR BASED DESIGN OF A CONTROL/STRUCTURAL SYSTEM

##### I. Introduction

Some of the difficulties encountered in controlling large space structural systems are attributed to their inherent flexibility. As the size of these systems increases, due to payload limitations, the total mass cannot be significantly increased. In the evolution of such systems, it often becomes necessary to include additional elements into the design such as those resulting from additional actuators, sensors, or experimental modules<sup>1</sup>.

Sometimes the resulting control may be optimal only for a prescribed structural design. But if we try to later change some of the structural design parameters -- even by a small amount -- then the previously designed control may no longer be able to satisfy the mission specifications. If we try to change some of the structural design parameters, perhaps the control system performance will be better than before in some sense -- i.e. more robust, better transient time constant, reduction of initial overshoot amplitudes, etc. On the other hand, a change of some other structural system parameters may improve the structural design, but at the expense of control system performance.

In Ref. 2, a combined structural and control optimization problem was formulated using an optimality criteria approach for the orientation and shape control of a free-free beam in orbit. The combined cost function included a form of the regulator cost, augmented with the (constrained) weight of the whole structure together with the appropriate Lagrange multiplier. Optimality criteria were derived for minimizing the combined cost function and the configuration of the structure

obtained was used for the synthesis of control laws using linear quadratic regulator theory. The configurations obtained by the combined approach required less control effort for shape and orientation control of the orbiting beams than that associated with the separately designed structure and LQR-based control systems.

For the large scale space structural design, it is important to reduce the mass of the structural system. The satisfaction of the control requirements during the combined control/structural design is also important. The multicriteria optimization approach will be needed for use in the field of structural redesign, which should allow a large amount of freedom and variety in selecting the potentially large number of design variables. In this study, we try to use the quadratic cost function and the control properties, such as the transient response time of the system attitude, as design criteria. The maximum allowable values of the structural mass and the saturation levels of the forces and torques provided by the control actuators are used as the system constraints. A free-free orbiting uniform beam with an articulated payload will be considered here as a simple model. The additional design of the beam diameter is based on LQR techniques using multicriteria which include the cost function and the transient response time of the attitude motion of the beam, subjected to the limited mass of the structure and the saturation levels of the actuators. The numerical optimization procedure and simulation is done using the IBM mainframe computer system.

## II. Equations of Motion

The dynamics of a long flexible beam in the plane of the assumed circular orbit can be expressed (after neglecting the second order effect) as <sup>2</sup>

$$\ddot{\theta} + 3\omega_o^2\theta = T_p/J \quad (1)$$

$$\mathbf{M} \ddot{\mathbf{Y}} + \mathbf{K} \mathbf{Y} = \mathbf{F} \mathbf{V} \quad (2)$$

Equation (1) describes the pitch motion of beam type satellites (rigid body motion) and equation (2) gives the vibratory motion of the same beam without damping, where

$\theta$  is the pitch angle

$T_p$  is the pitch torque

$\omega_o$  is the orbital frequency

$J$  is the transverse moment of inertia

$\mathbf{M}$  is the  $n \times n$  positive definite mass matrix

$\mathbf{K}$  is the  $n \times n$  positive definite stiffness matrix

$\mathbf{F}$  is the  $n \times p$  input distribution matrix

$\mathbf{Y}$  is the  $n \times 1$  displacement vector

$\mathbf{V}$  is the  $p \times 1$  vector of force inputs

Here the uniform beam with two additional masses in a circular orbit is considered ( Fig. 1).  $D$  and  $d$  stand for the outer diameter and the inner diameter of the beam, respectively. Based on the finite element method<sup>3</sup>, the beam is assumed to be divided into four elements with each element having the same geometrical size and material properties. Five force actuators and one torque actuator are assumed to be added to each of the five joints and at joint 3, respectively. The force actuators are assumed to produce forces parallel to the positive  $Y$  direction, whereas the torque is assumed to act about the  $Z$  axis. The two additional masses,  $m_l$  and  $m_r$ , are assumed to be attached to the joints 2 and 4, respectively. The mass matrix can be expressed by the sum of the beam mass matrix and the attached mass matrix, that is

$$\mathbf{M} = \mathbf{M}_S + \mathbf{M}_A \quad (3)$$

The beam mass matrix is represented by<sup>3</sup> :

$$\mathbf{M}_S = \begin{matrix} (10 \times 10) \\ \begin{bmatrix}
 \mathbf{M}_{11}^{(1)} & \mathbf{M}_{12}^{(1)} & 0 & 0 & 0 \\
 \mathbf{M}_{21}^{(1)} & \mathbf{M}_{22}^{(1)} + \mathbf{M}_{22}^{(2)} & \mathbf{M}_{23}^{(2)} & 0 & 0 \\
 0 & \mathbf{M}_{32}^{(2)} & \mathbf{M}_{33}^{(2)} + \mathbf{M}_{33}^{(3)} & \mathbf{M}_{34}^{(3)} & 0 \\
 0 & 0 & \mathbf{M}_{43}^{(3)} & \mathbf{M}_{44}^{(3)} + \mathbf{M}_{44}^{(4)} & \mathbf{M}_{45}^{(4)} \\
 0 & 0 & 0 & \mathbf{M}_{54}^{(4)} & \mathbf{M}_{55}^{(4)}
 \end{bmatrix} \end{matrix} \quad (4)$$

The attached mass matrix

$$\mathbf{M}_A = \begin{matrix} (10 \times 10) \\ \begin{bmatrix}
 0 & 0 & 0 & 0 & 0 \\
 0 & \mathbf{M}_L & 0 & 0 & 0 \\
 0 & 0 & 0 & 0 & 0 \\
 0 & 0 & 0 & \mathbf{M}_R & 0 \\
 0 & 0 & 0 & 0 & 0
 \end{bmatrix} \end{matrix} \quad (5)$$

where

$$\begin{bmatrix} \mathbf{M}_{11}^{(k)} & \mathbf{M}_{12}^{(k)} \\ \mathbf{M}_{21}^{(k)} & \mathbf{M}_{22}^{(k)} \end{bmatrix} = \frac{\rho A_0 l}{420} \begin{bmatrix} 156 & 22l & 54 & -13l \\ 22l & 4l^2 & 13l & -3l^2 \\ \dots & \dots & \dots & \dots \\ 54 & 13l & 156 & -22l \\ -13l & -3l^2 & -22l & 4l^2 \end{bmatrix}$$

$$\mathbf{M}_L = \begin{bmatrix} m_L & 0 \\ 0 & 0 \end{bmatrix} \quad \text{and} \quad \mathbf{M}_R = \begin{bmatrix} m_R & 0 \\ 0 & 0 \end{bmatrix}$$

Also the stiffness matrix of the beam can be expressed by <sup>3</sup>:

$$\mathbf{K} = \begin{bmatrix} \mathbf{K}_{11}^{(1)} & \mathbf{K}_{12}^{(1)} & \mathbf{0} & \mathbf{0} & \mathbf{0} \\ \mathbf{K}_{21}^{(1)} & \mathbf{K}_{22}^{(1)} + \mathbf{K}_{22}^{(2)} & \mathbf{K}_{23}^{(2)} & \mathbf{0} & \mathbf{0} \\ \mathbf{0} & \mathbf{K}_{32}^{(2)} & \mathbf{K}_{33}^{(2)} + \mathbf{K}_{33}^{(3)} & \mathbf{K}_{34}^{(3)} & \mathbf{0} \\ \mathbf{0} & \mathbf{0} & \mathbf{K}_{43}^{(3)} & \mathbf{K}_{44}^{(3)} + \mathbf{K}_{44}^{(4)} & \mathbf{K}_{45}^{(4)} \\ \mathbf{0} & \mathbf{0} & \mathbf{0} & \mathbf{K}_{54}^{(4)} & \mathbf{K}_{55}^{(4)} \end{bmatrix} \quad (6)$$

(10x10)

where

$$\begin{bmatrix} \mathbf{K}_{ij}^{(k)} & \mathbf{K}_{ij}^{(k)} \\ \mathbf{K}_{ij}^{(k)} & \mathbf{K}_{ij}^{(k)} \end{bmatrix} = \frac{E I}{l^3} \begin{bmatrix} 12 & 6l & -12 & 6l \\ 6l & 4l^2 & -6l & 2l^2 \\ \dots & \dots & \dots & \dots \\ -12 & -6l & 12 & -6l \\ 6l & 2l^2 & -6l & 4l^2 \end{bmatrix}$$

The joint between two elements  $i, j$  is referred by  $(ij)$  and the element number varies as  $k=1, 2, 3, 4$ ;  $l$  is the length of each element of the beam;  $\rho$  is the mass density; and  $E$  is Young's modulus.  $A_0$  and  $I$  are section area and section moment of inertia of the beam, respectively, which are dependent on the beam diameters,  $D$  and  $d$ .

Equations (1) and (2) can be written in state variable form as:

$$\dot{\mathbf{X}} = \mathbf{A} \mathbf{X} + \mathbf{B} \mathbf{U} \quad (7)$$

where the  $2(10+1) \times 1$  vectors,  $\dot{\mathbf{X}}$ ,  $\mathbf{X}$ , and the  $6 \times 1$  vector,  $\mathbf{U}$ , are given by:

$$\dot{\mathbf{X}} = [\dot{\theta} \quad \dot{\mathbf{Y}}^T \quad \ddot{\theta} \quad \ddot{\mathbf{Y}}^T]^T$$

$$\mathbf{X} = [\theta \quad \mathbf{Y}^T \quad \dot{\theta} \quad \dot{\mathbf{Y}}^T]^T$$

$$\mathbf{U} = [\tau_p \quad v_1 \quad v_2 \quad v_3 \quad v_4 \quad v_5]^T$$

The state matrix,  $\mathbf{A}$ , and the control matrix,  $\mathbf{B}$ , are given by

$$\mathbf{A} = \begin{bmatrix} \mathbf{0} & \mathbf{I} \\ (1 \times 11) & (11 \times 11) \\ \hline -3\omega_0^2 & \mathbf{0} & \mathbf{0} \\ \mathbf{0} & -\mathbf{M}^{-1} \mathbf{K} & \mathbf{0} \\ & & (11 \times 11) \end{bmatrix} \quad (8)$$

$$\mathbf{B} = \begin{bmatrix} \mathbf{0} \\ (11 \times 6) \\ \hline \mathbf{J}^{-1} & \mathbf{0} \\ \mathbf{0} & \mathbf{M}^{-1} \mathbf{F} \end{bmatrix} \quad (9)$$

### III. Additional Design Based on LQR

Based on LQR theory<sup>4</sup>, in general, the quadratic cost function is defined by

$$J = \int_0^{\infty} (\mathbf{X}^T \mathbf{Q} \mathbf{X} + \mathbf{U}^T \mathbf{R} \mathbf{U}) dt \quad (10)$$

subject to the state equation of the system from equation (7)

$$\dot{\mathbf{X}} = \mathbf{A} \mathbf{X} + \mathbf{B} \mathbf{U}$$

The cost function,  $J$ , is minimized under the optimal feedback control given by

$$\mathbf{U} = -\mathbf{R}^{-1} \mathbf{B}^T \mathbf{P} \mathbf{X} \quad (11)$$

where  $\mathbf{P}$  is the positive definite solution of the steady-state Riccati equation, which is

$$\mathbf{P} \mathbf{A} + \mathbf{A}^T \mathbf{P} - \mathbf{P} \mathbf{B} \mathbf{R}^{-1} \mathbf{B}^T \mathbf{P} + \mathbf{Q} = \mathbf{0} \quad (12)$$

From equations (4) and (5), we find the control system properties not only depend on the weighting matrices,  $\mathbf{Q}$  and  $\mathbf{R}$ , but also depend on the parameters of the structure and the actuator locations. If the structural parameters are fixed, the regulative range may be very limited for control design. It is possible that the change of structural design parameters could extend the regulative range and make the control and structural design satisfy the mission requirements.

Now we consider a class of additional design parameters,  $\mathbf{Z}$ , which could be varied while we design the control system. This means the control,  $\mathbf{U}$ , is now a function of  $\mathbf{Q}$ ,  $\mathbf{R}$ ,  $\mathbf{Z}$  and  $t$ . So the cost function,  $J$ , also is a function of  $\mathbf{Q}$ ,  $\mathbf{R}$  and  $\mathbf{Z}$ . Using the extremum principle, assuming that  $\mathbf{Z}^*$  results in an extremum of the system, we have as a necessary condition for the minimization of  $J$

$$\left. \frac{\partial J(\mathbf{Q}, \mathbf{R}, \mathbf{Z})}{\partial \mathbf{Z}} \right|_{\mathbf{Z} = \mathbf{Z}^*} = 0 \quad (13)$$

subject to some special control properties

$$\mathbf{g}(\mathbf{X}, \mathbf{Z}, t) = \mathbf{g}_0 \quad (14)$$

where  $\mathbf{g}_0$  is given from the design (mission) requirements.

From equation (13),  $\mathbf{Z}^*$  is obtained, for special cases analytically, or, more generally, by numerical means. The extremum point,  $\mathbf{Z}^*$ , may be not unique; thus, all extremum points must be compared in order to find the point at which the structural performance is optimal, such as the minimization of the total mass of the structure. Then, the optimal value of the structural design parameters may be incorporated into the control design to obtain the optimal control.

In the given simple model (Fig. 1), for example, we may select the section diameters,  $D$  and  $d$ , as the redesigned system variables and fix the transient response time of the pitch motion of the beam. Using the feasible directions of the search approach, the optimal values for the diameters would be obtained for the given system model and other parameters. For a different given model or parameter values, the optimization solution would be expected to yield different results.

#### IV. Design Multicriteria

In the LQR process, the assignment of  $\mathbf{Q}$  and  $\mathbf{R}$  values normally results from a step by step numerical search procedure. For actual LSS design, the interesting properties are the required mass of the structure, the system response time for damping rigid motions, and suppressing vibration, as well as the maximum values for the actuator forces, etc. A knowledge of the possible expected range of the boundary conditions will be helpful in selecting the weighting matrices,  $\mathbf{Q}$  and  $\mathbf{R}$ . For the combined control/structural optimal design, some design variables for both the structure and actuators should be considered. According to these, the control/structural design multicriteria for the system with additional design parameters,  $\mathbf{Z}$ ,

could be expressed by

$$J(\mathbf{Q}, \mathbf{R}, \mathbf{Z}) = \int_0^{\infty} \left[ \mathbf{X}^T(\mathbf{Z}, t) \mathbf{Q} \mathbf{X}(\mathbf{Z}, t) + \mathbf{U}^T(\mathbf{Z}, t) \mathbf{R} \mathbf{U}(\mathbf{Z}, t) \right] dt \quad (15)$$

$$\left. \frac{\partial J(\mathbf{Q}, \mathbf{R}, \mathbf{Z})}{\partial \mathbf{Z}} \right|_{\mathbf{Z} = \mathbf{Z}^*} = 0 \quad (16)$$

subject to

$$\dot{\mathbf{X}}(\mathbf{Z}, t) = \mathbf{A}(\mathbf{Z}) \mathbf{X}(\mathbf{Z}, t) + \mathbf{B}(\mathbf{Z}) \mathbf{U}(\mathbf{Z}, t) \quad (17)$$

$$\mathbf{g}(\mathbf{X}, \mathbf{Z}, t) = \mathbf{g}_0 \quad (18)$$

$$M(\mathbf{Z}) \leq M_{\max} \quad (19)$$

$$\|\mathbf{U}(\mathbf{Z}, t)\| \leq \mathbf{U}_{\max} \quad (20)$$

where  $\mathbf{g}_0$  is a design requirement

$M_{\max}$  is the limited mass of the structure

$\mathbf{U}_{\max}$  is the vector of maximum actuator force

$\mathbf{Z}$  is a vector of time-invariant design parameters

When  $\mathbf{g}_0$ ,  $M_{\max}$ ,  $\mathbf{U}_{\max}$  and the structural configuration are given, we can design the optimal structure,  $\mathbf{Z}^*$ , and optimal control,  $\mathbf{U}^*$ , using the additional design formulation based on LQR techniques

## V. Numerical Analysis

We have analyzed and designed an orbiting free-free beam using this technique, with pitch and other in-plane flexible modes included as degrees of freedom (see Fig. 1). Here we considered two cases. Case 1 is a uniform solid beam (inner diameter  $d=0$ ). Case 2 is a uniform tubular beam whose wall thickness is assumed constant ( $D-d=0.04$  ft). The material density of  $200 \text{ lb/ft}^3$ , Young's modulus of  $6E+9 \text{ lb/ft}^2$ , length of the beam of 130 ft and six actuator locations are assumed equal for both cases. Also the initial pitch angle,  $\theta_0$ , is assumed 6 degrees (0.105 rad) and the other initial state components and rates are assumed zero. Without losing general meaning, the weighting matrix,  $\mathbf{Q}$ , is assumed constant<sup>5</sup> and a diagonal matrix, that is

$$\mathbf{Q} = \text{trace} \left[ \underbrace{1000, \dots, 1000}_{11}, \underbrace{100, \dots, 100}_{11} \right]$$

and the weighting matrix,  $\mathbf{R}$ , is assumed a unitary matrix multiplied by a variable coefficient. By regulating the weighting matrix,  $\mathbf{R}$ , the response time for the rotational motion of the beam will satisfy the design requirement (here assumed ten seconds). Then the cost function values which depend on the diameter of the beam can be calculated by the multicriteria given by equations (15)–(20).

First, we suppose the additional payload mass to be 100 lb and to be added symmetrically to the beam at joints 2 and 4. The variation of the cost function with the outer diameter for the two cases is shown in Figs. 2 and 3. The first cost function extremum points for case 1 and case 2 are determined as  $D=0.45$  ft and  $D=0.32$  ft, respectively. If the beam diameters at these points satisfy the mission requirements, the structural design is optimal and so is the corresponding LQR based control design. Otherwise, the structural configuration, actuator locations or material properties should be changed. Comparing the two cases, we find the extremum points to be different, such that the optimal diameter for the solid beam is larger than that of the tubular beam. In this situation, the solid beam is heavier than

the tubular beam for the same required response time. According to the minimum mass requirement for large space structural design, the tubular beam may be much better because its mass is much less than that of the solid beam. From Fig. 2, we also can imply that the system may contain an additional extremum point for the cost function and its value may be less than the first extremum. If this happens, the first extremum point value of the diameter of the beam should be selected as the optimal solution.

Second, we try to increase additional payload mass up to 1,000 lb and still maintain symmetry. There also exist extremum points (see Figs. 4 and 5), but the diameter values corresponding to the extremum points differ from those when the payload mass is 100 lb. Comparing Figs. 2 and 4, or Figs. 3 and 4, we find the optimal diameter of the beam increases when the additional payload mass increases. This result indicates that the optimal values of the structural parameters are dependent on the payload added. Table 1 lists the optimal diameter values and their payload ratio for the uniform solid and tubular beams with three different payloads: 100 lb, 200 lb and 1,000 lb. It is clear that the payload ratio of the tubular beam is greater than that of the solid beam for the same control requirement (ten seconds of the transient response time). The payload ratio of the solid beam decreases when the payload increases, but the payload ratio of the tubular beam increases.

When additional payload masses are added asymmetrically with respect to the center of the beam, there are no big differences between the cost functions for the symmetric and asymmetric payloads (see Table 2). This may be explained by the fact that the incremental moment of inertia about the Z axis due to the payload masses is designed to be the same for both the symmetrical and asymmetrical distribution of the additional payload. Thus for practical system design it is probably useful to emphasize the symmetrical distribution of the additional payload wherever possible.

Figs. 6–9 provide the transient responses of pitch angle, two deformations, and corresponding control torque and forces for the nearly optimized uniform tubular beam (Fig. 3). Here the outer diameter of the beam is 0.3 ft which is near the optimal value. The wall thickness is still maintained at 0.02 ft. The transient

response time of pitch angle and all deformations are about ten seconds. Since the additional payload masses on the beam are symmetrically distributed, the deformations at joints 4 and 5 are the same as the deformations at joints 2 and 1, respectively, but their directions are opposite to each other. The maximum torque required is less than 5,000 ft-lb. All actuator forces are small and do not exceed 25 lb. If the solid beam is used instead of the tubular beam, for optimization, the control system requires 6,905 ft-lb maximum torque and 133 lb maximum force, which are larger than those for the tubular beam.

## VI. Conclusion

This paper reviews the effect of additional design parameters on the LQR based optimal design of space structural system. A multi-objective cost function which includes a form of the standard LQR regulator cost and its partial variation with respect to the additional design parameters is considered. The constraints are extended to the desired control properties. The optimal multicriteria are derived by minimizing the cost function and setting the variation of the cost function with respect to the design variables to zero. This approach is used to determine the optimum diameter of an orbiting free-free uniform beam with additional payload masses added. From the numerical results for two design models--a uniform solid beam and a uniform tubular beam, with two typical additional payloads added symmetrically and asymmetrically about the center of the beam, it is found that the optimal diameter occurs at the first extremum point of the variation of the cost function with respect to the diameter. It is also found that the tubular beam is superior to the solid beam for meeting both minimum mass requirements as well as desired transient and control requirements. The study proves that the multicriteria design approach should give better results from both the structural designer's and the control designer's points of view.

## VII. References

1. "A Program for Methodology Development for CSI Design," NASA Analytical Design Methods (ADM) Team Report, September 9, 1988
2. Satyanarayana, K. and Bainum, P. M., "Use of Optimality Criterion Techniques in the Combined Design and Control of Large Space Structures," AAS/AIAA Astrodynamics Specialist Conference, Stowe, Vermont, August 7-10, 1989, Paper No. AAS 89-437
3. Ross, C.T.F., Finite Element Methods in Structural Mechanics, Ellis Horwood, Limited, England, 1985
4. Bainum, P. M., Reddy, A.S.S.R., Li, F. and Xu, J., "The Dynamics and Control of Large Flexible Space Structures--XII," Final Report, NASA Grant NSG-1414, Suppl II, Howard University, September 1989
5. Ali, B., "Control System Design for Space Station," Master's Thesis, Mechanical Engineering, Howard University, December 1989

Table 1: Comparison of Optimal Diameter and Payload Ratio of Uniform Solid and Tubular Beams for Payloads: 100, 200 and 1,000 lb

Payload (lb)	Diameter (ft)		Payload Ratio	
	Solid	Tubular	Solid	Tubular
100	0.45	0.32	2.4%	22%
200	0.75	0.42	2.0%	30%
1,000	1.60	1.50	1.9%	30%

Table 2: Comparison of Cost Function Value Varied with Diameter, D, for Symmetric and Asymmetric Payloads (500 & 500 lb; 900 & 100 lb) for the Uniform Solid and Tubular Beams

Diameter D	Solid Beam		Tubular Beam	
	$J_{sym}$	$J_{asym}$	$J_{sym}$	$J_{asym}$
1.3	30.025	30.024	34.437	34.530
1.4	28.902	28.901	33.939	33.937
1.5	27.525	27.524	33.845	33.843
1.6	26.505	26.504	33.856	33.853
1.7	27.942	27.941	33.865	33.863
1.8	29.152	29.151	33.875	33.873
1.9	30.778	30.777	33.885	33.883

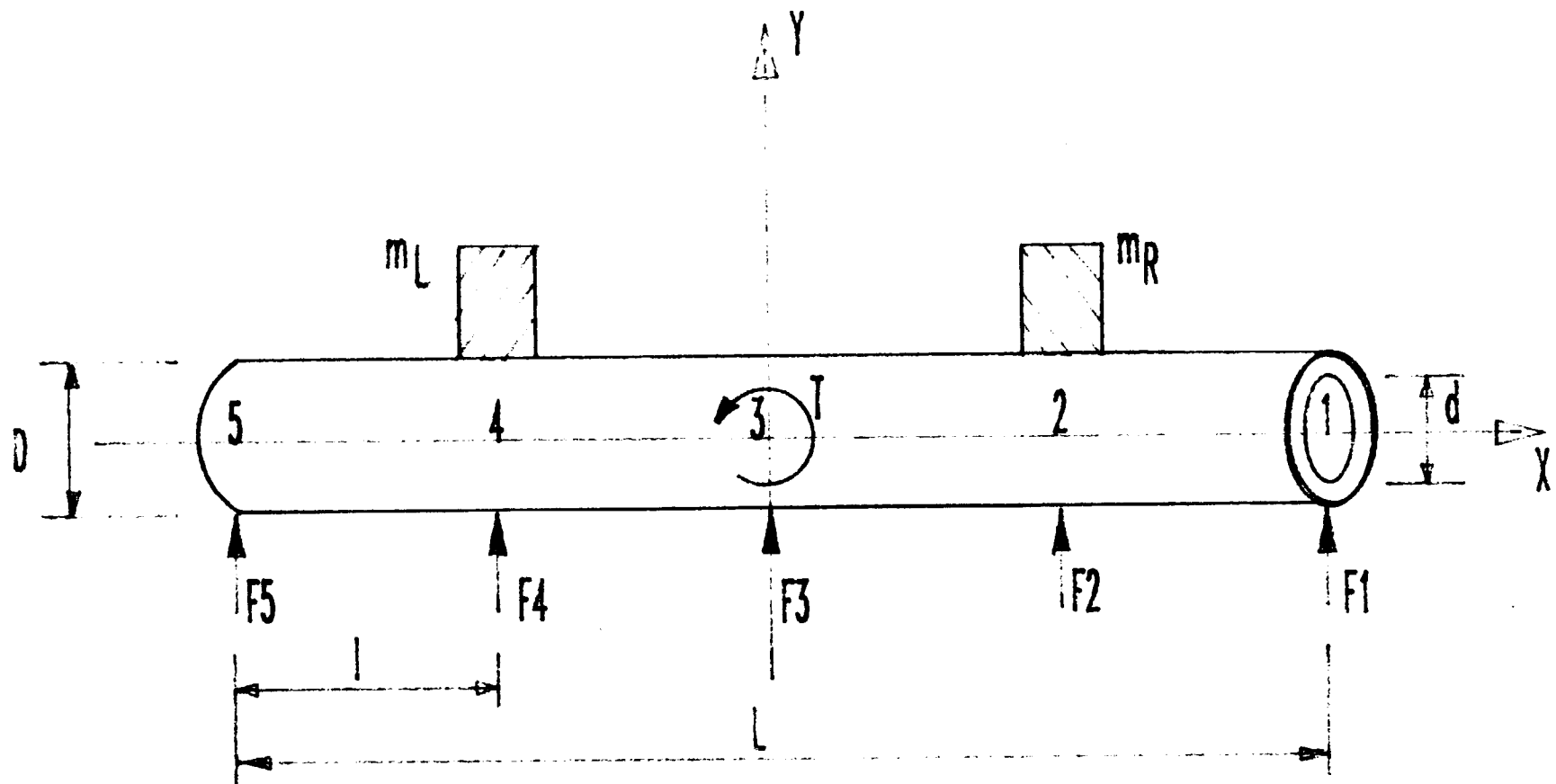


Fig. 1 Configuration of Orbiting Free-free Uniform Beam with two Additional Payload Masses

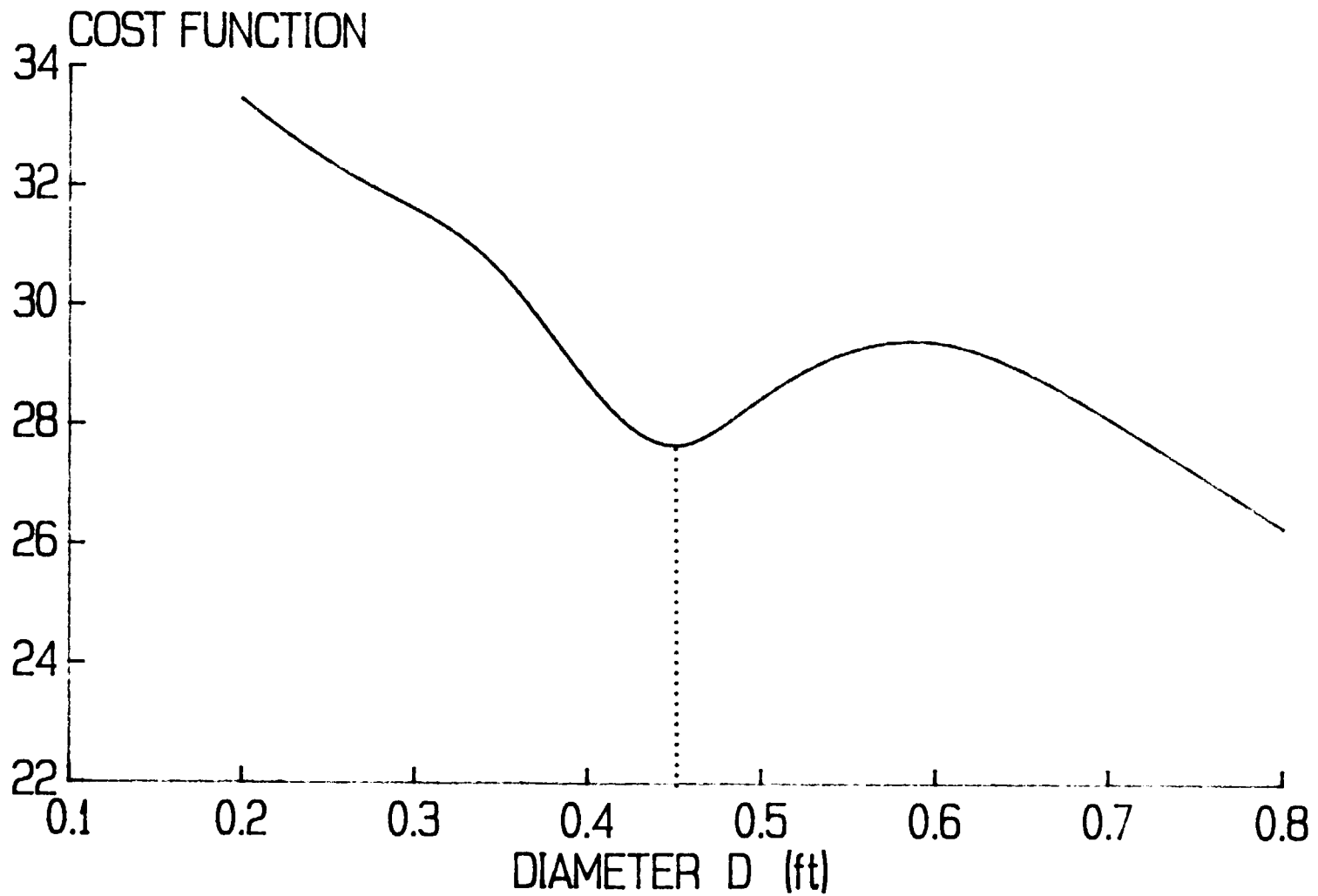


Fig. 2 Cost Function vs Diameter of the Uniform Solid Beam (here  $d=0$ ) when two 50 lb Payloads are Added to the Beam at Joints 2 and 4, Symmetrically

4.17  
THE QUALITY OF YOUR COPY IS

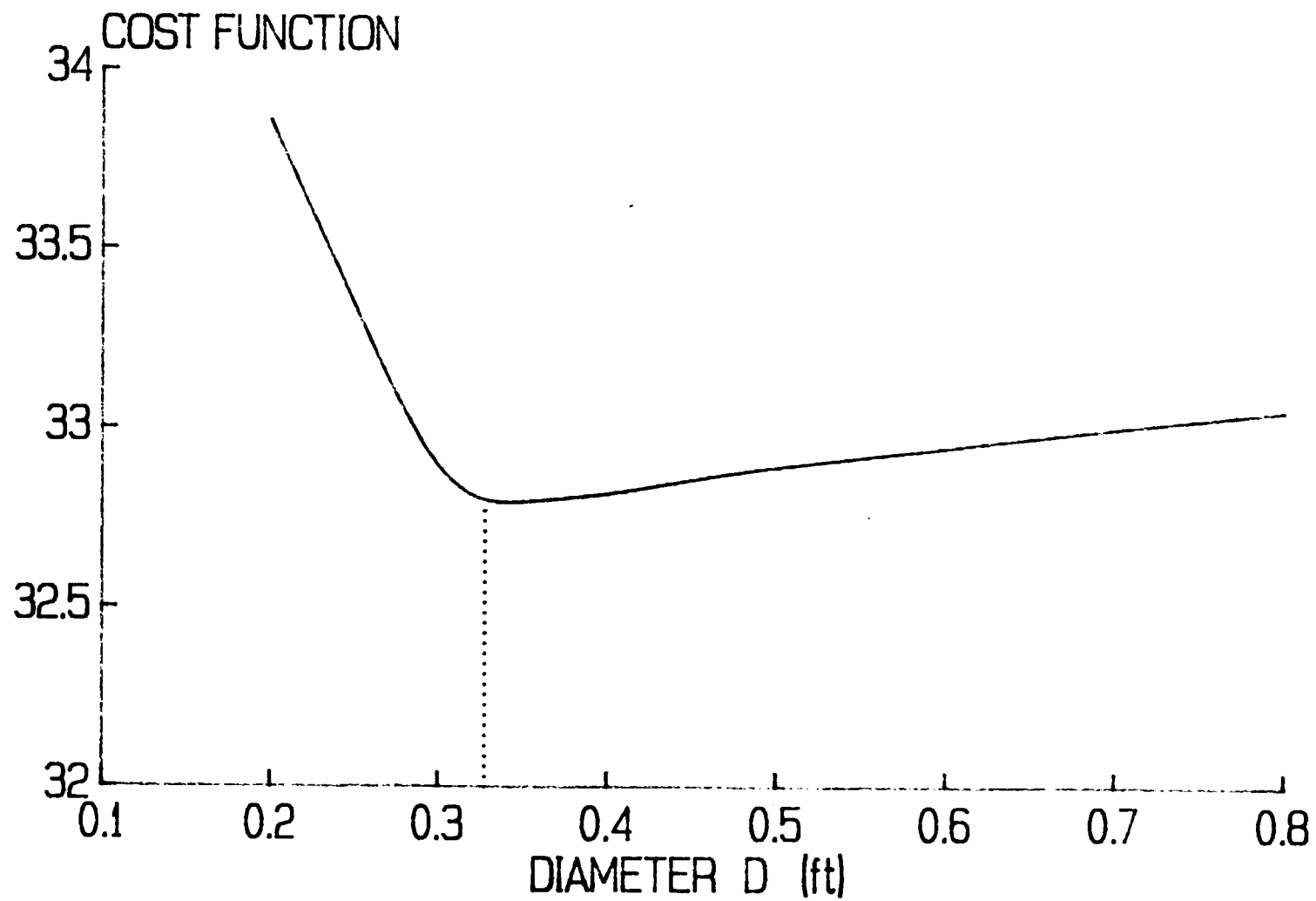


Fig. 3 Cost Function vs Diameter of the Uniform Tubular Beam (here  $D-d=0.04$  ft) when two 50 lb Payloads are Added to the Beam at Joints 2 and 4, Symmetrical ly

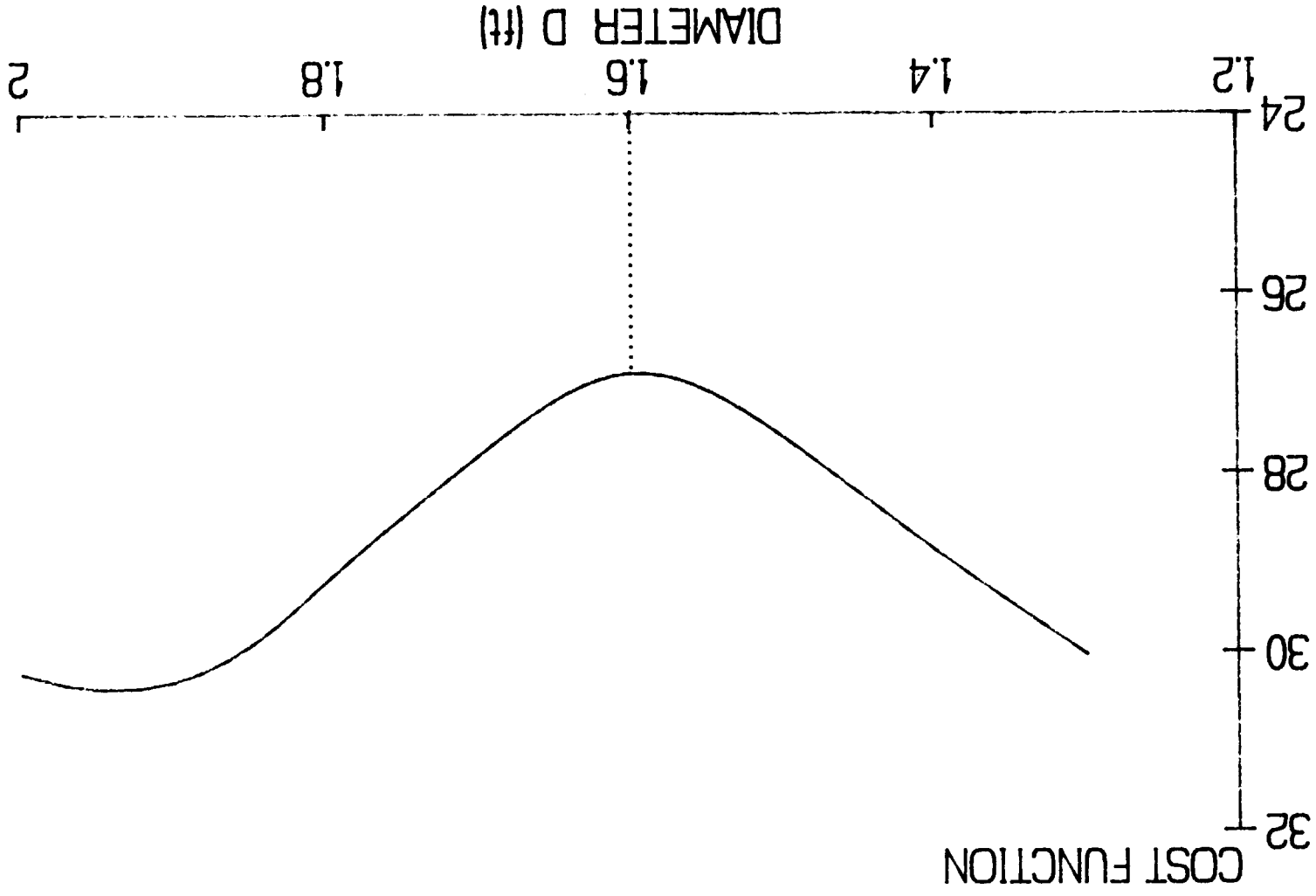


Fig. 4 Cost Function vs Diameter of the Uniform Solid Beam (here  $d=0$ ) when two 500 lb Payloads are Added to the Beam at Joints 2 and 4, Symmetrically

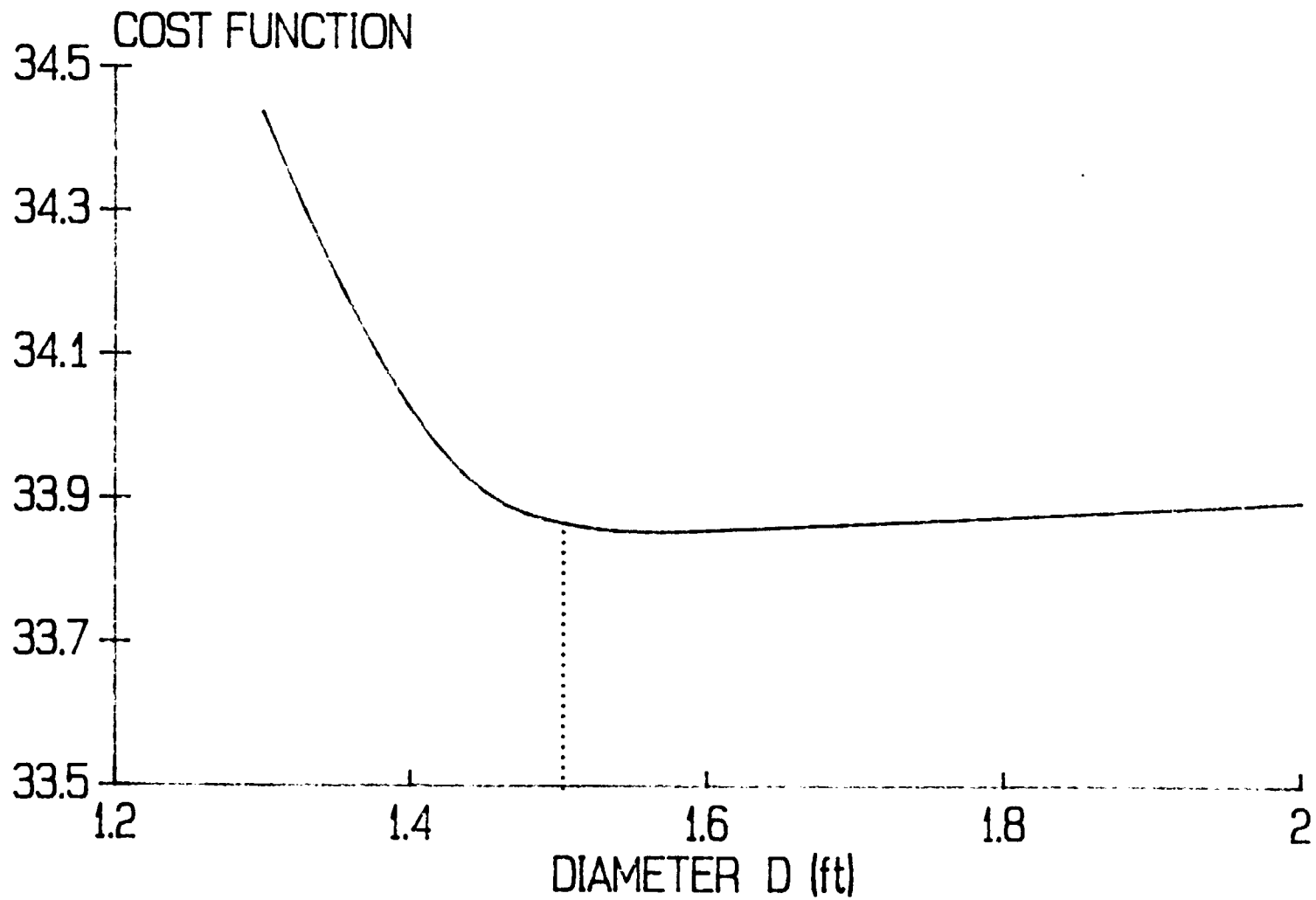


Fig. 5 Cost Function vs Diameter of the Uniform Tubular Beam (here  $D-d=0.04$  ft) when two 500 lb Payloads are Added to the Beam at Joints 2 and 4, Symmetrically

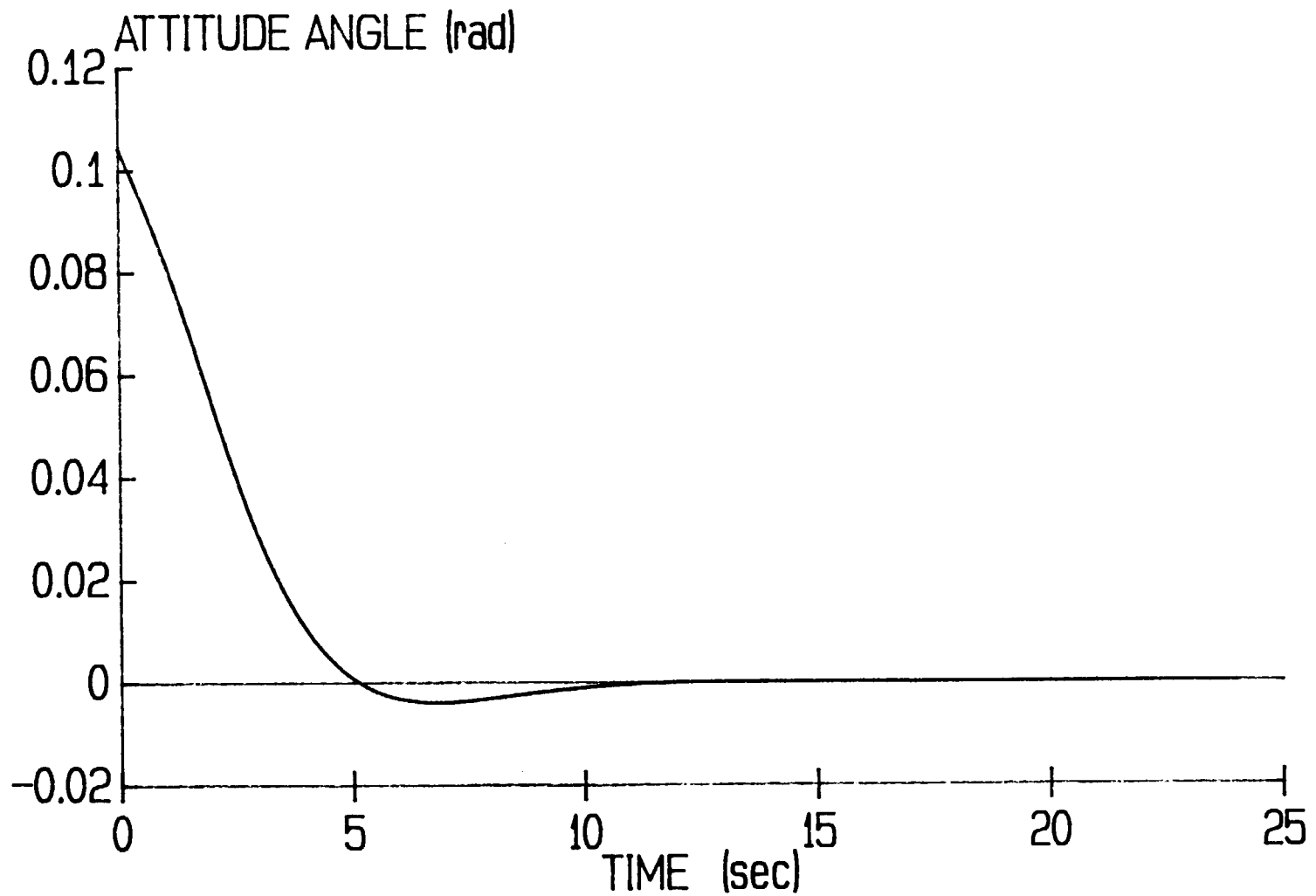


Fig. 6 Response of the Attitude Angle in-Plane for the Uniform Tubular Beam with two 50 lb Payloads at Joints 2 and 4, Symmetrically [here  $D=0.3$  ft and  $D-d=0.04$  ft]

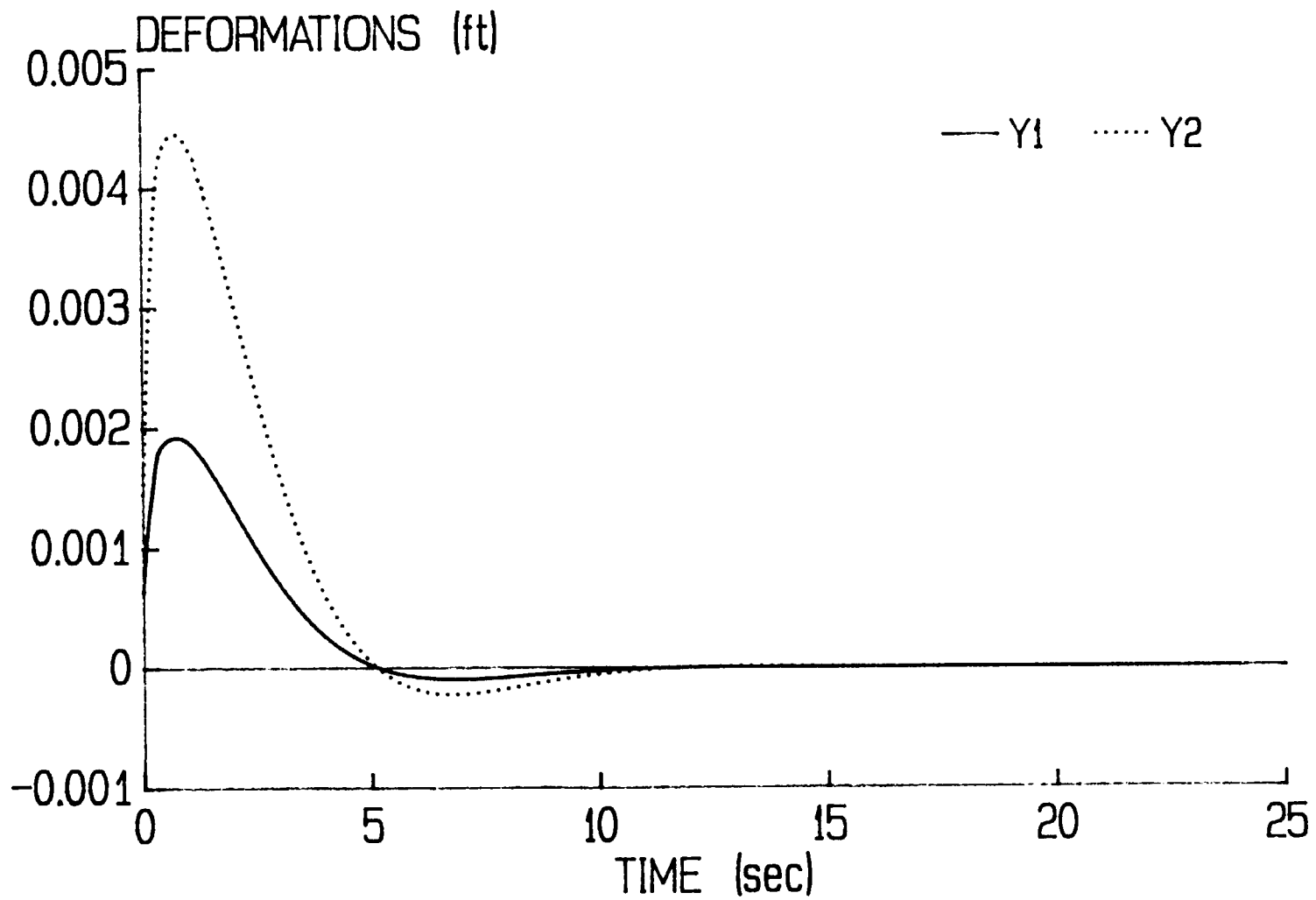


Fig. 7 Response of Deformations Parallel to the Y Axis at Joints 1 and 2 for the Uniform Tubular Beam with two 50 lb Payloads at Joints 2 and 4, Symmetrically [here  $D=0.3$  ft and  $D-d=0.04$  ft]

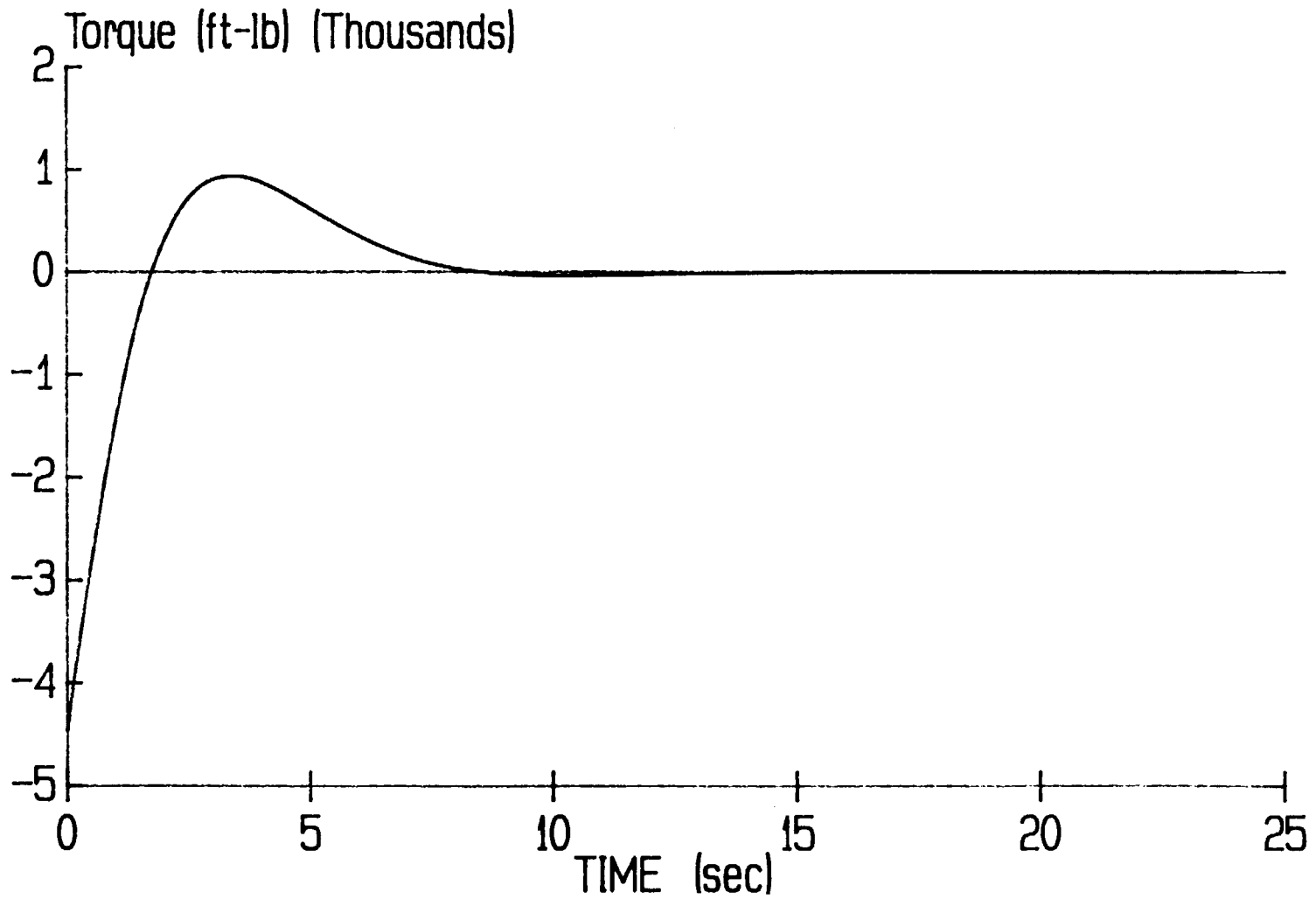


Fig. 8 Control Torque Trajectory at Joint 3 in Z direction for the Uniform Tubular Beam with two 50 lb Payloads at Joints 2 and 4, Symmetrically [here  $D=0.3$  ft and  $D-d=0.04$  ft]

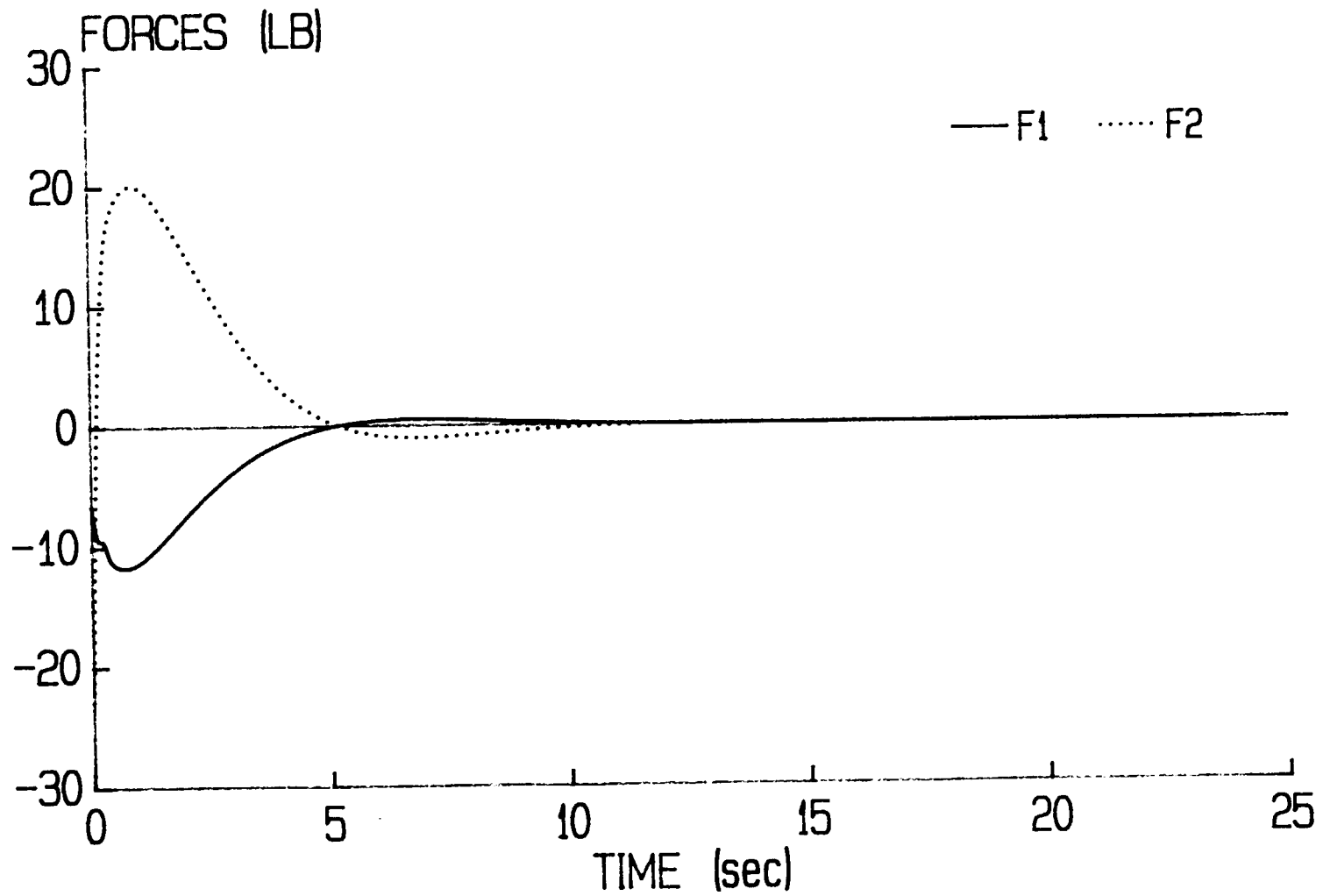


Fig. 9 Control Force Trajectories at Joints 1 and 2 Parallel to the Y Axis for the Uniform Tubular Beam with two 50 lb Payloads at Joints 2 and 4, Symmetrically [here  $D=0.3$  ft and  $D-d=0.04$  ft]

## V. CONCLUSIONS AND RECOMMENDATIONS

Pontryagin's maximum principle has been applied to study the rapid slewing of the SCOLE orbital configuration in three dimensions. The quasilinearization technique for solving the resulting nonlinear two point boundary value problem has been successfully used for several different examples. The results indicate that the linearized system model can represent the nonlinear system adequately for simulating the major motions, but not as well for the secondary motions. The nonlinear quadratic terms of the main body (Shuttle) angular velocity can not be neglected for large-amplitude rapid maneuvers. The differences between the rigid and flexible nonlinear system responses are small because the flexible vibrations are successfully suppressed during the maneuvers simulated here.

In addition it is seen that the structural offset of the SCOLE mast attachment to the reflector is associated with a first order nonlinear effect. The mast shortening is associated with only a second order nonlinear effect and should be considered when the mast deformations are outside of the linear range. Gravitational-gradient effects may be safely neglected for all rapid slew maneuvers considered.

For further research it is recommended to extend the application of the maximum principle and the two point boundary value problem to more complicated systems proposed for the future CSI program.

A multi-objective cost function which includes a form of the standard LQR regulator cost and its partial variation with

respect to additional design parameters is studied here. This approach can be employed to determine the optimal diameter of a free-free orbiting uniform beam with additional payload masses added when constraints are placed on the maximum total mass, control saturation levels, and transient settling times. This study proves that the multicriteria design approach should produce superior results as compared with combinations of separate structural and control system design approaches. Extensions are recommended to consider more complex systems representative of proposed candidate CSI systems.

The current (1990-91) grant work has been redirected to lend greater support to the Controls/Structures Interaction (CSI) program and focuses on specific CSI evolutionary configurations.